HEAVY TRUCK MODELING AND ESTIMATION FOR VEHICLE-TO-VEHICLE COLLISION AVOIDANCE SYSTEMS

DISSERTATION

Presented in Partial Fulfillment of the Requirements for the Degree Doctor of Philosophy in the Graduate School of The Ohio State University

By

Sage M. Wolfe, MSME

Graduate Program in Mechanical Engineering

The Ohio State University

2014

Dissertation Committee:

Dennis A. Guenther, PhD, Advisor

Gary J. Heydinger, PhD

Junmin Wang, PhD

Anthony F. Luscher, PhD

ABSTRACT

This dissertation details the development of a state and position estimator for articulated heavy trucks based entirely on freely available on-board signals. The estimator consists of a quasi-linear vehicle dynamics model, tire cornering stiffness estimator, Kalman filter, and position integrator. Results from testing show that the estimator can provide lane-level (1.5 m) positioning accuracy in urban environments for the duration of typical GPS outages. A hybrid kinematic-dynamic model allows estimation of hitch angle to within half of a degree over the practical range of articulation angles. This presents novel contributions to the state of the art of trailer tire cornering stiffness estimation and hitch angle estimation.

Government research has estimated that vehicle-to-vehicle (V2V) collision avoidance systems can address 72% of heavy truck crashes, but this requires localization of the truck and trailer in a variety of environments. Studies have shown that GPS cannot be reliably used for V2V in urban and some suburban environments. This estimator offers a potential supplement to GPS for V2V systems in these environments.

Moreover, the current V2V messaging framework does not include an estimate of hitch angle. This can lead to missed warnings and false positives when the implicit assumption of zero hitch angle is grossly violated, such as turning at an intersection. Results from this research indicate that a reliable estimate can be provided without the addition of new sensors.

ACKNOWLEDGMENTS

I would like to thank the following Vehicle Research & Test Center personnel for their invaluable assistance in this research: Dr. Sughosh Rao, Joshua Every, Dr. Kamel Salaani, Frank Barickman, Gavin Howe, Guogang Xu, Randy Landes, and Dr. Riley Garrott.

I would also like to thank Drs. Denny Guenther, Gary Heydinger, Junmin Wang, and Tony Luscher for advising me and serving on this committee.

Many thanks to the National Highway Traffic Safety Administration (NHTSA) for funding this work.

Finally, thanks to my girlfriend, Jessica Christine, for generating the kinematics and dynamics diagrams found throughout this text.

VITA

1988 .... Born in Athens, Ohio

2010 .... BS Mechanical Engineering, The Ohio State University, Columbus, Ohio

2011 .... MS Mechanical Engineering, The Ohio State University, Columbus, Ohio

2010 – Present .... Graduate Research Associate, The Ohio State University, Columbus, Ohio

PUBLICATIONS

1. So, J., Park, B., Wolfe, S., and Dedes, G. (2014). "Development and Validation of a Vehicle Dynamics-Integrated Traffic Simulation Environment Assessing Surrogate Safety." Pending publication in ASCE Journal of Computing in Civil Engineering.

2. Dedes, G., Wolfe, S., Guenther, D., Park, B., So, J., Mouskos, K.,. . . Heydinger, G. (2012). "A Simulation Design of an Integrated GNSS/INU, Vehicle Dynamics, and Microscopic Traffic Flow Simulator for Automotive Safety." RSS2011 Special Issue of Advances in Transportation Studies an International Journal, 41-52.

FIELDS OF STUDY

Major Field: Mechanical Engineering

Specialization: Vehicle Dynamics

TABLE OF CONTENTS

LIST OF FIGURES

LIST OF TABLES

CHAPTER 1

INTRODUCTION

Today's passenger cars and heavy trucks contain more safety systems than ever before, yet crashes continue to occur. This chapter begins by describing the benefits of a new active safety paradigm known as 'V2V' (vehicle-to-vehicle). The limitations of the system are explored and research is proposed to address the needs of the system. The chapter concludes with an overview of the research conducted and an outline of this dissertation document.

1.1 Literature Review

This chapter section presents a review of publications related to V2V and general vehicle dynamics modeling. Publications related to more specific topics of interest are discussed in later chapters for the sake of clarity. As examples: references that discuss the tuning of a Kalman filter are presented in Section 2.4 where the details of the Kalman filter are laid out. Prior art relating to the estimation of hitch angle is presented alongside new models for the same in Section 3.2.3.

1.1.1 V2V Benefits and Motivation for Research

In recent years, vehicles at all price points have incorporated a variety of impressive and capable active safety systems [1]. These systems, e.g. adaptive cruise control and active lane keeping, autonomously perform a variety of tasks using on-board controllers that take in sensor data from the vehicle. In literature, this is termed the 'egocentric' approach.

Despite these advancements, heavy truck fatal crashes per 100 million vehicle miles traveled increased from 1.11 to 1.42 during the period of 2009–2012 – an increase of 28% (2012 is the last year for which such data are currently available). Similarly, injury (nonfatal) crashes involving heavy trucks and resulting in injuries increased from 19 per 100 million vehicle miles to 29, a 53% increase over the four year period [2]. For two-vehicle fatal crashes, the three most common pre-crash scenarios were head-on (31%), other vehicle front to truck rear (19%), and truck front to other vehicle left (14%) as seen in Table 1.1.

Table 1.1: Percentage of Principal Impact Points in Two-Vehicle Fatal Crashes Involving Large Trucks, 2012 [2]

Impact Point on Large Truck	Impact Point on Other Vehicle (%)				
	Front	Left Side	Right Side	Rear	Total
Front	31	14	11	6	62
Left Side	9	1	1	0	11
Right Side	6	1	0	0	7
Rear	19	1	0	0	20
Total	**65**	**17**	**12**	**6**	**100**

In layman's terms, we need to prevent head-on collisions, keep people from rear ending trucks, and stop trucks from striking other vehicles in intersections. Studies conducted by researchers at Battelle and Virginia Tech indicate that radar- or video-based forward collision warning (FCW) systems have the ability to reduce heavy truck rear-end collisions by 21%, but head-on and intersection collisions virtually require a vehicle-to-vehicle (V2V) approach to obtain significant benefits [3]. Under this paradigm, vehicles broadcast their locations, speeds, headings, vehicle sizes, etc. over the air using a communications protocol known as Dedicated Short Range Communications (DSRC), similar to a Wi-Fi connection. A 2010 National Highway Traffic Safety Administration (NHTSA) study found that a combined V2V/V2I (vehicle-to-infrastructure) safety system could address 72% of heavy truck crashes involving unimpaired drivers, whereas an egocentric system could only address 64% of crashes [4]. V2V technology allows for a suite of collision avoidance programs aimed at mitigating various types of crashes – head-on, lane changing, intersections, road departures, and so on. Additionally, the sister technology, V2I, allows for curve speed warnings and a wide variety of information exchange, e.g. traffic conditions.

Work is being done on V2V outside the United States as well. Following a number of research projects, the German vehicle manufacturers Audi, BMW, Daimler, and Volkswagen formed an organization known as the Car 2 Car Communication Consortium (C2C-CC) in order to standardize V2X (vehicle-to-x, where x might be 'vehicle' or 'infrastructure') communications. Today members of C2C-CC include all European car manufacturers, a large number of suppliers, academia, and the telecommunications industry. Their studies have shown that 86% of crashes resulting in injury or death are due to driver error (including impairment, misjudgment of road conditions, etc.) that could potentially be addressed with V2V systems [5]. Efforts are shifting from small-scale research to large-scale field operational testing. In their first phase, C2C-CC intends to augment egocentric sensors by providing data about vehicles further ahead in the same direction of travel (ignoring, for example, vehicles crossing at intersections). Even with this limited approach, they expect to address up to 35% of crashes [5].

The effect of this first phase, or 'Early Warning' approach, is that the driver receives a warning some seconds before they reach the potential danger – and before a warning could be provided by an egocentric system. This warning means the driver can react sooner, creating a safety margin. Because V2V systems can 'see' further than egocentric sensors, the 'Early Warning' V2X approach can be more effective than the egocentric approach.

1.1.2 Selected V2V Limitations: GPS Accuracy and Availability

The efficacy of V2V safety systems critically depends upon GPS (Global Positioning System) accuracy and availability. The Crash Avoidance Metrics Partnership (CAMP), an industry consortium, published a study in 2011 regarding the potential benefits of V2V systems. A significant portion of this effort was devoted to studying the accuracy and availability of GPS in a variety of environments using a range of GPS receivers and processing algorithms. CAMP has defined an accuracy of 1.0–1.5 m (RMS relative position error) as being precise enough to enable lane-level positioning and 5–10 m as being precise enough to enable road-level positioning [6][7]. In urban canyons, they achieved RMS relative accuracy of 9.5–12.2 m and thus concluded, "GNSS-only techniques cannot be used reliably in this particular environment." Additionally, they found that on a tree-lined street typical of a residential neighborhood, positioning data were unavailable for approximately 21% of the time [7].

GPS availability gaps were also studied. Gaps were defined as the time interval when no relative positioning solution is available. This interval was affected by the positioning method used. In the single-point (SP) method, each vehicle calculates and broadcasts its own position (requiring a minimum of four satellite signals). In the real-time kinematic (RTK) method, raw GPS observables are shared and relative positioning is performed autonomously by each vehicle, resulting in enhanced accuracy. This requires that the vehicles exchange four *common* satellite observables. This more stringent requirement leads to more frequent and longer gaps [7].

With the SP method, 96–100% of gaps were less than 15 s and the average gap was 2–3.5 s depending on GPS receiver type. In general, the SP method would produce a position estimate almost immediately after seeing four satellites. With the RTK method, gap length varied widely with receiver type. Average gaps ranged from 8.6–19.7 s and some gaps were 70 s or higher. Additionally, the RTK method required 4–5 s to produce a position estimate after four common satellites were available [7].

In research conducted in parallel with [8], it was shown that warning timing (i.e., the temporal difference between when a warning should be issued and when it is actually issued) degrades rapidly with decreasing GPS accuracy.

1.1.3 Selected V2V Limitations: Current V2V Message Set

The current V2V message set does not include a field for the articulation angle of heavy trucks; they are implicitly assumed to be straight at all times [9]. This oversimplification can lead to both false positives and missed warnings. While articulation angles are small in highway driving, consider the case of a heavy truck turning left in an urban intersection as an example. This poses two problems. First, the vehicles traveling straight ahead to the right of the truck may receive a forward collision warning (FCW) since their on-board threat arbitration module will project the trailer into their lane. Secondly, vehicles who are oncoming to the truck's final lane may receive no warning even though the trailer is still blocking the intersection.

1.1.4 Vehicle Dynamics Modeling

Vehicle dynamics modeling is a mature field and many books are dedicated to the topic, such as [10], [11], and [12]. Theoretical work began in the 1920s with Rolls-Royce, but as Bill Milliken notes in *Race Car Vehicle Dynamics*, "the beginning of a systematic attack on automobile stability and control" came from British engineer Maurice Olley in the 1930s during his time with Cadillac. Within three years of taking the position, he was responsible for the introduction of the independent front suspension in the United States [10]. Olley's early work, including what can be considered the earliest vehicle dynamic models, can be found in the comparatively recently released (circa 2002) *Chassis Design: Principles and Analysis* [13].

Milliken discusses a concept in [10] called the "Ladder of Abstraction." At the top of this ladder is the complete reality of the vehicle-driver combination. Near the top of the ladder are advanced driving simulators on mobile platforms. Such simulators provide users with visual, aural, and tactile feedback and are well-suited to studying naturalistic driver behavior in a safe environment [14]. The development of a vehicle dynamics model for such a simulator is described in [15]. As one moves down the ladder, additional simplifying assumptions are added to the model. Multibody dynamics programs remove the real driver from the simulation and instead use a closed-loop driver model or open-loop inputs. This class of programs simulates the dynamics (and often elastic compliance) of individual components and has broad applications beyond vehicle dynamics. One specific example is ADAMS (Automatic Dynamic Analysis of Mechanical Systems) and its various ADAMS/Car packages [16]. Slightly further down the ladder of abstraction are lumped-parameter vehicle dynamics simulation programs. TruckSim, which was used as a reference simulation to develop the models in Chapters 2 and 3, is an example of a lumped-parameter vehicle dynamics simulation program. In contrast to ADAMS, users of TruckSim would enter curves that describe suspension kinematics rather than describe individual suspension components, hence the lumped-parameter nature [17].

The models discussed so far have hundreds of degrees of freedom (DOF) and are intended to run on relatively high-performance computers. Near the middle of the ladder of abstraction are n-DOF models of modest n, say $4 > n > 30$. Ghike et al. describe the development of a 14-DOF model suitable for use in active chassis control systems [18]. Segal describes the validation of a 15-DOF model used to study the effects of the roadside environment on safety [19]. Berntop describes a 6-DOF model to be used for general vehicle dynamics simulation [20]. At the bottom of the ladder of abstraction are extremely simple models, perhaps with a single DOF. Gillespie describes such a model – at this level of reduction, a single equation – used to study longitudinal acceleration in [12].

The modeling choices an engineer must make center around a tradeoff between two goals: fidelity and simplicity. A racing team engaged in driver training will need such fidelity that an advanced driving simulator is required. A car company engaged in simulation of ride comfort will value the fidelity of a multibody dynamics program to the faster runtime of a moderate DOF simulation. When designing active chassis controls, a car company will be forced to use a lower order model capable of running in real-time on an automotive ECU. This research faces similar limitations, i.e. the vehicle dynamics model must be developed with the goal of feasible real-time implementation on an automotive ECU.

1.1.4.1 Lateral Dynamic Models

The simplest type of model useful for this research is the linear 2-DOF lateral dynamic model, or 'bicycle' model. It is described in [10] as having lateral velocity and yaw rate as its degrees of freedom with steer angle as the control input. It is termed a ‘bicycle’ model because it neglects lateral load transfer and accordingly compresses the vehicle to a single track. It neglects longitudinal load transfer, pitch motion, roll motion, aerodynamic effects, and compliance effects. Forward speed is treated as a constant parameter rather than a state variable (DOF). Tires are considered to be in their linear range, below about 0.4 g [10]. References [11] and [12] also contain 2-DOF lateral dynamic models, as does [21]. Pacejka provides a model of a single-track car-trailer combination [21].

1.1.4.2 Parameter Estimation

If a lateral acceleration sensor is present, the bicycle model can also be used to estimate some vehicle parameters. Estimation of linear tire cornering stiffness in conjunction with a bicycle model can be found in [22] and [23]. Several authors used a bicycle model and GPS data to estimate tire cornering stiffness (see [24], [25], [26]). Baffet et al. use a bicycle model in conjunction with a sliding mode observer and Kalman filter to estimate tire cornering stiffness [27].

1.1.4.3 Heavy Truck Models

According to a historical survey of heavy truck dynamic modeling by Bernard et al., theoretical work on heavy trucks began in the 1950s and simulations on analog computers were carried out in the 1960s [28]. The earliest known work, on the snaking of trailers, was published by Williams in 1951 [29].

A number of more recent articulated heavy truck lateral dynamic models were also identified and studied. However, a new model was developed due to the incompatibility of other models with this research or other inconveniences presented by those found in the literature. Rao produced a model that assumed a measured hitch angle [30]. Alexander et al. produced a tractable model, but it was intended only for use when hitch angle is small [31]. Salaani also produced a feasible model, but it used an inconvenient coordinate system [32]. Hac and Deng both created car-trailer models extensible to the heavy truck case, but required calculation of hitch forces [33], [34]. Luijten used a bicycle model to study the yaw (jackknife) stability of articulated heavy vehicles [35]. Bareket et al. produced a lateral dynamic model for a driving simulator that used a table lookup approach for roll and pitch motion [36].

1.2 Outline of Research

1.2.1 Research Goals

The goal of this research is to address the limitations of V2V systems as outlined in Sections 1.1.2 and 1.1.3 without adding hardware costs to the vehicle. This means providing a sensor-less solution for positioning the vehicle and determining the articulation angle based on already available on-board signals.

Since position is an integrated quantity, the error of such an estimator naturally grows without bound over long time scales. Accordingly, the position estimate provided by this system is not designed to replace GPS – it is intended to augment GPS. It is expected that the V2V system will primarily use GPS for positioning and that this estimate will be used when GPS is unavailable or unreliable (and perhaps to determine when GPS is unreliable). Since the goal is to keep the system functioning in the face of GPS gaps, the work done by CAMP referenced in Section 1.1.2 gives some insight into what the capabilities of this system should be. Accuracy of 1.0–1.5 m RMS (lane-level positioning) should be maintained for average gaps, which may be up to 20 s depending on the positioning method and receiver type. Accuracy of 5 m RMS (road-level positioning) should be maintained for the longer gaps of up to 70 s.

A single GPS receiver cannot provide a measurement of hitch angle. This requires additional sensors, such as dual GPS receivers on the trailer (and communication with the tractor) or direct measurement via a sensor located on the tractor. Even a simple kinematic model of trailer motion requires knowledge of side slip velocity. (GPS provides velocity data, of course, but not longitudinal and lateral velocity – only their vector sum.) Thus this system will also be useful when GPS is available as it solves the hitch angle problem without adding additional sensors. With some assumptions, a target for hitch angle accuracy can be derived. For example, consider a 53 ft (16.2 m) trailer and a desired accuracy (of the rear of the trailer) of 1.0 m. If the tractor's position and heading are correct, this implies that the hitch angle must be accurate to $\pm \arctan\left({}^{1.0}/_{16.2}\right) = \pm 3.5$ deg. In accordance with the fact that the tractor's position and heading may be known imperfectly, an accuracy of ±2 deg has been chosen as a goal for this research.

This research is supported by NHTSA, the division of the Department of Transportation responsible for vehicle safety. They are currently researching V2V safety systems. This project helps them to advance the state of the art of V2V, understand its limitations, and consider what regulatory changes might be necessary for its success.

1.2.2 Dissertation Outline

Chapter 1 has explained the benefits attainable with V2V safety systems and their current limitations. The remainder of the dissertation will be devoted to explaining research designed to address these issues.

Chapter 2 describes the modeling for the unarticulated (trailer-less) case (or 'three-axle model'). This consists of a quasi-linear vehicle lateral dynamics model that uses wheel speeds and steer angle as input. A parameter estimation scheme has been developed to provide the model with values of tire cornering stiffness. The estimates provided by the vehicle dynamics model are fused via Kalman filtering with on-board measurements of lateral acceleration and yaw rate, both available from the tractor's electronic stability control (ESC) system. Finally, Chapter 2 concludes with a brief validation of the model using TruckSim as a reference.

Chapter 3 describes the modeling for the articulated (tractor-trailer) case (or 'five-axle model') and discusses some of the modeling issues encountered with this more complex system. It also explains the modifications made to the cornering stiffness estimator and Kalman filter to extend them to the articulated case. A kinematic (as opposed to dynamic) method of estimating articulation angle is derived. Finally, TruckSim is used to validate the articulated model and compare the kinematic and dynamic methods for estimating articulation angle.

Chapter 4 contains an experimental validation of the models. First, the test vehicle and instrumentation are discussed. The remainder focuses mostly on the more complex five-axle model. Several scenarios were developed to examine cornering stiffness estimation, urban driving, and highway driving. The results are examined and the kinematic and dynamic models for estimating articulation angle are again compared.

Chapter 5 examines how this research benefits the state of the art of V2V safety systems. This chapter also describes some of the additional work required to implement this research and what limitations might be faced in practice.

1.2.3 Conclusion

This chapter has introduced the dissertation. It began with a literature review of V2V and vehicle dynamics modeling. Respectively, these represent the motivation for this research and the means by which it was accomplished. The goals of the research program were specified and an overview of the dissertation was provided.

Chapter References

[1] Highway Loss Data Institute, “Mercedes-Benz collision avoidance features: initial results.” Bulletin, Vol. 29, No. 7, April 2012.

[2] National Highway Traffic Safety Administration, “Traffic Safety Facts, 2012 Data, Large Trucks.” DOT HS 811 868, `http://www-nrd.nhtsa.dot.gov/Pubs/811868.pdf`, May 2014. Online; accessed June 10, 2014.

[3] F. S. Barickman, “NHTSA VRTC HV Forward Collision Avoidance and Mitigation Research.” Government/Industry Brake Research Presentation, 2012.

[4] W. Najm, J. Koopmann, J. Smith, and J. Brewer, “Frequency of Target Crashes for Intellidrive Safety Systems.” DOT HS 811 381, 2010.

[5] C. Weiss, “V2x communication in Europe – from research projects towards standardization and field testing of vehicle communication technology,” *ComNet (Computer Networks)*, vol. 55, no. 3103-3119, 2011.

[6] Crash Avoidance Metrics Partnership, “Enhanced Digital Mapping Project Final Report.” DOT DTFH61-01-X-00014, November 2004.

[7] Crash Avoidance Metrics Partnership, “Vehicle Safety Communications - Applications (VSC-A) Final Report.” DOT DTNH22-05-H-01277, May 2011. Appendix E.

[8] Sage Wolfe, “Integration of CarSim into a Custom Cosimulation Program for Automotive Safety.” Master’s Thesis, The Ohio State University, 2011.

[9] D. S. R. C. Technical Committee, “Dedicated Short Range Communications (DSRC) Message Set Dictionary,” *SAE Standard J2735*, November 2009.

[10] W. Milliken and D. Milliken, *Race Car Vehicle Dynamics*. Warrendale, PA: SAE, 1995.

[11] R. Rajamani, *Vehicle Dynamics and Control*. New York: Springer, 2012.

[12] T. Gillespie, *Fundamentals of Vehicle Dynamics*. Warrendale, PA: SAE, 1992.

[13] W. Milliken, D. Milliken, and M. Olley, *Chassis Design: Principles and Analysis*. Warrendale, PA: SAE, 2002.

[14] NHTSA, “The national advanced driving simulator (NADS).” `http://www.nhtsa.gov/Research/Driver+Simulation+(NADS)/The+National+Advanced+Driving+Simulator+(NADS)`. Online; accessed June 11, 2014.

[15] M. K. Salaani, “Development and Validation of a Vehicle Model for the National Advanced Driving Simulator.” Doctoral Dissertation, The Ohio State University, 1996.

[16] Mechanical Simulation Corporation, "Product datasheet - adams/car." http://www.mscsoftware.com/sites/default/files/ds_adams-car_ltr_w_0.pdf. Online; accessed June 11, 2014.

[17] Mechanical Simulation Corporation, "Trucksim brochure." http://www.carsim.com/downloads/pdf/trucksim_handout.pdf. Online; accessed June 11, 2014.

[18] C. Ghike and T. Shim, "14 degree-of-freedom vehicle model for roll dynamics study," *SAE*, no. 2006-01-1277, 2006.

[19] D. Segal, "Highway-vehicle-object simulation model - 1976 engineering manual - validation." FHWA Report No. FHWA-RD-76-165, February 1976.

[20] K. Berntop, "Derivation of a six degrees-of-freedom ground-vehicle model for automotive applications," *Technical Report, Lund University, Department of Automatic Control*, no. ISRN LUTFD2/TFRT–7627–SE, 2006.

[21] H. B. Pacejka, *Tire and Vehicle Dynamics*. Warrendale, PA: SAE, 2002.

[22] C. Lundquist and T. Schon, "Recursive identification of cornering stiffness parameters for an enhanced single track model," *Proceedings of the 15th IFAC Symposium on System Identification*, vol. 15, no. 1, 2009.

[23] C. Sierra, E. Tseng, A. Jain, and H. Peng, "Cornering stiffness estimation based on vehicle lateral dynamics," *Vehicle System Dynamics: International Journal of Vehicle Mechanics and Mobility*, vol. 44, no. 1, 2007.

[24] D. Bevly, R. Daily, and W. Travis, "Estimation of critical tire parameters using GPS based sideslip measurements," *SAE*, no. 2006-01-1965, 2006.

[25] W. Sienel, "Estimation of the tire cornering stiffness and its application to active car steering," *Proceedings of the 36th IEEE Conference on Decision and Control*, vol. 5, no. 4744-4749, 1997.

[26] R. Anderson and D. Bevly, "Estimation of tire cornering stiffness using gps to improve model based estimation of vehicle states," *Proceedings of IEEE Intelligent Vehicles Symposium*, no. 801-806, 2005.

[27] G. Baffet, A. Charara, and D. Lechner, "Estimation of vehicle sideslip, tire force and wheel cornering stiffness," *Control Engineering Practice*, vol. 17, no. 1255-1264, 2009.

[28] J. Bernard and J. Shannan, "Simulation of heavy vehicle dynamics," *SAE*, no. 902270, 1990.

[29] D. Williams, "The mathematical theory of the snaking of two-wheeled trailers, with practical rules and devices for preventing snaking," *Proceedings of the Institution of Mechanical Engineers: Automobile Division*, 1951. pp. 175-190.

[30] S. Rao, "Development of a Hardware in the Loop Simulation System for Heavy Truck ESC Evaluation and Trailer Parameter and State Estimation." Doctoral Dissertation, The Ohio State University, 2013.

[31] L. Alexander, M. Donath, M. Hennessey, V. Morellas, and C. Shankwitz, "A lateral dynamic model of a tractor–trailer: Experimental validation." MN DOT Report, Contract 73168 TOC 174, November 1996.

[32] M. Salaani, "The application of understeer gradient in stability analysis of articulated vehicles," *International Journal of Heavy Vehicle Systems*, vol. 16, no. 1/2, 2009.

[33] A. Hac, D. Fulk, and H. Chen, "Stability and control considerations of vehicle-trailer combination," *SAE*, no. 2008-01-1228, 2008.

[34] W. Deng and X. Kang, "Parametric study on vehicle-trailer dynamics for stability control," *SAE*, no. 2006-01-1965, 2003.

[35] M. Luijten, "Lateral dynamic behaviour of articulated commercial vehicles." Master's thesis, Eindhoven University of Technology, August 2010.

[36] Z. Bareket and P. Fancher, "Truck or bus dynamic modeling for a driving simulator," *Technical Report, University of Michigan, Transportation Research Institute*, no. UMTRI-91-26, 1991.

CHAPTER 2
THREE-AXLE LATERAL DYNAMIC HEAVY TRUCK MODEL

2.1 Introduction

This chapter describes the development of the three-axle lateral dynamic model of the heavy truck. The term ‘three-axle’ refers to the front steer axle and the tandem rear axles of a heavy truck (without trailer).

First, the structure of this model (i.e. its states and parameters) and its derivation are presented along with the assumptions and approximations employed therein. The derivation is examined using both Newton’s Second Law and Lagrange’s Equation. The coupled differential equations of motion are converted to a continuous-time state space representation using MATLAB®. MATLAB® is then used to discretize the system. Next, a recursive least squares cornering stiffness estimation scheme based on two different measurements is introduced. A Kalman filter is then developed based on extant signals available from the electronic stability control (ESC) system. Finally, the model is validated using TruckSim as a reference.

2.2 Derivation

A quasi-linear three-axle bicycle model was derived using Newton's Second Law (Equation 2.1) and Lagrange's Equation (Equation 2.2). The model is quasi-linear in that the cosine of road wheel steer angle appears in the state and input matrices, though it could be neglected as this is very near unity. Forward velocity, u, is treated as a constant parameter instead of a state variable. This is because the model is intended to run at 100 Hz, which far exceeds the bandwidth of forward velocity (i.e., it can be considered constant for $^1/_{100}$ s). At each time step, the model is updated with new values for u and the cosine of steer angle.

$$\sum \vec{F} = m\vec{a} \tag{2.1}$$

$$\frac{d}{dt}\left(\frac{\delta T}{\delta \dot{q}_i}\right) - \frac{\delta T}{\delta q_i} = Q_{q_i} \tag{2.2}$$

In Lagrange's Equation, the Lagrangian, L, represents the difference of the sums of kinetic energy (T) and potential energy (V) in terms of the generalized coordinates, $\underline{q}$. This is expressed in body-fixed coordinates of lateral position, y, and yaw angle, Ψ. A free-body diagram of the system, along with details of its parameters, are given in Figure 2.1. This is a right-handed coordinate system with 'forward' positive in the longitudinal direction, 'left' positive in the lateral direction, and counterclockwise (as viewed from above) positive in the yaw direction. Note that since the coordinates are body-fixed, $y(t) = 0 \ \forall \ t$ despite the fact that $\dot{y}(t) = v \neq 0$ in general. (Energy is independent of position, it is dependent only on velocity.) The Lagrangian, L, for this system is given in Equation 2.3. Note that potential energy, V, is zero.

$$L = T - V = T = \frac{1}{2}m_1(u^2 + v^2) + \frac{1}{2}J_1\dot{\Psi}^2 \tag{2.3}$$

Applying Equation 2.2 to Equation 2.3 results in two coupled differential equations which form the "inertial terms" of the system. They are coupled due to the relationship shown in Equation 2.4. This relationship, well-known in vehicle dynamics, exists

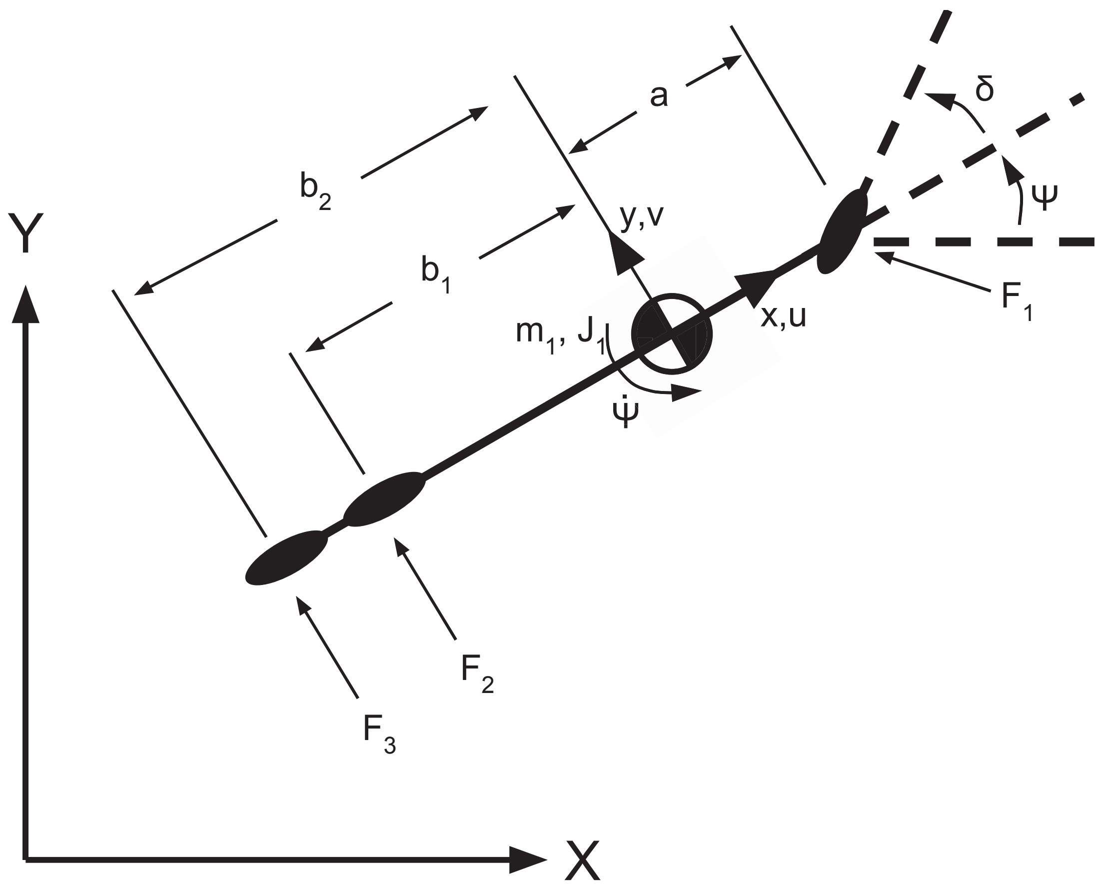

Figure 2.1: Free-Body Diagram, Three-Axle Model

because the body-fixed frame is moving with forward velocity u and rotating with angular velocity $\dot{\Psi}$. A formal derivation of this relationship is given in [1]. Since we wish to track Ψ, we augment the system with the equation $\dot{\Psi} = \dot{\Psi}$. When converted to discrete time, this will result in the equation $\Psi_{k+1} = \Psi_k + \dot{\Psi}_k T_s$ (which is more obviously an integrator). Due to the coupling and quasi-linearity of this problem, we ultimately wish to deal with it in a state space representation. Thus the inertial terms, augmented with what will become the yaw angle integrator, are expressed as $\mathbf{M}\underline{\dot{\mathbf{x}}}$ where $\mathbf{M}$ is given in Equation 2.5 and $\underline{\dot{\mathbf{x}}}$ is given in Equation 2.6.

$$\frac{d}{dt}(v) = \dot{v} + u\dot{\Psi} \tag{2.4}$$

$$\mathbf{M} = \begin{bmatrix} m_1 & 0 & u\,m_1 \\ 0 & J_1 & 0 \\ 0 & 0 & 1 \end{bmatrix} \tag{2.5}$$

$$\underline{\dot{\mathbf{x}}} = \begin{pmatrix} \dot{v} \\ \ddot{\Psi} \\ \dot{\Psi} \end{pmatrix} \tag{2.6}$$

Where:

$\dot{v}$: side-slip acceleration of tractor CG

$\ddot{\Psi}$: yaw acceleration of tractor

$\dot{\Psi}$: yaw rate of tractor

Rows 1 and 2 of $\mathbf{M}\underline{\dot{\mathbf{x}}}$ correspond to the ma terms derived using Equation 2.1. From inspection, we can see that the generalized forces, Q_{q_i}, will be equal to the sum of forces in the y direction for $q_i = y$ and the sum of moments about the CG for $q_i = \Psi$. (These can also be independently derived via virtual work expressions. Virtual work expressions are further explained in Section 3.2.1, where they are more useful.) This yields the following equations (please refer to Figure 2.1 for a depiction of the forces and parameters):

$$Q_y = \sum F_y = F_1 \cos\delta + F_2 + F_3 \tag{2.7}$$

$$Q_\Psi = \sum M_{CG} = aF_1 \cos\delta - b_1 F_2 - b_2 F_3 \tag{2.8}$$

Equations 2.7 and 2.8 require that the lateral tire forces, F_i, be calculated. Here, several assumptions common to the field of vehicle dynamics are applied. Forces are calculated using a lumped, linear cornering stiffness (C_{α_i}), i.e. $F_i = C_{\alpha_i}\alpha_i,\ C_{\alpha_i} > 0\ \forall\ i$. Slip angle, α_i, is defined as the angle between the instantaneous velocity vector and the heading angle of the tire. For a diagram and expressions for slip angles, refer to Appendix A.1. Consistent with the coordinate system, slip angles are considered positive counterclockwise so that a positive slip angle produces a positive lateral force using a positive value of cornering stiffness. (Correspondingly, a positive steer input produces a positive yaw rate response.) Linearity of cornering stiffness is a valid assumption for low-g (sub-limit) maneuvers [2]. Furthermore, heavy truck tires tend to be more linear in cornering stiffness than light vehicle tires ([3], [4] and comparison of validated tire models in CarSim/TruckSim). Additionally, slip angles are assumed small. This is because each slip angle contains a term for the arctangent of (negative) lateral velocity divided by forward velocity. Thus $\arctan\alpha_i \approx \alpha_i$ [2]. Finally, since this is a bicycle model, slip angles are treated as being equal for tires on a given axle. In a turn, the forward velocity of the outside wheel will be increased by an amount equal to the yaw rate multiplied by half the track width, while the inside wheel's velocity will be retarded by the same amount. Thus this is a good approximation as the slip angle of the outside wheels will be overestimated in magnitude by an amount similar to which the slip angle of the inside wheels is underestimated. Furthermore, these contributions to forward velocity are generally small relative to the mean forward velocity of the tractor, u.

Now that the tire forces have been quasi-linearized, they can be expressed in the form $\mathbf{K}\underline{\mathbf{x}} + \mathbf{F}\mathbf{u}$, where $\mathbf{K}$ is given in Equation 2.9 and $\mathbf{F}$ is given in Equation 2.10. The state vector, $\underline{\mathbf{x}}$, and input, $\mathbf{u}$, are given in Equation 2.11. (Note: this input, $\mathbf{u}$, is not to be confused with forward velocity, u. It is simply due to the conventions of state space and vehicle dynamics that they share the same character.)

$$\mathbf{K} = \begin{bmatrix} \frac{1}{u}\left[-\cos(\delta)C_{\alpha 1} - C_{\alpha 2} - C_{\alpha 3}\right] & \frac{1}{u}\left[-a\cos(\delta)C_{\alpha 1} + b_1 C_{\alpha 2} + b_2 C_{\alpha 3}\right] & 0 \\ \frac{1}{u}\left[-a\cos(\delta)C_{\alpha 1} + b_1 C_{\alpha 2} + b_2 C_{\alpha 3}\right] & \frac{1}{u}\left[-a^2\cos(\delta)C_{\alpha 1} - b_1^2 C_{\alpha 2} - b_2^2 C_{\alpha 3}\right] & 0 \\ 0 & 1 & 0 \end{bmatrix} \tag{2.9}$$

$$\mathbf{F} = \begin{bmatrix} \cos(\delta)C_{\alpha 1} \\ a\cos(\delta)C_{\alpha 1} \\ 0 \end{bmatrix} \tag{2.10}$$

$$\underline{\mathbf{x}} = \begin{pmatrix} v \\ \dot{\Psi} \\ \Psi \end{pmatrix}, \quad \mathbf{u} = \delta \tag{2.11}$$

Where:

v : side-slip velocity of tractor CG

$\dot{\Psi}$: yaw rate of tractor

Ψ : yaw angle of tractor

δ : road wheel steer angle of tractor

With the inertial (left hand side) and stiffness/forcing (right hand side) terms formulated, they can be combined as shown in Equation 2.12. This is essentially the matrix form of Equation 2.1 with the right and left hand sides exchanged. This is readily converted to state space form by inverting the mass matrix and multiplying each side by $\mathbf{M}^{-1}$, as shown in Equation 2.13. This continuous-time representation can then be converted to the discrete-time representation shown in Equation 2.14. In both cases, these matrix manipulations are carried out numerically in MATLAB®, i.e. after the values of parameters, etc. have been used to fill in the matrices.

$$\mathbf{M}\underline{\dot{\mathbf{x}}} = \mathbf{K}\underline{\mathbf{x}} + \mathbf{F}\mathbf{u} \tag{2.12}$$

$$\underline{\dot{\mathbf{x}}} = \mathbf{M}^{-1}\mathbf{K}\underline{\mathbf{x}} + \mathbf{M}^{-1}\mathbf{F}\mathbf{u} = \mathbf{A}\underline{\mathbf{x}} + \mathbf{B}\mathbf{u} \tag{2.13}$$

$$\underline{\mathbf{x}}_{k+1} = \mathbf{A}_k\underline{\mathbf{x}}_k + \mathbf{B}_k\mathbf{u}_k \tag{2.14}$$

The model requires values for tire cornering stiffness. The estimation of these quantities is described in Section 2.3. Since the vehicle position estimator is intended to provide localization under normal driving conditions, a simple linear tire model is used. It is expected that in practice the lateral acceleration of the truck will rarely exceed 0.3 g. Nonetheless, the estimator has shown good results even with peak lateral accelerations exceeding 0.5 g (see Section 4.4).

The model, as presented thus far, predicts and tracks the states of the system. In order to track position, it is augmented with two simple integrators. Equation 2.15 is an integrator for global X position and Equation 2.16 is an integrator for global Y position.

$$\hat{X}_{k+1} = \hat{X}_k + \left(\hat{u}_k \cos\hat{\Psi}_k - \hat{v}_k \sin\hat{\Psi}_k\right) T_s \tag{2.15}$$

$$\hat{Y}_{k+1} = \hat{Y}_k + \left(\hat{u}_k \sin\hat{\Psi}_k + \hat{v}_k \cos\hat{\Psi}_k\right) T_s \tag{2.16}$$

Because the goal of this system is to track the position of the truck, the problem is significantly difficult. State estimates that would be acceptable for dynamic controls, e.g. vehicle stability control, are inadequate for position estimation. This is because small errors in yaw rate are integrated to become significant errors in yaw angle (or heading). If the vehicle is traveling at significant speeds (e.g. highway driving), error accumulates very rapidly with time if the heading is incorrect. For this reason, the estimator was augmented with a Kalman filter. The Kalman filter uses measurements of lateral acceleration and yaw rate – both freely available signals from the electronic stability control (ESC) system. The specifics of the Kalman filter implementation are described in Section 2.4.

2.3 Tire Cornering Stiffness Estimator

To be reasonably accurate, the vehicle position estimator must have good values for tire cornering stiffness. Since the vehicle manufacturer is likely to be the entity programming such a position estimator in practice, one may think that cornering stiffness is a 'fair' thing to take as a known value. However, due to tire replacement, tire wear, varied inflation pressure, road surface conditions, and so on, an on-line estimator is required.

Parameter estimation, at its core, is similar to solving an algebraic equation. If you apply an unknown force to a one pound block and measure its acceleration to be one g, you can surmise that you have applied one pound of force.

In this case, we are interested in estimating three parameters – the cornering stiffness of each axle of the vehicle (this is the vector $\hat{\phi}$). Since this is compared to a single measured quantity, y (not to be confused with the generalized coordinate), multiple measurements are taken and the three cornering stiffnesses are fitted to the data in a least squares sense (since it is done by looking backwards, it is termed 'recursive least squares' or RLS). Additionally, new data is weighted more heavily than old data, a technique known as 'forgetting,' or 'recursive least squares with forgetting.' To continue the analogy, the process is complicated by the fact that the equivalent of the known mass, X, is a changing vector made up mostly of state variables. Equations 2.17 – 2.19 give the structure of the RLS scheme [5].

$$\hat{\phi}(k) = \hat{\phi}(k-1) + L(k)(y(k) - X^T(k)\hat{\phi}(k-1)) \tag{2.17}$$

$$L(k) = P(k-1)X(k)(\lambda + X^T(k)P(k-1)X(k))^{-1} \tag{2.18}$$

$$P(k) = (I - L(k)X^T(k))P(k-1)\frac{1}{\lambda} \tag{2.19}$$

Where:

$\hat{\boldsymbol{\phi}}$: parameter estimate column vector

X : row vector that scales $\hat{\phi}$ to y

L : gain vector

P : covariance matrix

λ : forgetting factor

RLS schemes were created based on two different measurements: lateral acceleration (y_1) and yaw acceleration (y_2). (Yaw acceleration was calculated by numerically differentiating the measured yaw rate.) The details are given below in Equations 2.20 – 2.24. Note that although the vehicle position estimator is intended for cases when GPS is unavailable, the tire cornering stiffness estimator would only run when GPS is available and thus the most recent information is available to construct high-fidelity state estimates. Although the measurements and states used to make up the X vectors are supplied to the tire cornering stiffness estimator by the dynamic model, the tire cornering stiffness values used by the dynamic model are not updated throughout a run. The tire cornering stiffness values used by the dynamic model are constant for a given run. On a real vehicle, with a real V2V system, a formal algorithm for how and when to update the tire cornering stiffnesses of the dynamic model would need to be developed.

Figure 2.2 shows an example of the estimator at work. Note that it is typical for the estimator to converge to different values based on the level of excitation. Here the solid lines ($C_{\alpha i}(1)$) correspond to the estimate from lateral acceleration and the dashed lines ($C_{\alpha i}(2)$) correspond to the estimate from the yaw acceleration measurement. In general, the estimates from lateral acceleration measurements were more reliable and accurate. This is fortunate since it is a commonly available quantity and does not involve taking a (noisy) derivative. This favored formulation – RLS with forgetting, single-track 'bicycle' model, linear cornering stiffness, and lateral acceleration as a measurement – is a popular method for on-line estimation [6],[7].

It is worth emphasizing the 'lumped' nature of Equations 2.20 and 2.21. Consider Equation 2.20. It is a restatement of Newton's Second Law, i.e. that the lateral acceleration of the tractor is equal to the lateral force applied by the tires divided by the mass of the tractor. This lateral force is modeled as the sum of products of slip angle estimates and cornering stiffness estimates. In addition to the fact that the slip angle estimates are built from state estimates (refer to Appendix A.1.2 for slip angle expressions), this neglects several other effects such as steering gear compliance, body roll, static toe, suspension compliance, normal load variation, etc. This scheme provides an estimate of the lumped cornering stiffness of the entire axle, i.e. the scaling factor that best defines (in a least squares sense) the input-output relationship between slip angle estimates and estimated lateral force. In practice, this *in situ* estimation can provide cornering stiffness estimates that differ significantly from what would be measured *ex situ* on a tire test machine [8]. Pacejka refers to this as the 'effective axle cornering stiffness' [4]. Owing to uncertainties both in tires (inflation pressure, wear, road friction coefficient, construction, compound) and trucks

(Ackerman, alignment, steering compliance, loaded weight, axle loads), no party has the information necessary to predict *in situ* effective axle cornering stiffness and thus it must be estimated online.

$$y_1 = a_y = \frac{1}{m_1} X_1 \phi \tag{2.20}$$

$$y_2 = \ddot{\Psi} = \frac{1}{J_1} X_2 \phi \tag{2.21}$$

$$\phi = \begin{pmatrix} C_{\alpha 1} \\ C_{\alpha 2} \\ C_{\alpha 3} \end{pmatrix} \tag{2.22}$$

$$X_1 = \begin{bmatrix} \left(\delta \cos(\delta) - \cos(\delta) \dfrac{v + a\dot{\Psi}}{u} \right) & \dfrac{-v + b_1 \dot{\Psi}}{u} & \dfrac{-v + b_2 \dot{\Psi}}{u} \end{bmatrix} \tag{2.23}$$

$$X_2 = \begin{bmatrix} a\cos(\delta) \left(\delta - \dfrac{v + a\dot{\Psi}}{u} \right) & b_1 \dfrac{v - b_1 \dot{\Psi}}{u} & b_2 \dfrac{v - b_2 \dot{\Psi}}{u} \end{bmatrix} \tag{2.24}$$

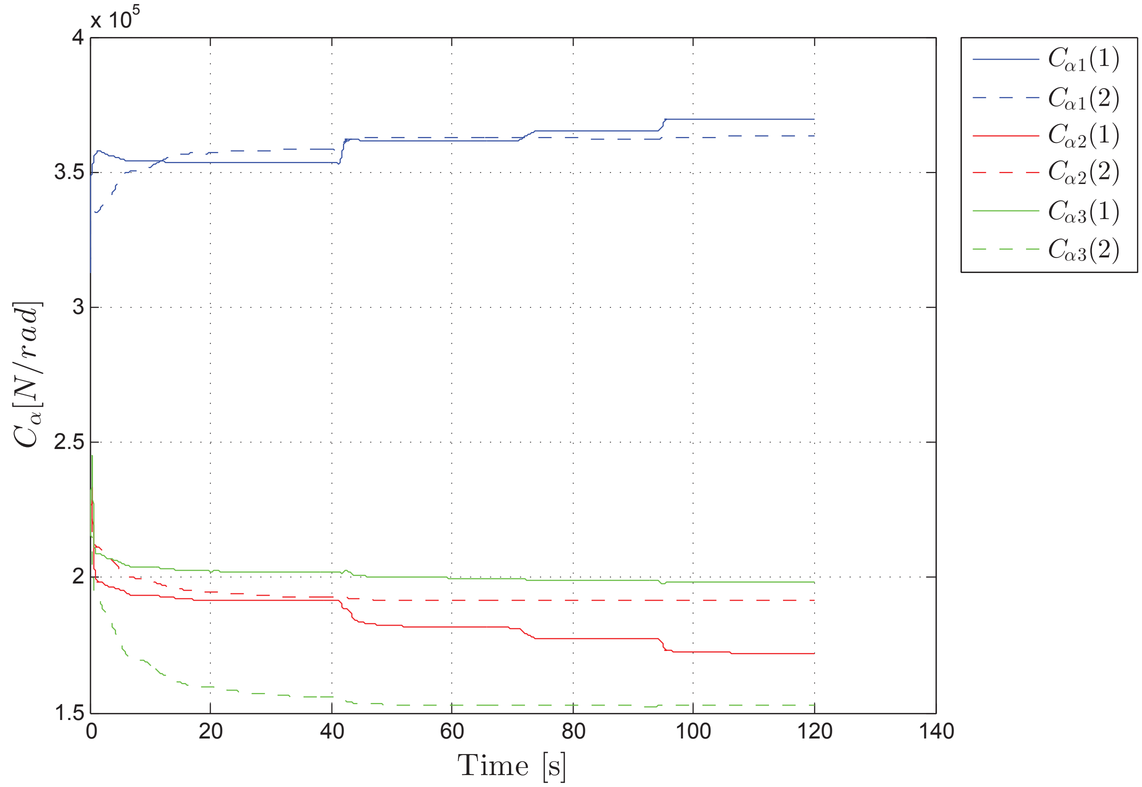

Figure 2.2: Cornering Stiffness Estimate, Three-Axle Model.
[(1): $y = a_y$, (2): $y = \ddot{\Psi}$]

2.4 Kalman Filter

Even with accurate cornering stiffness values, a Kalman filter (KF) is required for acceptable positioning accuracy. This is because small errors in yaw rate integrate with time to significant errors in heading (yaw) angle. Once the heading is misaligned, positioning errors grows rapidly. Thus the Kalman filter's primary function is to maintain the correct heading angle. The Kalman filter is well-known and its background and derivation will not be provided (for the original paper, see [9]). However, the equations and the specifics of its implementation will be discussed. While many formulations of the Kalman filter are possible, the convention followed here is similar to that outlined in [10]. The measurements used, $\underline{\mathbf{z}}_k$, are lateral acceleration and yaw rate, both available from the tractor ESC system.

Initialization proceeds as outlined in Equations 2.25-2.28, where $E\langle\cdot\rangle$ denotes the expected value operator. First, the best estimate of the current state vector is loaded as in Equation 2.25. In practice, this would be the last known data from before the loss of GPS. Second, the state covariance matrix, $\mathbf{P}$, is initialized. The diagonal terms represent the mean squared error in the initial values of the state vector. If these errors are unbiased and uncorrelated, the off-diagonal elements are zero (this is what is done here) [11]. Next, the measurement noise covariance matrix, $\mathbf{R}$, is initialized. It has a similar significance as the state covariance matrix: its diagonal terms represent the mean squared error of the measurements. The off-diagonal terms represent cross-correlations of measurement error and are set to zero as in [10]. Lastly, the process noise covariance matrix, $\mathbf{Q}$, is initialized. This matrix represents errors in the model due to noise and unmodeled disturbances (e.g. gusts of wind) and its off-diagonal terms are also set to zero [10]. Essentially, the process noise covariance matrix is used to account for the fact that the lateral dynamic model is only an approximation to the true physical system and accordingly the model's predictions will tend to be imperfect.

While the initialization of covariance matrices has been presented in terms of their mathematical significance, they are used by engineers as tuning parameters [12]. At its core, a Kalman filter is an intelligent scheme for averaging the results of a model and one or more measurements in such a way as to produce the best estimate (the estimate with the lowest mean squared expected error). It accomplishes this by calculating filter gains based on, among other things, the relative magnitude of the entries in the covariance matrices. For instance, setting the values of $\mathbf{R}$ comparatively low implies that the sensors make accurate measurements. As seen in Equation 2.32, a smaller $\mathbf{R}$ in the denominator results in a larger value of $\mathbf{K}$. In the update step, Equation 2.33, this will increase the magnitude of the second term, which is the correction term based on the measured values, $\underline{\mathbf{z}}_k$. Thus setting the values of $\mathbf{R}$ low causes the Kalman filter to 'trust' the sensors more (and the model comparatively less). Although the covariance matrices are largely used as tuning parameters, there have been some published efforts to determine these matrices numerically based on acquired data [13].

First, the following parameters are initialized:

$$\underline{\hat{\mathbf{x}}}_0^- = E\langle \underline{\mathbf{x}}_0 \rangle \tag{2.25}$$

$$\mathbf{P}_0^- = E\langle \underline{\tilde{\mathbf{x}}}_i \underline{\tilde{\mathbf{x}}}_i^T \rangle \tag{2.26}$$

$$\mathbf{R} = E\langle \underline{\tilde{\mathbf{z}}}_i \underline{\tilde{\mathbf{z}}}_j^T \rangle \tag{2.27}$$

$$\mathbf{Q} = E\langle \underline{w}_i \underline{w}_j^T \rangle \tag{2.28}$$

The following time (model) update occurs at each time step (refer to the text following these equations for a discussion of Equation 2.30):

$$\underline{\hat{\mathbf{x}}}_k^- = \mathbf{A}_{k-1} \underline{\mathbf{x}}_{k-1}^+ + \mathbf{B}_{k-1} \mathbf{u}_{k-1} \tag{2.29}$$

$$\mathbf{H}_k = \begin{bmatrix} 0 & u_k & 0 \\ 0 & 1 & 0 \end{bmatrix} \tag{2.30}$$

The covariance matrix is also updated at each time step:

$$\mathbf{P}_k^- = \mathbf{A}_{k-1} \mathbf{P}_{k-1}^+ \mathbf{A}_{k-1}^T + \mathbf{Q} \tag{2.31}$$

The gain is calculated to minimize the expected variance of the estimate:

$$\mathbf{K}_k = \mathbf{P}_k^- \mathbf{H}_k^T \left(\mathbf{R} + \mathbf{H}_k \mathbf{P}_k^- \mathbf{H}_k^T \right)^{-1} \tag{2.32}$$

Using the Kalman gain and residual term, the estimate is updated:

$$\underline{\mathbf{x}}_{k-1}^{+} = \underline{\mathbf{x}}_{k}^{-} + \mathbf{K}_{k}\left(\mathbf{z}_{k} - \mathbf{H}_{k}\underline{\mathbf{x}}_{k}^{-}\right) \tag{2.33}$$

Finally, covariance propagation is calculated to be used at the next time step:

$$\mathbf{P}_{k}^{+} = \left(\mathbf{I} - \mathbf{K}_{k}\mathbf{H}_{k}\right)\mathbf{P}_{k}^{-} \tag{2.34}$$

Where:

$$\underline{\tilde{\mathbf{x}}}_{\mathbf{k}} = \underline{\hat{\mathbf{x}}}_{\mathbf{k}} - \underline{\mathbf{x}}_{\mathbf{k}} \tag{2.35}$$

$$\underline{\tilde{\mathbf{z}}}_{\mathbf{k}} = \underline{\hat{\mathbf{z}}}_{\mathbf{k}} - \underline{\mathbf{z}}_{\mathbf{k}} \tag{2.36}$$

$$\underline{\mathbf{z}}_{\mathbf{k}} = \left[a_{y}\ \dot{\Psi}\right]^{T} \tag{2.37}$$

The Kalman filter works by comparing a measured value to that predicted by a model. In this case, one of the measurement is lateral acceleration. However, lateral acceleration is not a state of the model. It is the role of the **H** matrix to map states to measurements. Lateral acceleration includes a term for pure side slip acceleration ($\dot{v}$), which is not an available model state (though it could be estimated using the continuous time **A** and **B** matrices). This is theoretically available by taking a numerical derivative of v but this will not be done due to the noise concerns imposed by a real system. Instead, the following approximation is used (reflected in Equation 2.30). This approximation has been shown to work well with real truck data, even when maneuvers exceed 0.5 g of lateral acceleration.

$$\hat{z}_{k}\left(1\right) = a_{y} = \dot{v} + u\dot{\Psi} \approx u\dot{\Psi} \tag{2.38}$$

2.5 TruckSim Validation

A scenario was devised in TruckSim to test the performance of the vehicle state and positioning estimation system. The scenario shown in Figure 2.3 was created to represent typical highway driving. It includes a double lane change as well as two gradual ninety degree curves. This scenario is two minutes long. In each of the following plots, 'Model' refers to the three-axle lateral dynamic model without the Kalman filter augmentation (or 'open-loop'), 'KF' refers to the Kalman filtered model, and 'TruckSim' represents the reference data provided by TruckSim. In this plot (as well as Figures 2.5–2.6), the 'TruckSim' line is lying directly over top of the 'KF' line for the majority of the data.

A plot of the position error (the Euclidean distance between the estimated and TruckSim-reported positions) as a function of time for both the 'open-loop' model and the Kalman filtered ('KF') model is shown in Figure 2.4. While the KF model remains within four meters of the TruckSim results, the open-loop model diverges significantly (>60m). Note that the error in the open-loop model is actually quite small until approximately one minute. At this point, error grows rapidly. The yaw angle estimate, given in Figure 2.5, begins to diverge at about this time and is the reason for the rapid accumulation of error. And of course, the source of error in yaw angle is due to an error in yaw rate (which is integrated to yield yaw angle). This is shown in Figure 2.6. Since the Kalman filter is using TruckSim-generated values of yaw rate, the agreement between the KF model and TruckSim is expected. Although not shown, lateral acceleration has similarly good agreement for the same reason.

This validation exercise shows that the KF model does a good job of predicting the position of the heavy truck when given accurate signals to feed back on. Noise was not added to the signals; the effects of using 'real' truck data (with its noise) will be explored in Section 4.4.

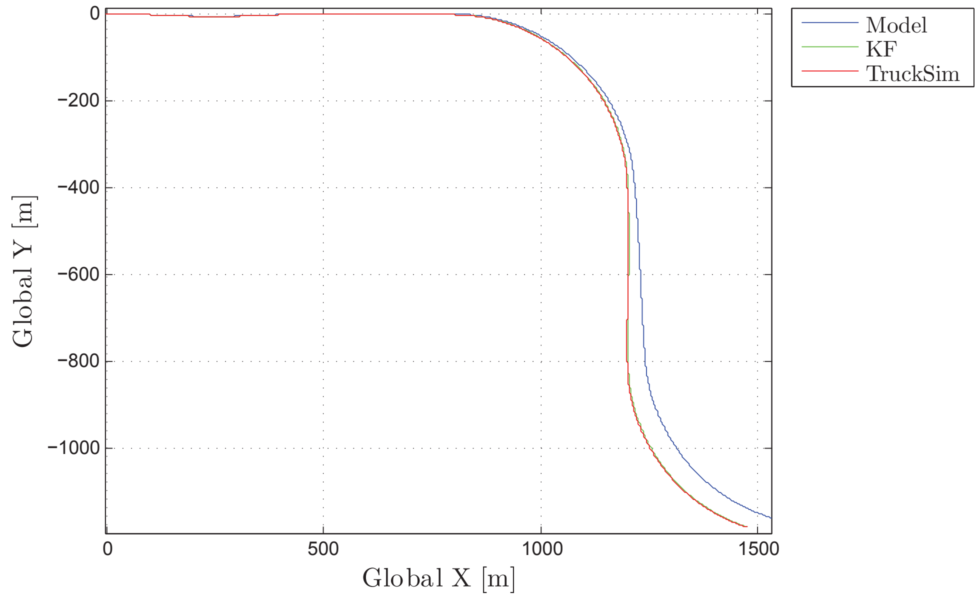

Figure 2.3: Path Prediction, Three-Axle Model

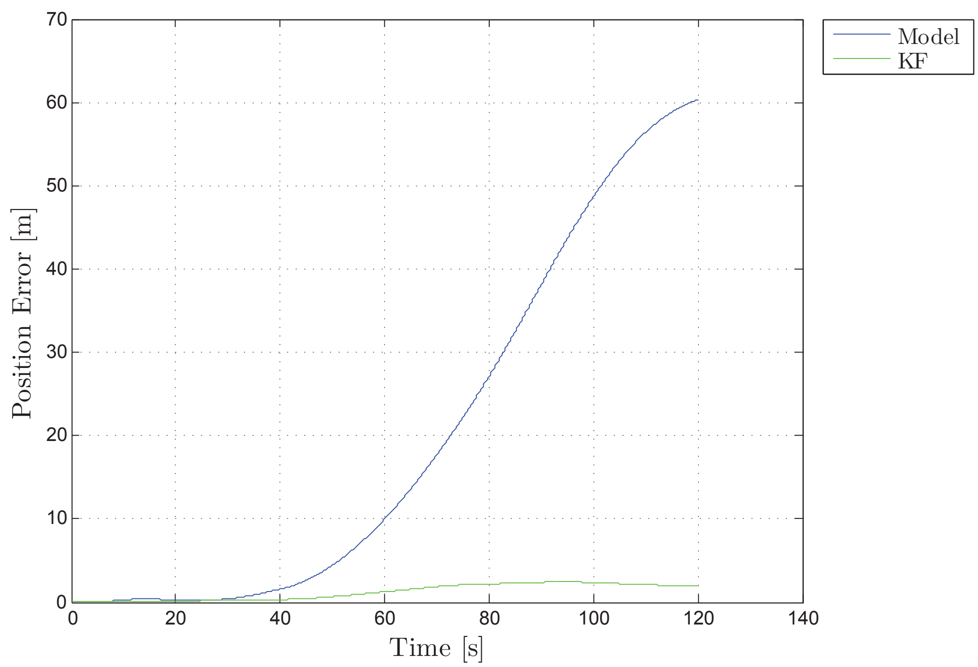

Figure 2.4: Global Position Error, Three-Axle Model

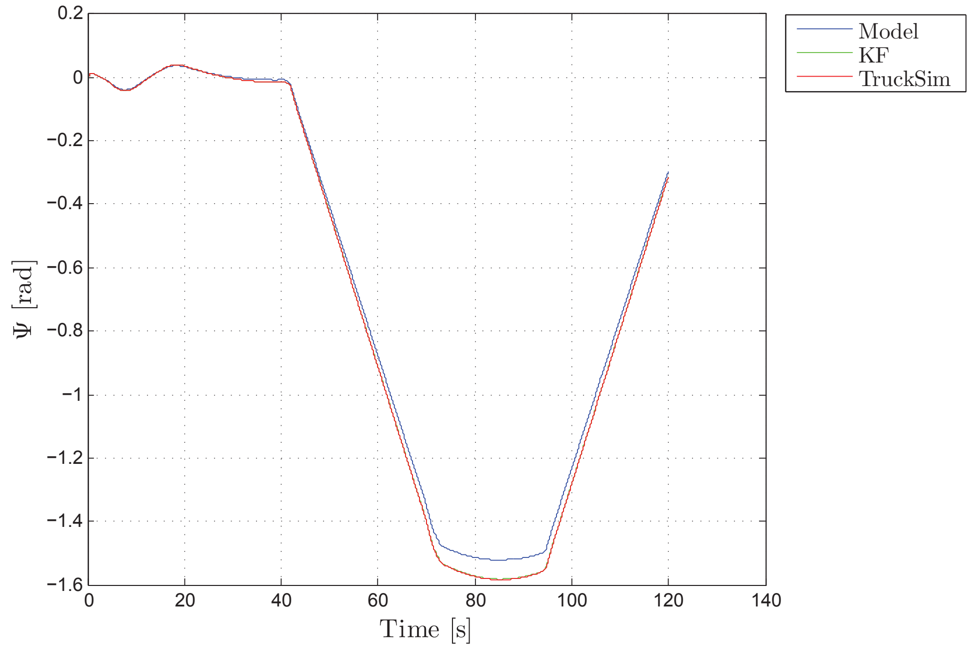

Figure 2.5: Yaw Angle, Three-Axle Model

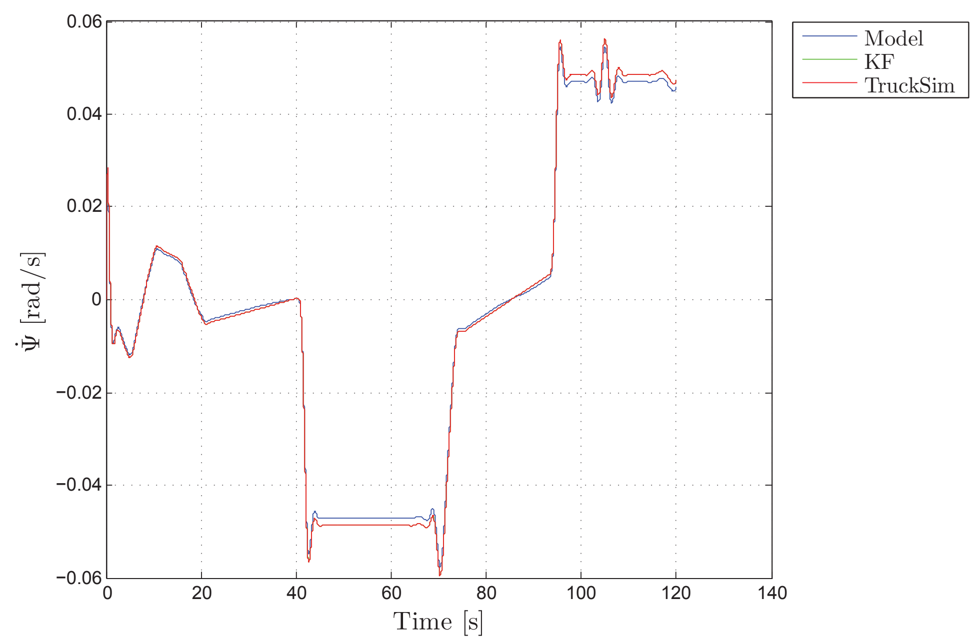

Figure 2.6: Yaw Rate, Three-Axle Model

2.6 Conclusion

This chapter has presented the development and simulation-based validation of the three-axle lateral dynamic heavy truck model. The derivation of the bicycle model has been presented from the perspective of Newtonian and Lagrangian mechanics. The details of its accompanying mathematical constructs, the Kalman filter and the RLS tire cornering stiffness estimator, have been explained. Analysis has shown that the lateral acceleration approximation of the Kalman filter works well ($a_y \approx u\dot{\Psi}$). Testing of the RLS tire cornering stiffness estimator has shown that lateral acceleration is a suitable measurement for parameter estimation. Results from TruckSim simulation have shown that the model can accurately predict the location of the heavy truck when supplied with accurate measurements. The work presented here will be extended in the next chapter to the tractor-trailer combination, or five-axle case.

Chapter References

[1] R. Rajamani, *Vehicle Dynamics and Control*. New York: Springer, 2012.

[2] W. Milliken and D. Milliken, *Race Car Vehicle Dynamics*. Warrendale, PA: SAE, 1995.

[3] R. Ervin, C. Winkler, J. Bernard, and R. Gupta, "Effects of tire properties on truck and bus handling." DOT Report UM-HSRI-76-11, June 1976.

[4] H. B. Pacejka, *Tire and Vehicle Dynamics*. Warrendale, PA: SAE, 2002.

[5] S. Rao, "Development of a Hardware in the Loop Simulation System for Heavy Truck ESC Evaluation and Trailer Parameter and State Estimation." Doctoral Dissertation, The Ohio State University, 2013.

[6] C. Lundquist and T. Schon, "Recursive identification of cornering stiffness parameters for an enhanced single track model," *Proceedings of the 15th IFAC Symposium on System Identification*, vol. 15, no. 1, 2009.

[7] C. Sierra, E. Tseng, A. Jain, and H. Peng, "Cornering stiffness estimation based on vehicle lateral dynamics," *Vehicle System Dynamics: International Journal of Vehicle Mechanics and Mobility*, vol. 44, no. 1, 2007.

[8] L. Alexander, M. Donath, M. Hennessey, V. Morellas, and C. Shankwitz, "A lateral dynamic model of a tractor–trailer: Experimental validation." MN DOT Report, Contract 73168 TOC 174, November 1996.

[9] R. E. Kalman, "A new approach to linear filtering and prediction problems," *Transactions of the ASME, Journal of Basic Engineering*, no. 82, 1960. pp. 35-45.

[10] J. Farrell, *Aided Navigation: GPS with High Rate Sensors*. New York: McGraw-Hill, 2008.

[11] A. Gelb, *Applied Optimal Estimation*. Cambridge, Mass.: The MIT Press, 1974.

[12] R. Plessis, *Poor Man's Explanation of Kalman Filtering or How I Stopped Worrying and Learned to Love Matrix Inversion*. Monterey, Cali.: Taygeta Scientific, 1967.

[13] M. Rajamani and J. Rawlings, "Estimation of the disturbance structure from data using semidefinite programming and optimal weighting," *Texas-Wisconsin Modeling and Control Consortium*, no. 2007-02, 2007.

CHAPTER 3

FIVE-AXLE LATERAL DYNAMIC ARTICULATED HEAVY TRUCK MODEL

3.1 Introduction

This chapter describes the development of the five-axle lateral dynamic model of the articulated heavy truck. The term 'five-axle' refers to the front steer axle, tandem rear truck axles, and tandem trailer axles.

First, the structure of this model (i.e. its states and parameters) and its derivation are presented along with the assumptions and approximations employed therein. Owing to the complexity of this system, the derivation is based entirely on Lagrange's Equation. Virtual work expressions are explained and an example is given. The effects of various assumptions embedded in the Lagrangian are examined. The coupled differential equations of motion produced by Lagrange's Equation are converted to a continuous-time state space representation using MATLAB®. MATLAB® is then used to discretize the system. Next, the extension of the cornering stiffness estimation scheme and Kalman filter from the three- to five-axle case are presented. Finally, the model is validated using TruckSim as a reference.

3.2 Derivation

A quasi-linear five-axle model for the articulated heavy truck was derived using Lagrange's equation (Equation 2.2). The model is not completely linear because the mass and stiffness matrices of the model, $\mathbf{M}$ and $\mathbf{K}$, include terms for the cosine of hitch angle. Additionally, the stiffness and forcing matrices, $\mathbf{K}$ and $\mathbf{F}$, include terms for the cosine of road wheel steer angle. As in Section 2.2, forward velocity, u, is treated as a constant parameter instead of a state variable. Accordingly, the model matrices are recomputed at each time step. A sketch of the model with states, lateral tire forces, and parameters can be seen in Figure 3.1. The states of the model are listed below. Since the position estimator is intended to provide localization under normal driving conditions, a simple linear tire model is used. It is expected that in practice the lateral acceleration of the truck will rarely exceed 0.3 g.

v : lateral velocity of tractor CG

$\dot{\Psi}$: yaw rate of tractor

Ψ : yaw angle of tractor

$\dot{\gamma}$: hitch rate

γ : hitch angle

Equation 3.1 shows the Lagrangian for the five-axle model. Note that the first two terms, corresponding to tractor energy, are the same as Equation 2.3 and the following two, corresponding to trailer energy, are of similar form. The generalized coordinates are lateral position, y, yaw angle, Ψ, and hitch angle, γ. Again, potential energy is zero. Equations 3.2–3.4 contain the details of the trailer velocity terms. A comparison of results based on the treatment of Equation 3.3 can be found in Section 3.2.2. Diagrams detailing slip angles and equations for the calculation of tire forces can be found in Appendix A.1.

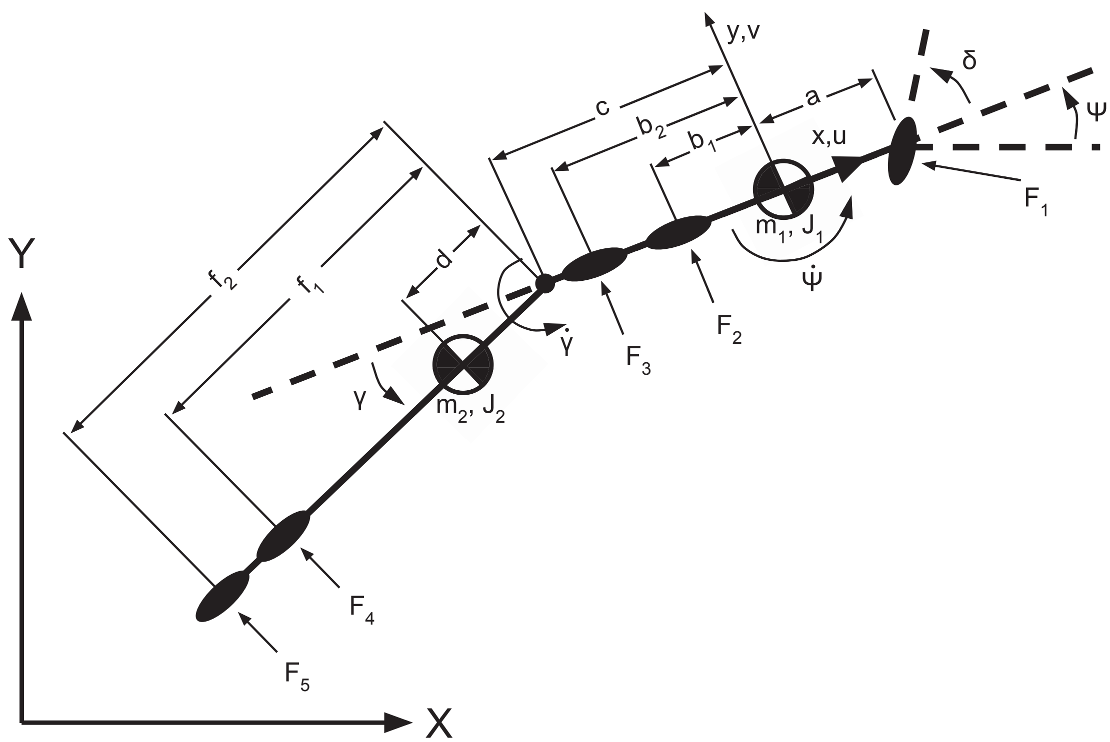

Figure 3.1: Five-Axle Articulated Bicycle Model

Thus:

$$L = T - V = \frac{1}{2}m_1(u^2 + v^2) + \frac{1}{2}J_1\dot{\Psi}^2 + \frac{1}{2}m_2(u_{trailer}^2 + v_{trailer}^2) + \frac{1}{2}J_2\omega_2^2 \tag{3.1}$$

Where:

$$\omega_2 = \dot{\Psi} + \dot{\gamma} \tag{3.2}$$

This equation states that the total angular velocity of the trailer is equal to the sum of the tractor angular velocity and the angular velocity of the hitch coupling.

$$u_{trailer} = u + d\sin\gamma\left(\dot{\Psi} + \dot{\gamma}\right) \approx u \tag{3.3}$$

This equation states that the forward velocity of the trailer CG (in the tractor's local frame) is equal to the tractor forward velocity plus some terms which can be neglected as being comparatively small. These terms arise when the truck is not straight ($\sin\gamma \neq 0$) and the trailer is yawing ($\omega_2 \neq 0$), but these are both small numbers compared to u.

$$v_{trailer} = v - (c + d\cos\gamma)\,\dot{\Psi} - d\cos\gamma\dot{\gamma} \tag{3.4}$$

This equation states that the side-slip velocity of the trailer CG (in the tractor's local frame) is equal to the tractor side-slip velocity plus some other terms multiplied by the tractor yaw rate and the hitch rate. Unlike Equation 3.3, these other terms cannot be neglected. In this case, the angular rates are being multiplied by $\cos\gamma$, which is generally very close to unity.

Evaluating Equation 2.2 using the Lagrangian from Equation 3.1 results in three (one for each generalized coordinate) coupled differential equations which can be expressed as $\mathbf{M}\underline{\dot{\mathbf{x}}}$. These are the inertial terms; the left-hand side of Equation 2.12. Though several derivations were carried through by hand, these calculations are somewhat involved and most were computed by a MATLAB® program. Products of states were ignored (treated as zeros) in most derivations. This is a common assumption in vehicle dynamics modeling, see e.g. [1]. The effect of ignoring products of states will be examined in Section 3.2.2.

Evaluation of the virtual work terms, explained in Section 3.2.1, results in coupled stiffness and forcing terms of which can be expressed as $\mathbf{K}\underline{\mathbf{x}}+\mathbf{F}\mathbf{u}$ (the right-hand side of Equation 2.12). The three differential equations were augmented with integrators for yaw angle and hitch angle in order to track these states.

At this point in the derivation, the parameters of the matrices are replaced with numerical values. MATLAB® can then be used to convert the model to state space format by multiplying each side by $\mathbf{M}^{-1}$ as was done for the three-axle model. The system is then transformed to a discrete time representation (see Equation 2.14).

Parametric values for the $\mathbf{M}$, $\mathbf{K}$, and $\mathbf{F}$ matrices; $\underline{\mathbf{x}}$ and $\dot{\underline{\mathbf{x}}}$ vectors; and control input can be found in Appendix A.2.

3.2.1 Virtual Work Expressions

To formulate the right-hand side of Equation 2.12, the virtual work expressions, Q_{q_i}, must be calculated for $q_i = y$, $q_i = \Psi$, and $q_i = \gamma$. These represent the work done on the system by external forces. They are calculated graphically as follows. First, the system is drawn in an arbitrary state. Next, the system is drawn as if it had been displaced by the virtual displacement δq_i while holding *all other coordinates fixed*. Then, the sum of virtual work is expressed as in Equation 3.5. The virtual work expression is calculated by dividing the sum of virtual work by the virtual displacement as shown in Equation 3.6. These virtual work expressions are also known as *generalized forces*, owing to the fact that they are force (or moment) terms corresponding to generalized coordinates.

$$W_{q_i} = \sum F\left(\delta q_i\right) \tag{3.5}$$

$$Q_{q_i} = \frac{W_{q_i}}{\delta q_i} \tag{3.6}$$

A specific example is provided for the case of $q_i = \Psi$ in this section. Figure 3.2 shows the virtual displacement of the system by the generalized coordinate Ψ. The sum of the virtual work, W_Ψ, is expressed in Equation 3.7. Note that the terms are of the dimension $F \cdot L$ multiplied by $\delta\Psi$. This is torque multiplied by angular displacement, which has units of work (energy). The resulting virtual work expression, Q_Ψ, is shown in Equation 3.8. Even though Q_Ψ represents a torque (i.e., its terms are of the dimensions $F \cdot L$), the appropriate expression is obtained through the general method. This is because the moment arms are properly accounted for through the displacement terms in Equation 3.7. Virtual displacement diagrams and virtual work expressions for the other two coordinates are presented in Appendix A.1.

The virtual work is:

$$W_\Psi = a\cos\delta F_1\delta\Psi - b_1 F_2\delta\Psi - b_2 F_3\delta\Psi - (c\cos\gamma + f_1) F_4\delta\Psi - (c\cos\gamma + f_2) F_5\delta\Psi \tag{3.7}$$

Dividing by $\delta\Psi$ yields the virtual work expression:

$$Q_\Psi = \frac{W_\Psi}{\delta\Psi} = a\cos\delta F_1 - b_1 F_2 - b_2 F_3 - (c\cos\gamma + f_1) F_4 - (c\cos\gamma + f_2) F_5 \tag{3.8}$$

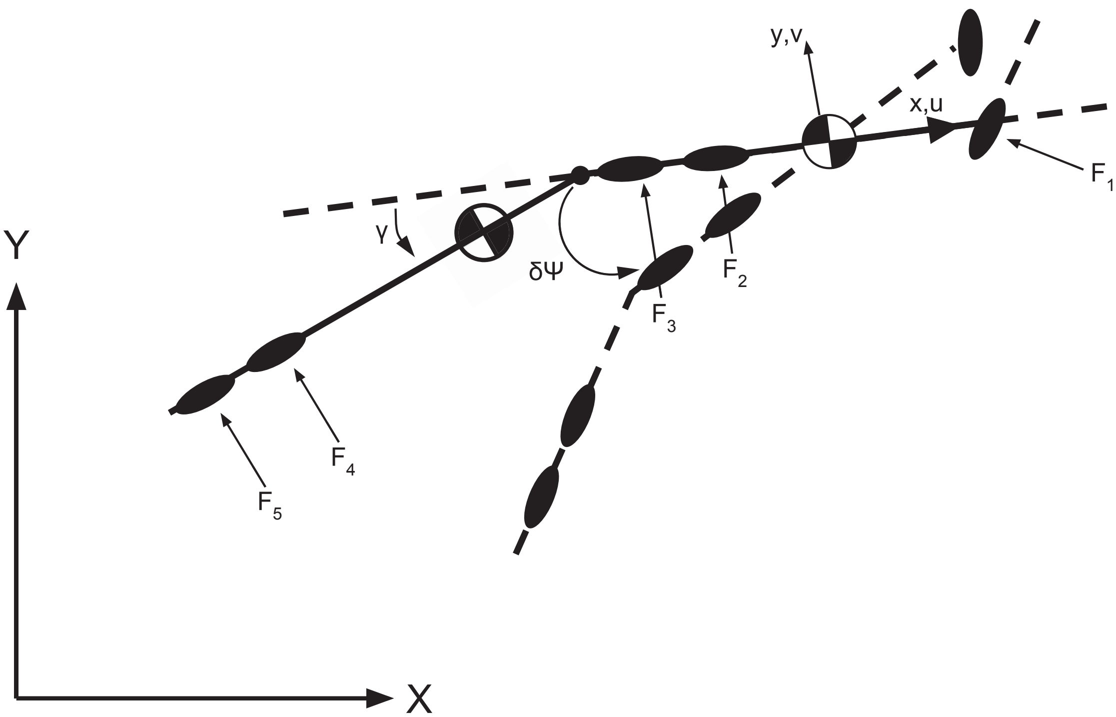

Figure 3.2: Virtual Displacement by $\delta\Psi$

3.2.2 Comparison of Derivations

The model behaves differently when various assumptions are used for Equations 3.3-3.4. In all cases, the Kalman filter is 'strong' enough to produce good positioning results if it has good signals available to it (for yaw rate in particular) and appropriately tuned covariance matrices ($\mathbf{Q}$, $\mathbf{R}$). However, some model revisions tend to produce poor estimates of lateral velocity, hitch rate, and hitch angle (depending on the maneuver, they may also produce good results – but they did not produce good results for all maneuvers studied).

In each of the following plots, 'Model' refers to the five-axle model without the Kalman filter augmentation ('open-loop'), 'KF' refers to the Kalman filtered model that feeds back on TruckSim signals, and 'TruckSim' represents the reference data provided by TruckSim. For hitch rates and angles, 'KinHat' and 'KinGPS' legend entries refer to computation of the hitch rate via Equation 3.12 and numerical integration to yield hitch angle. The difference between 'KinHat' and 'KinGPS' is that in the 'Hat' case, values for u, v, and $\dot{\Psi}$ are taken from the Kalman filtered model whereas in the 'GPS' case they are taken from TruckSim data (equivalent to a perfect dual GPS).

Figure 3.3 shows the global position estimates produced during a two-minute highway driving scenario using Revision 3 of the model. Although the open-loop model does not track the path well, the Kalman filtered model follows the path closely due to the clean, accurate yaw rate signal from TruckSim. Figure 3.4 shows the hitch angle estimates from Revision 3. The open-loop model shows incorrect polarity (sign) and a very small amplitude relative to the TruckSim results. The Kalman filter attempts to correct the magnitude by increasing it, but the sign is still wrong. Figure 3.5 shows the hitch rate estimates produced by Revision 3. Similar to the hitch angle, the sign of hitch angle is wrong and its amplitude too low for the open-loop model. This plot also shows one of the peculiarities of the Kalman filter. At $t \approx 60$ s, the hitch rate estimated by the Kalman filter model is nonzero, even though the estimated hitch angle is not changing. This is because the Kalman filter can independently adjust its estimate of each state (and therefore it is not as simple as $\gamma_{k+1} = \gamma_k + \dot{\gamma}_k T_s$).

These plots should be contrasted with those in Section 3.5.1 where results from Revision 4 are presented. Table 3.1 summarizes the results of a number of different model revisions containing different implicit assumptions. Revision 3 may be considered representative of those models with 'No' in the last column while Revision 4 may be considered representative of those with 'Yes' in the last column.

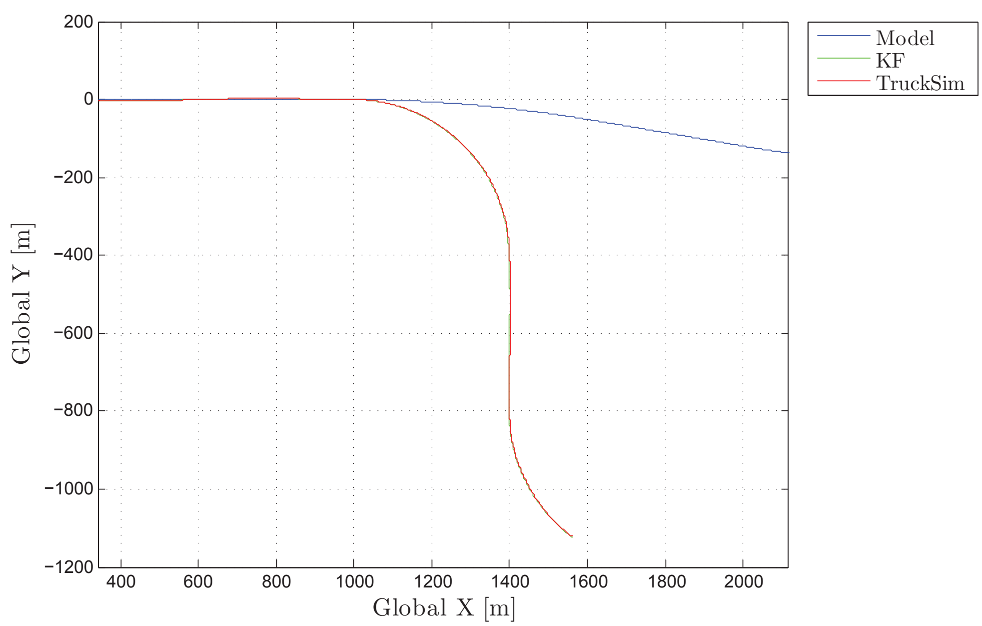

Figure 3.3: Highway Scenario Path Prediction, Five-Axle Model Revision 3

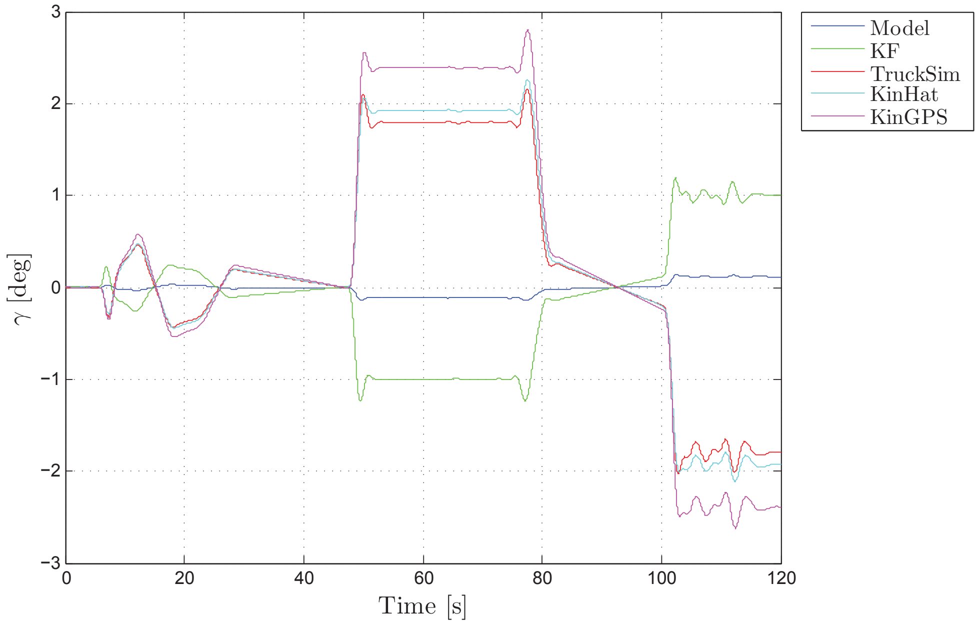

Figure 3.4: Highway Scenario Hitch Angle, Five-Axle Model Revision 3

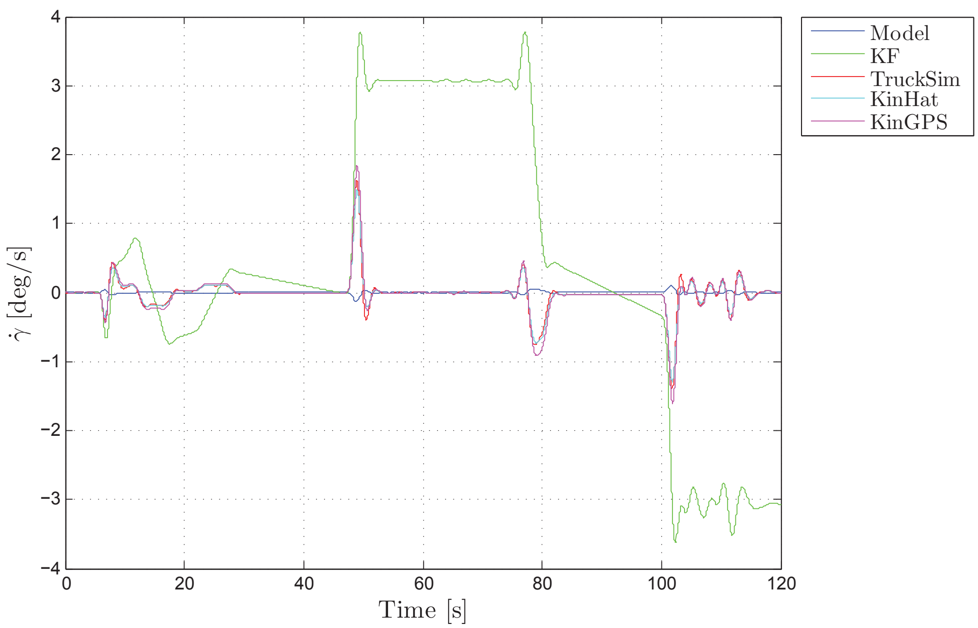

Figure 3.5: Highway Scenario Hitch Rate, Five-Axle Model Revision 3

Table 3.1: Effects of Various Assumptions on Model Performance

Rev	cos(γ)	sin(γ)	$u_{trailer}$ = $u_{tractor}$?	Predicts γ well?
3	cos(γ)	sin(γ)	No.	No.
4	1	0	Yes.	Yes.
5	cos(γ)	sin(γ)	No.	No.
6	cos(γ)	0	Yes.	Yes.
7	1	γ	No.	No.
8	cos(γ)	γ	No.	No.

Note that the models which work well, Revisions 4 and 6, both approximate trailer longitudinal velocity to be the same as tractor longitudinal velocity ($u_{tractor} = u_{trailer} \leftrightarrow \sin\gamma = 0$). This is believed to occur because of unmodeled longitudinal dynamics acting as a noise input to the system. In the three-axle case, u only appears in the mass matrix, $\mathbf{M}$, due to the $u\dot{\Psi}$ term of lateral acceleration. (Of course, u appears in the stiffness matrix of both systems due to slip angle relationships.) Similarly, if $u_{trailer} \approx u_{tractor}$, then u only appears in the five-axle model's mass matrix as a $u\dot{\Psi}$ term (i.e., in the third column). However, if $u_{trailer} \neq u_{tractor}$, u also appears in the mass matrix multiplied by $\dot{\gamma}$, i.e. in the fifth column (cf. $\mathbf{M}_3$ and $\mathbf{M}_4$ in Appendix A.2).

When tested with TruckSim data, model Revisions 4 and 6 both worked equally well (refer to Section 3.5). Accordingly, both were used for the field testing validation shown in Chapter 4. The results in this case were again nearly identical, which should be expected as the cosine of hitch angle is very close to unity most of the time. However, Revision 4 predicted hitch angle slightly better for high articulation angles (approximately 30 degrees). It is counterintuitive that Revision 4 (which simplifies cosine of hitch angle to unity) would outperform Revision 6 (which uses its estimate of hitch angle and calculates its cosine) at high articulation angles, but it is worth remembering that these are both very simple models of a very complex system. Perhaps, then, the detail omitted by Revision 4 is offset by another unmodeled error source.

How close is $u_{trailer}$ to $u_{tractor}$? Figure 3.6 shows three velocities for the highway driving scenario: 'Model,' the tractor velocity as estimated by averaging wheel speeds (tractor only) reported by TruckSim; 'TruckSim,' the longitudinal velocity of the tractor CG as reported by TruckSim; and 'Trailer,' the velocity of the trailer in the direction of the tractor's heading as calculated by Equation 3.3 using TruckSim signals. At this scale, the signals are indistinguishably similar. Figure 3.7 shows the same plot with a much smaller scale, which indicates that the velocities are close (within 0.03 m/s) for the duration of the maneuver.

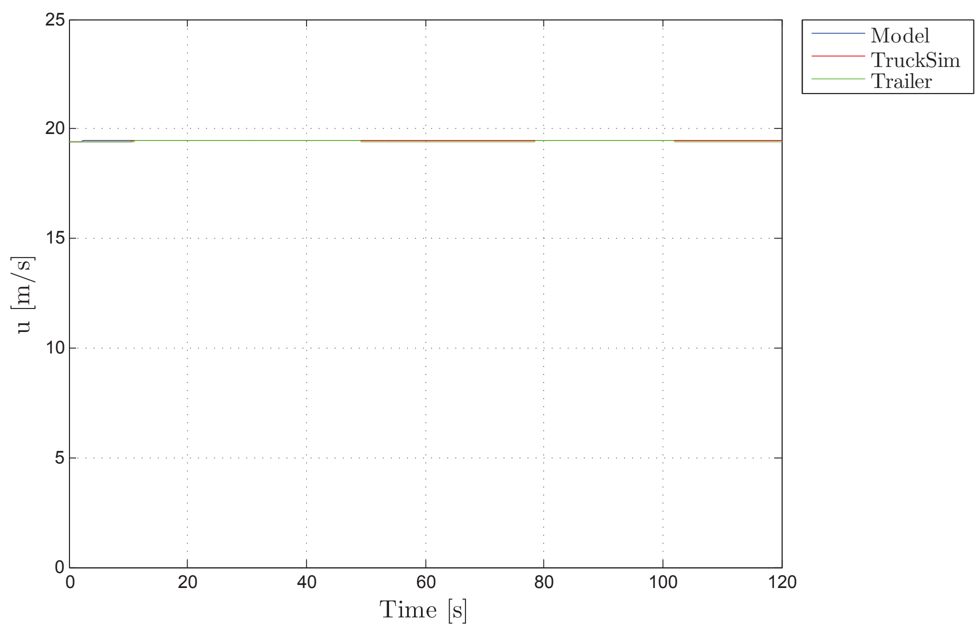

Figure 3.6: Longitudinal Velocities for Highway Driving Case

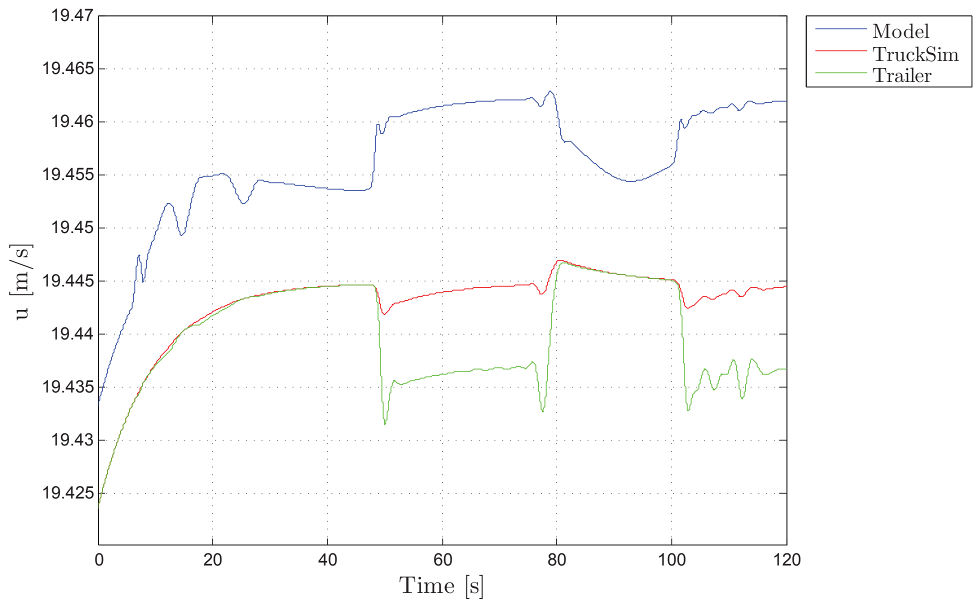

Figure 3.7: Longitudinal Velocities for Highway Driving Case (scale smaller)

In Table 3.1, the difference between Revisions 3 and 5 is not apparent. The differential equations of motion were calculated using the same Lagrangian and were derived both by hand and using MATLAB®. Revision 3 treats $\cos\gamma$ as a constant parameter (like u) to be updated in the mass matrix at each time step. Revision 5, on the other hand, uses closed-form operating point linearization via the Jacobian (carried out via MATLAB®). This model does not neglect products of states. For background on this form of linearization, refer to [2] or [3].

Revision 5 was calculated in the following manner: starting with the differential equations of motion, MATLAB® was used to algebraically manipulate the system into the form $\dot{\underline{\mathbf{x}}} = f\left(\underline{\mathbf{x}}, \mathbf{u}, u\right)$, i.e. explicitly in terms of $\dot{\underline{\mathbf{x}}}$ (this is equivalent to $\mathbf{M} = \mathbf{I}$). The resulting functions were used to calculate the Jacobian, which was decomposed into two parts so that the system could be expressed in the form of Equation 2.13, i.e. state space form. The resulting $\mathbf{A}$ matrix was very complex, with some entries containing hundreds of terms. This is not thought to be a tractable solution for real-time implementation, but instead was used as a validity check for the quasi-linearization accomplished in Revision 3 by placing terms such as $\cos\gamma$ inside the **M** and **K** matrices.

The continuous-time **A** matrices of Revisions 3 and 5 were compared. During a simulation run, the (numerical) **A** matrices and eigenvalues of both models were saved for comparison. Equations 3.9 and 3.10 show the **A** matrices and eigenvalues of model Revisions 3 and 5 respectively. These values are taken from the highway driving case examined in Sections 2.5 and 3.5.1. Note the extremely close agreement, suggesting that the quasi-linearization technique is valid and that products of states are inconsequential.

$$\mathbf{A}_3 = \begin{bmatrix} -3.3416 & -30.2102 & 0 & -16.5485 & -7.3492 \\ -0.0740 & -15.9041 & 0 & -9.9695 & 2.9290 \\ 0 & 1 & 0 & 0 & 0 \\ 0.2557 & 14.3187 & 0 & 5.1522 & -15.0846 \\ 0 & 0 & 0 & 1 & 0 \end{bmatrix}, \lambda_3 = \begin{bmatrix} 0 \\ -3.7283 + 6.1068i \\ -3.7283 - 6.1068i \\ -3.3185 + 1.4577i \\ -3.3185 - 1.4577i \end{bmatrix} \quad (3.9)$$

$$\mathbf{A}_5 = \begin{bmatrix} -3.3416 & -30.2102 & 0 & -16.5485 & -7.3492 \\ -0.0740 & -15.9041 & 0 & -9.9695 & 2.9289 \\ 0 & 1 & 0 & 0 & 0 \\ 0.2557 & 14.3187 & 0 & 5.1522 & -15.0846 \\ 0 & 0 & 0 & 1 & 0 \end{bmatrix}, \lambda_5 = \begin{bmatrix} 0 \\ -3.7283 + 6.1068i \\ -3.7283 - 6.1068i \\ -3.3185 + 1.4577i \\ -3.3185 - 1.4577i \end{bmatrix} \quad (3.10)$$

3.2.3 Kinematic Hitch Rate

As listed in Section 3.2, hitch angle (γ) is a state of the five-axle model. Accordingly, the dynamic model naturally produces an estimate of hitch angle while running. However, this dynamic model requires knowledge of a large number of vehicle parameters (e.g. trailer inertia). For this reason, a simple kinematic model was investigated.

The kinematic model was derived based on the assumption that the trailer wheels do not side slip, a common assumption for low-speed turning [4]. This is, of course, not true in practice. Side slip is necessary to produce lateral force, but side slip velocity is small in comparison to the orthogonal 'forward' component of velocity [4]. In order for the trailer to be able to turn, the instant center of the trailer is located between its wheels. In this case there are two rear axles, so the instant center is located in between them (point F) to minimize side slip. A kinematic diagram of the trailer is shown in Figure 3.8.

If the velocity of the hitch point and a few other parameters are known, the hitch rate can be calculated. The hitch point velocities are shown in green. Rotating these velocities by the angle γ results in the velocities shown in blue. The relationship between the velocity of point F and the hitch point is shown in Equation 3.11 [5]. Substitution of the relevant velocities and parameters yields Equation 3.12. This hitch rate is numerically integrated to estimate hitch angle. Since hitch angle appears in Equation 3.12, this estimation process should begin at a time when hitch angle can be assumed zero, such as straight driving.

Side slip velocity cannot be measured with a single GPS. A single GPS can only provide the vector sum of side slip and longitudinal velocity (or 'total' velocity). However, the five-axle model can provide an estimate. The effects of using estimated and 'known' velocities will be shown in Section 3.5. Also note that the parameters c and L_f are subject to adjustment by the user, as the kingpin and rear axle locations can be moved. Refer to Figure 3.1 for a sketch of the model with parameters.

$$\vec{v}_H = \vec{v}_F + \vec{r}_{H/F} \times \omega \tag{3.11}$$

$$\dot{\gamma} = \frac{\left(v - c\dot{\Psi}\right)\cos\gamma - u\sin\gamma}{L_f} - \dot{\Psi} \tag{3.12}$$

Some previous work has been done to estimate articulation angle, but this has

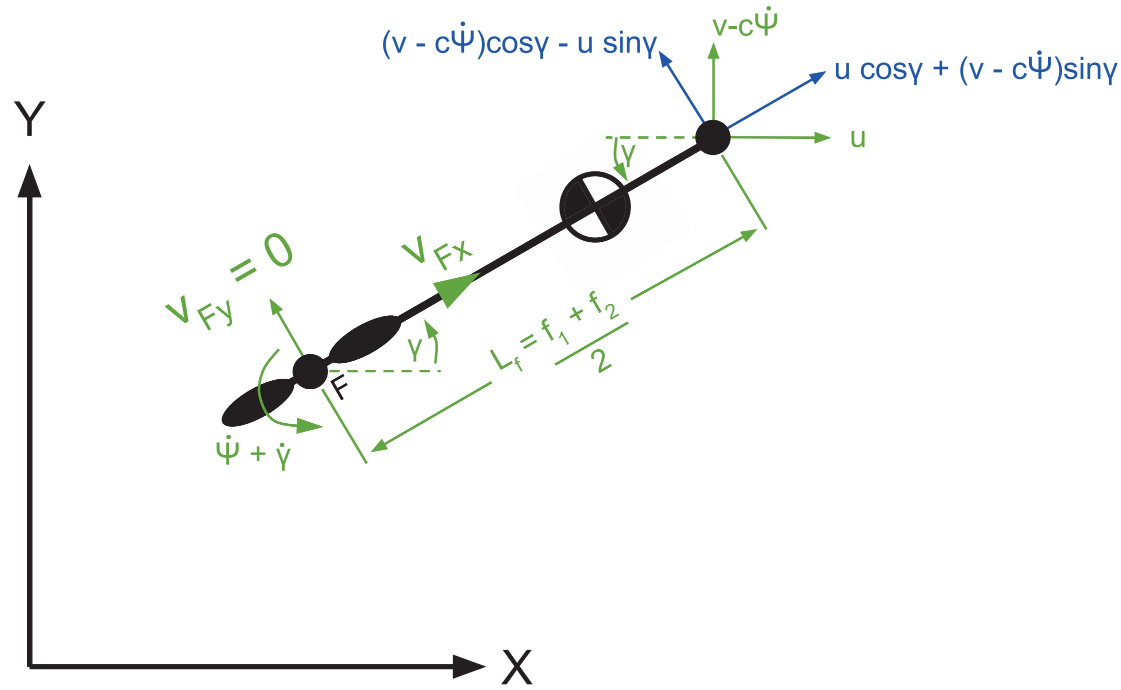

Figure 3.8: Diagram for Kinematic Determination of Hitch Rate

primarily been concerned with jackknife detection and prevention. Chu et al. designed an estimator based on a state observer, but this study had several limitations. It required lateral velocity as a measured signal, was not very accurate at high hitch angles (ca. ± 2 deg at $\gamma = 10$ deg), and was only tested against a 21-DOF simulation (no physical validation) [6]. Dunn created a model to detect jackknifing under heavy braking, but this required measuring longitudinal slip ratio and had similar accuracy issues at higher hitch angles [7]. Zhou et al. also described prediction of hitch angle based on a state space model in a paper regarding jackknife prevention. However, no results of hitch angle prediction were shown, no physical validation was carried out, and the system required a yaw rate sensor on the trailer [8].

3.3 Tire Cornering Stiffness Estimator

The cornering stiffness estimation scheme detailed in Section 2.3 was modified for the five-axle case. Equations 2.17–2.19 were used without modification. However, some of the quantities in the equations themselves changed. Since there are five axles, ϕ now contains five lumped axle cornering stiffnesses. In the three-axle case, both lateral acceleration and yaw acceleration were investigated as measurements ($y_1 = a_y$, $y_2 = \ddot{\Psi}$). Based on the results of the three-axle case and the availability of sensors, only lateral acceleration was investigated as a measurement for the five-axle cornering stiffness estimator ($y = a_y$).

However, the treatment of this measurement was not so simple due to the coupling of the system. In the three-axle case, the first equation of the model can be stated as "the sum of the lateral tire forces is equal to the tractor's mass multiplied by its lateral acceleration." This made it very simple to separate the equation in terms of the lateral acceleration measured, known mass, estimated slip angles, and cornering stiffnesses to be estimated. In the five-axle case, the same equation would be stated as "the sum of lateral tire forces is equal to the sum of tractor and trailer mass multiplied by lateral acceleration plus coupling terms multiplied by yaw acceleration and hitch acceleration." These coupling terms complicated the matter and were treated in several different ways. In the first case, these terms were neglected entirely ($y_1 = a_y$). In the second case, the transient terms were estimated based on the continuous time state space model and the measurement was augmented by this value ($y_2 = a_y + \hat{t}_1 + \hat{t}_2$). In the final case, the transient terms were calculated using TruckSim values ($y_3 = a_y + t_1 + t_2$). Though this is not feasible in practice, it provided a benchmark by which y_1 and y_2 were measured. Equation 3.13 shows the measurement term while Equations 3.14 and 3.15 give the exact form of the transient coupling terms. Equation 3.16 lists the quantity to be estimated, i.e. the vector of cornering stiffnesses and Equation 3.17 gives the vector that maps ϕ to lateral forces, i.e. slip angle estimates.

$$y = a_y + t_1 + t_2 = \frac{1}{m_1 + m_2} X\phi \tag{3.13}$$

$$t_1 = \frac{-m_2\ddot{\Psi}\left(c + d\cos\gamma\right)}{m_1 + m_2} \tag{3.14}$$

$$t_2 = \frac{-m_2\ddot{\gamma}d\cos\gamma}{m_1 + m_2} \tag{3.15}$$

$$\phi = \begin{pmatrix} C_{\alpha 1} \\ C_{\alpha 2} \\ C_{\alpha 3} \\ C_{\alpha 4} \\ C_{\alpha 5} \end{pmatrix} \tag{3.16}$$

$$\begin{aligned} X = \Bigg[& \left(\delta\cos(\delta) - \cos(\delta)\frac{v + a\dot{\Psi}}{u}\right) \qquad \frac{-v + b_1\dot{\Psi}}{u} \qquad \frac{-v + b_2\dot{\Psi}}{u} \\ & \frac{-\cos\gamma v + \cos\gamma\left(c + f_1\cos\gamma\right)\dot{\Psi} + \cos^2\gamma f_1\dot{\gamma}}{u} + \gamma\cos\gamma \\ & \frac{-\cos\gamma v + \cos\gamma\left(c + f_2\cos\gamma\right)\dot{\Psi} + \cos^2\gamma f_2\dot{\gamma}}{u} + \gamma\cos\gamma \Bigg] \end{aligned} \tag{3.17}$$

Figure 3.9 shows the three measurements y_1, y_2, and y_3 and Figure 3.10 shows the corresponding cornering stiffness estimates during a ramp and hold maneuver. This entails quickly ramping the steering to the value required to generate approximately 0.2 g and holding it there while maintaining constant forward speed. The ramp and hold maneuver was found to be the most suitable for cornering stiffness estimation. This was believed to be because constant lateral acceleration provided a strong signal to the estimator while the quasi-steady nature caused Equations 3.14 and 3.15 to go to zero. This suggests that in practice constant radius turns such as highway exit ramps may provide suitable excitation for the cornering stiffness estimator.

In steady state, y_1 tracked y_3 (the 'truth' value) better than y_2. However, using y_2, the measurement that included estimates of the dynamic coupling terms of Equations 3.14 and 3.15, produced better estimates of tire cornering stiffness (refer to Figure 3.10). For example, consider $C_{\alpha 1}$ and $C_{\alpha 5}$. The estimates generated using y_1 (appended by (1)) are vastly different (about an order of magnitude) while those generated by y_2 (appended by (2)) are less than a factor of two different, suggesting the estimates produced by y_2 are more physically reasonable. In simulation, using estimates produced by y_2 was found to work better than using estimates produced by y_1.

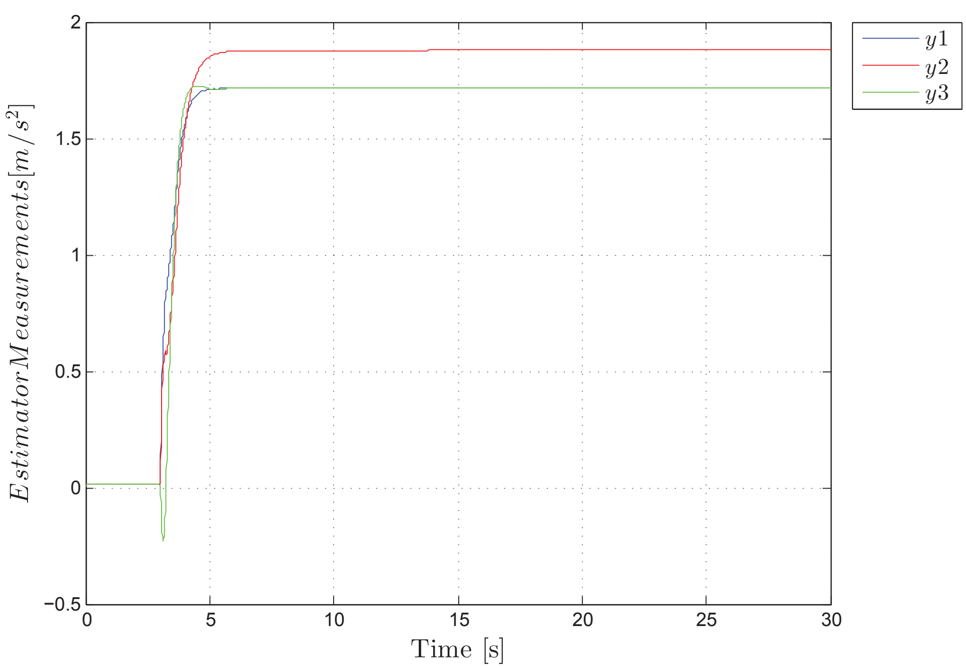

Figure 3.9: Measurements for Tire Cornering Stiffness Estimation, Five-Axle Model

We now take note of the fact that this represents a new contribution to the field of tire cornering stiffness estimation. Previous researchers have created methods to

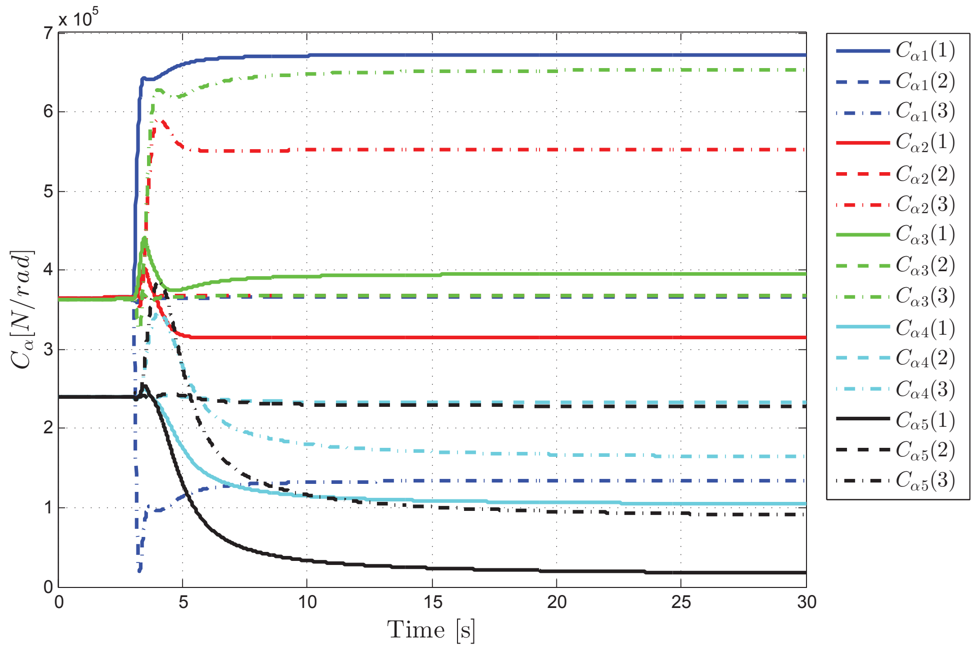

Figure 3.10: Cornering Stiffness Estimate, Five-Axle Model.
[(1): $y = y_1$, (2): $y = y_2$, (3): $y = y_3$]

estimate the tire cornering stiffnesses ('effective axle cornering stiffnesses' in Pacejka's terminology) of passenger cars under a variety of assumptions. Anderson et al. developed a method to estimate the cornering stiffness of passenger car tires based on a Kalman filter using dual GPS and a yaw rate gyro as measurements [9]. However, dual GPS is not typically available. Sienel produced an estimation scheme that requires only lateral acceleration and yaw rate, but involves numerically calculating time derivatives of steer angle (steer rate) and lateral acceleration (jerk) and thus the signals must be filtered [10]. Wesemeier et al. developed a model that calculates static gains of the bicycle model, i.e. the input-output relationships that lateral acceleration and yaw rate have with steer angle at a given steady trim. The advantage of Wesemeier's approach is that cornering stiffness can be estimated without knowing the vehicle's moment of inertia [11]. Baffet et al. created an observer model that calculates tire cornering stiffnesses based only on the following extant signals: yaw rate, lateral acceleration, steer angle, and wheel angular velocities [12]. You et al. described a model that identifies cornering stiffness based on extant signals and also produces an estimate of road bank angle [13].

However, comparatively little work has been done to identify cornering stiffnesses of trailer tires. Alexander et al. calculated trailer tire cornering stiffness by identifying the transfer function coefficients relating steer angle to yaw rate at various constant speeds (an off-line estimation method) [14]. Though the mathematics are unclear, it seems that the researchers have considered only two effective axle cornering stiffnesses – that of the steer axle and that of all other axles (rear tractor tandem and trailer tandem), since the results are organized in this fashion and equal among the non-steered axles. This is in contrast to other research which might lump tandem axles (e.g. both trailer axles) but not all non-steered axles, presumably due to the wide variations in normal force possible in practice [7]. Hac et al. estimated trailer tire cornering stiffness using measurement of trailer lateral acceleration and yaw rate, which are are not commonly available. This was done off-line with a least squares method [15].

3.4 Kalman Filter

In contrast with the cornering stiffness estimator, very little modification was necessary to extend the three-axle Kalman filter to the five-axle case. Equations 2.25–2.34 were used directly, though the terms in the equations were modified, e.g. $\mathbf{Q}$ became a 5×5 matrix instead of a 3×3. The five-axle Kalman filter utilizes the same measurements: lateral acceleration and tractor yaw rate. The same approximation of lateral acceleration was used, i.e. $a_y \approx u\dot{\Psi}$, and this results in the $\mathbf{H}$ matrix shown in Equation 3.18.

$$\mathbf{H}_k = \begin{bmatrix} 0 & u_k & 0 & 0 & 0 \\ 0 & 1 & 0 & 0 & 0 \end{bmatrix} \tag{3.18}$$

3.5 TruckSim Validation

The model presented in this chapter was tested with TruckSim and the various tuning parameters (e.g. $\mathbf{R}$) were adjusted to provide good results. Model Revisions 4 and 6 provided nearly identical results, and only the results from Revision 4 are presented here. Both Revisions 4 and 6 will be investigated in Chapter 4 to determine if either has an advantage when using field data. In each of the following plots, 'Model' refers to the five-axle model without the Kalman filter augmentation, 'KF' refers to the Kalman filtered model, and 'TruckSim' represents the reference data provided by TruckSim. For hitch rates and angles, 'KinHat' and 'KinGPS' legend entries refer to computation of the hitch rate via Equation 3.12 and numerical integration to yield hitch angle. The difference between 'KinHat' and 'KinGPS' is that in the 'Hat' case, values for u, v, and $\dot{\Psi}$ are taken from the Kalman filtered model whereas in the 'GPS' case they are taken from TruckSim data (equivalent to a perfect dual GPS). In general, the difference is slight and suggests that perhaps the kinematic solution can be used without dual GPS. In neither case is a TruckSim signal for γ provided.

3.5.1 Highway Driving Scenario

First, the scenario from Section 2.5 was simulated for the five-axle case using the cornering stiffness estimate shown in Figure 3.10. The path prediction of this model is shown in Figure 3.11 and the RMS position error as a function of time is shown in

Figure 3.12. Figure 3.13 shows the roadwheel steering input. The forward velocity was given earlier in Figure 3.6.

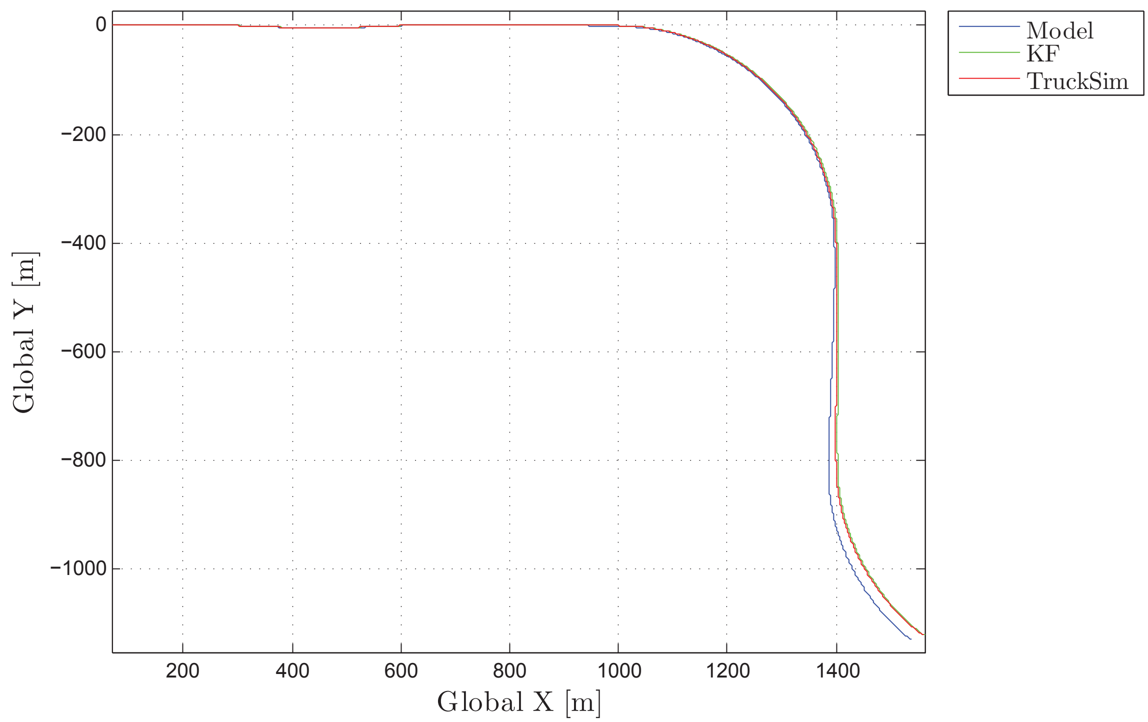

Figure 3.11: Highway Scenario Path Prediction, Five-Axle Model

It is clear from Figures 3.11 and 3.12 that the Kalman filter is greatly improving the performance of the model. Because the Kalman filter is feeding back on very clean TruckSim signals, it is able to provide excellent corrections. This can be seen in Figures 3.14, 3.15, and 3.15 which show the lateral acceleration, yaw rate, and yaw (heading) angle for this scenario respectively. Note that the Kalman filter data is essentially 'line-over-line' with TruckSim due to the quality of the signals.

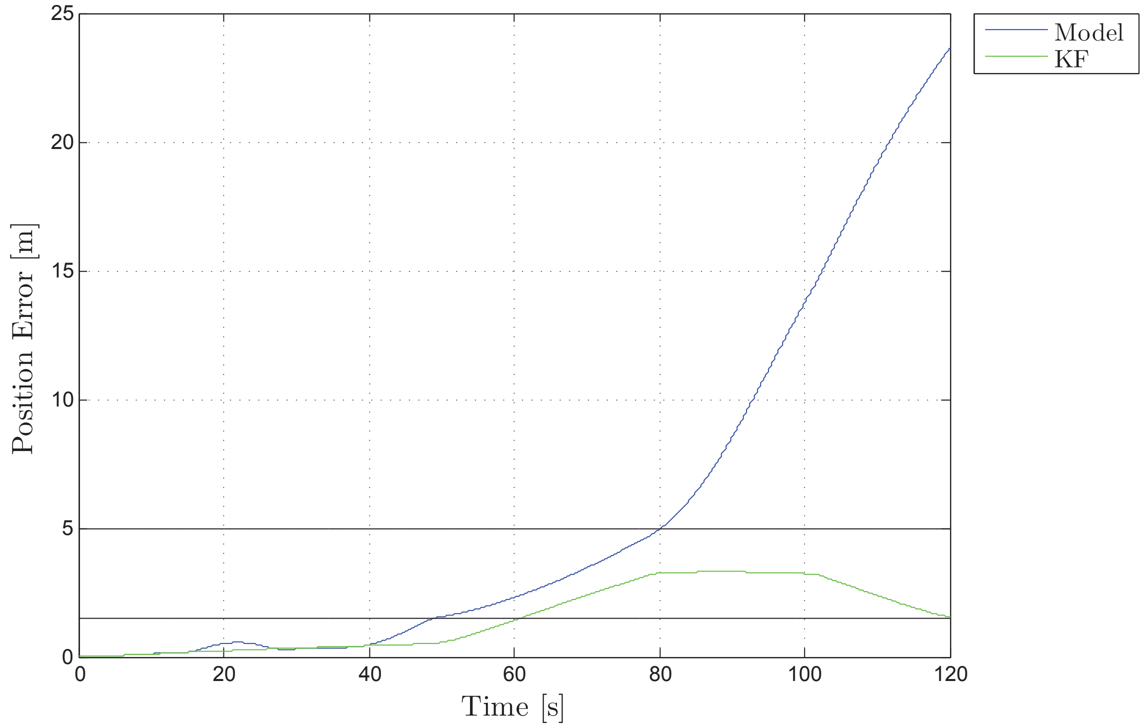

Figure 3.12: Highway Scenario Global Position Error, Five-Axle Model

Figures 3.17 and 3.18 show the hitch angle and hitch rate, respectively. For this case, the dynamic model predicts hitch angle more accurately than the kinematic model and the Kalman filter is helpful for the dynamic model. However, it is worth noting that the absolute value of hitch angle is fairly low (peak $\approx$ 2 deg). The kinematic model using TruckSim data ('KinGPS') is slightly more accurate than the model which uses Kalman filter model data ('KinHat').

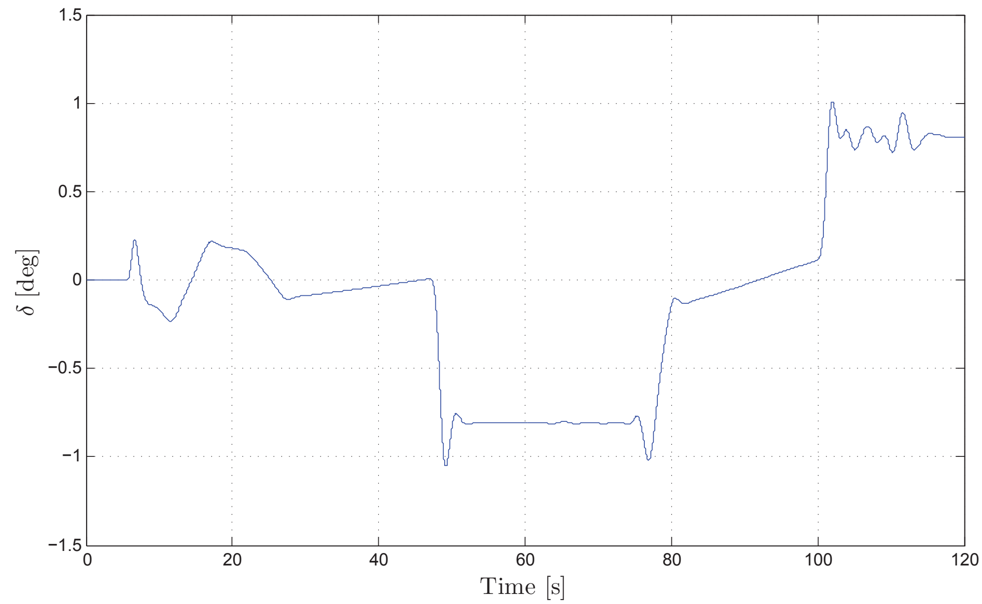

Figure 3.13: Highway Scenario Roadwheel Steering Angle, Five-Axle Model

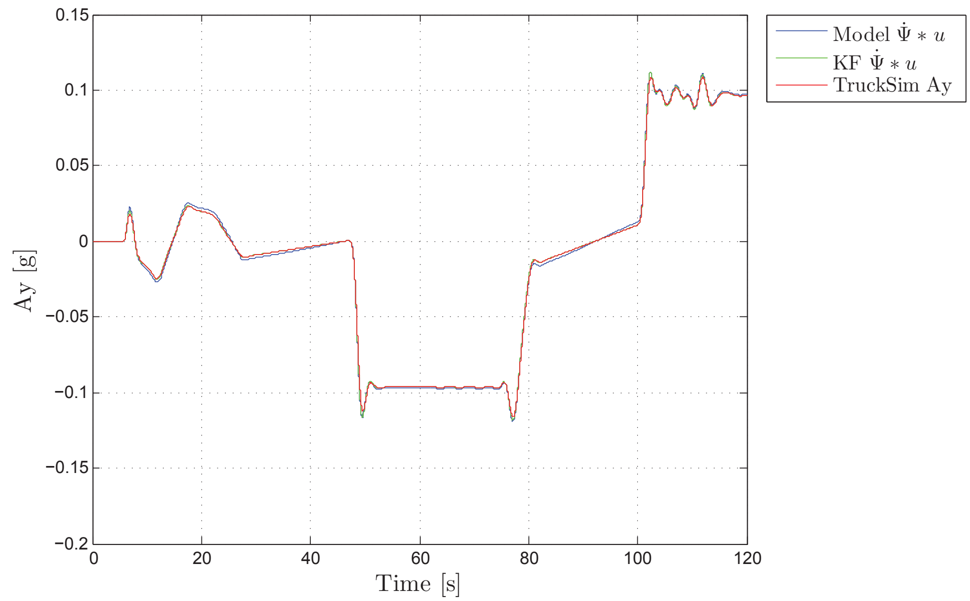

Figure 3.14: Highway Scenario Lateral Acceleration, Five-Axle Model

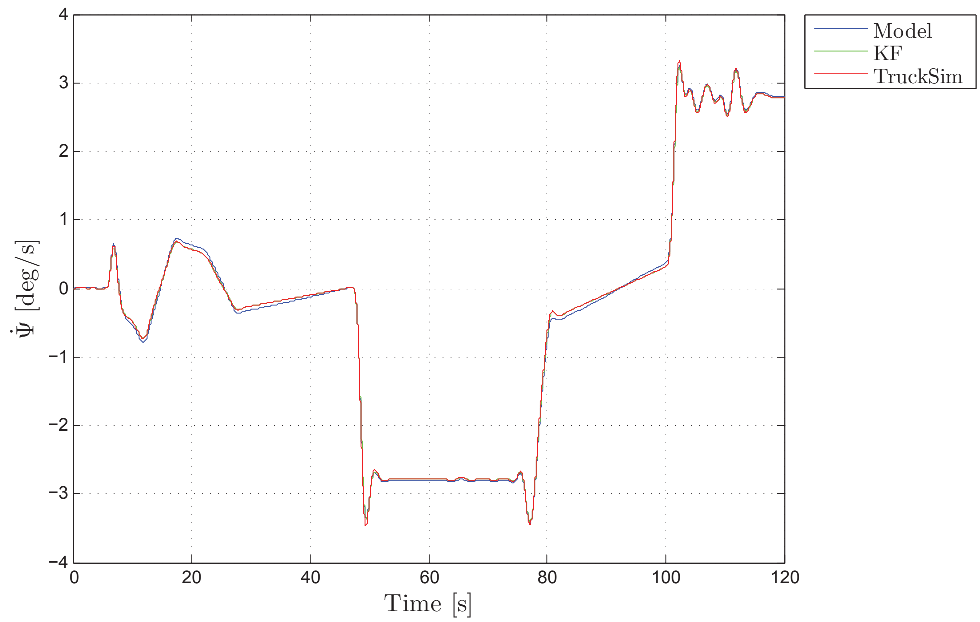

Figure 3.15: Highway Scenario Yaw Rate, Five-Axle Model

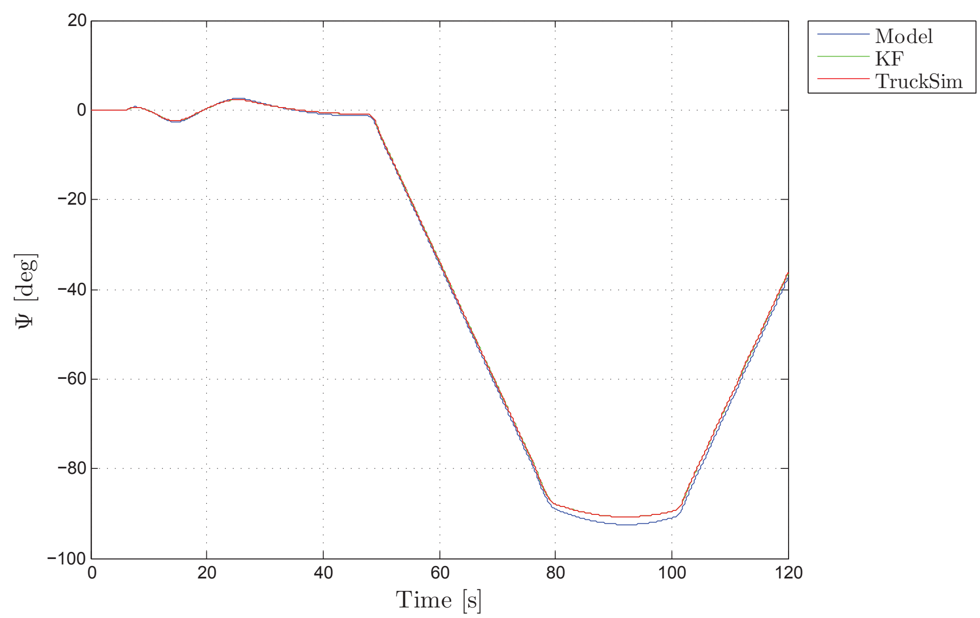

Figure 3.16: Highway Scenario Yaw Angle, Five-Axle Model

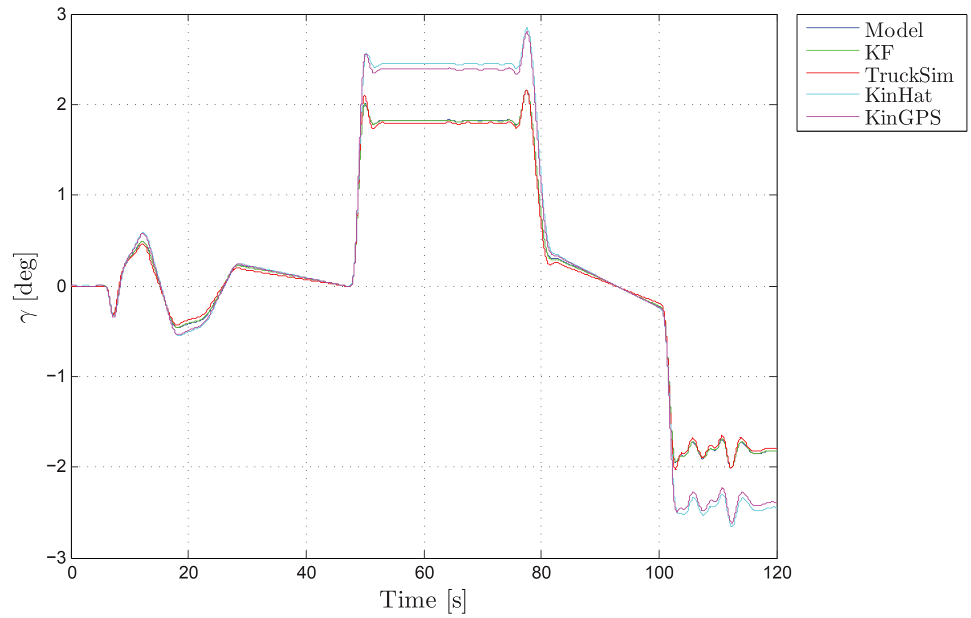

Figure 3.17: Highway Scenario Hitch Angle, Five-Axle Model

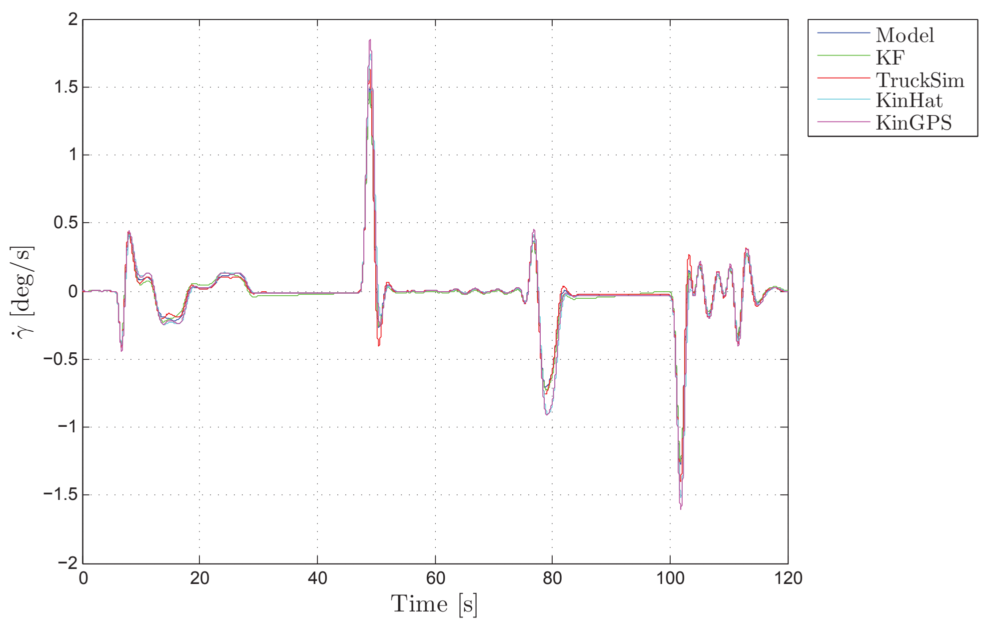

Figure 3.18: Highway Scenario Hitch Rate, Five-Axle Model

3.5.2 Urban Driving Scenario

Next, an urban driving scenario was developed. This consists of three straight sections connected by right and left turns ($R = 20$ m). The path prediction of this model is shown in Figure 3.19 and the RMS position error as a function of time is shown in Figure 3.20. Figure 3.21 shows the roadwheel steering input and speed is shown in Figure 3.22. Due to the tight radius of curvature and correspondingly high hitch angles, the trailer longitudinal velocity (in the tractor's frame, not its own) differs significantly from the tractor's at some points.

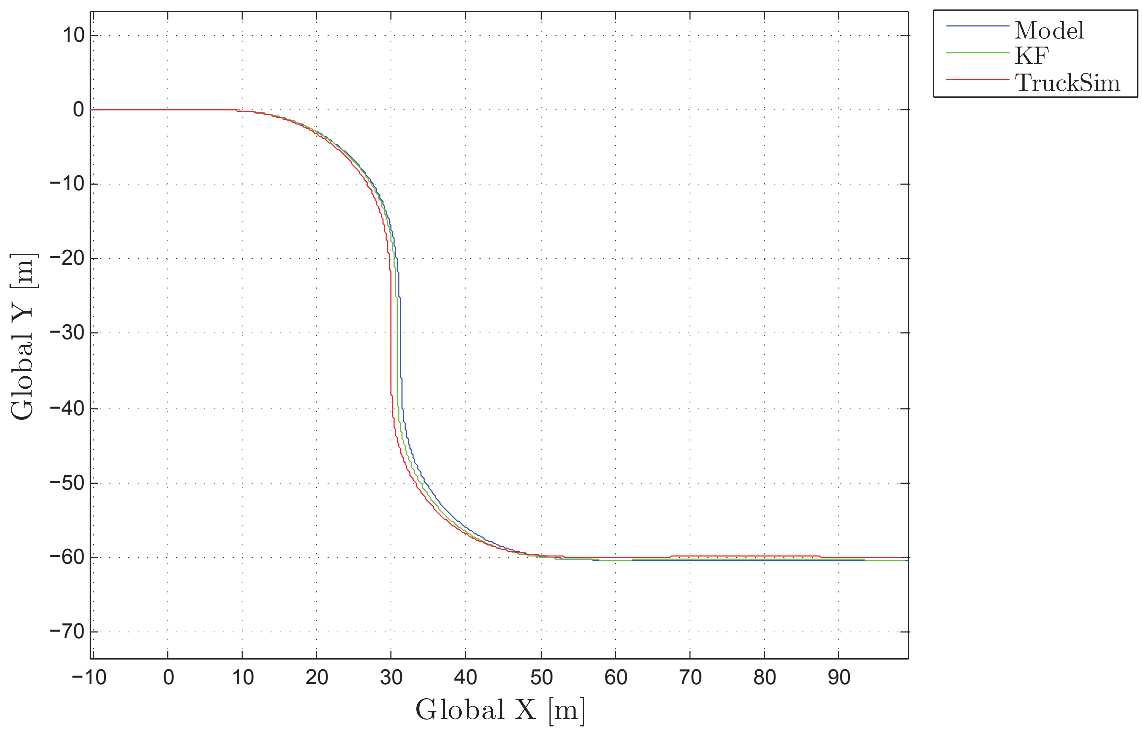

Figure 3.19: Urban Scenario Path Prediction, Five-Axle Model

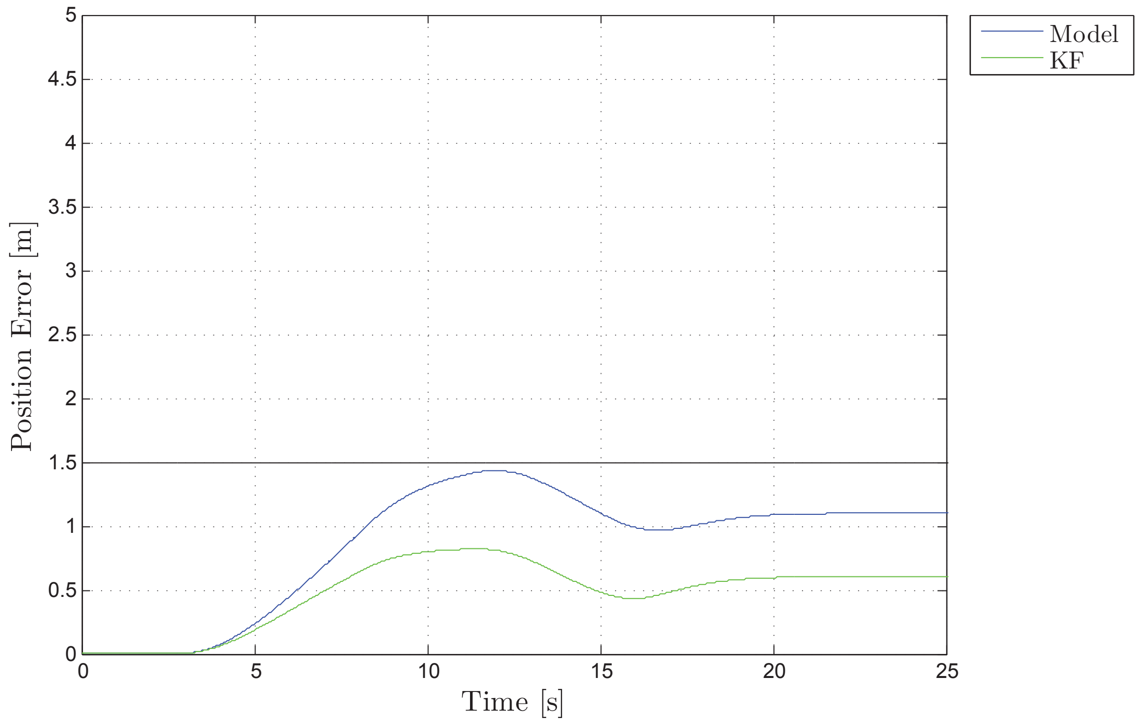

Figure 3.20: Urban Scenario Global Position Error, Five-Axle Model

It is clear from Figures 3.19 and 3.20 that the Kalman filter is improving the performance of the model. While the open-loop model reaches a peak RMS position error of nearly 1.5 m, the Kalman filtered model never exceeds 1 m of error.

Figures 3.26 and 3.27 show the hitch angle and hitch rate, respectively. For this case, the kinematic model predicts hitch angle more accurately than the dynamic model.

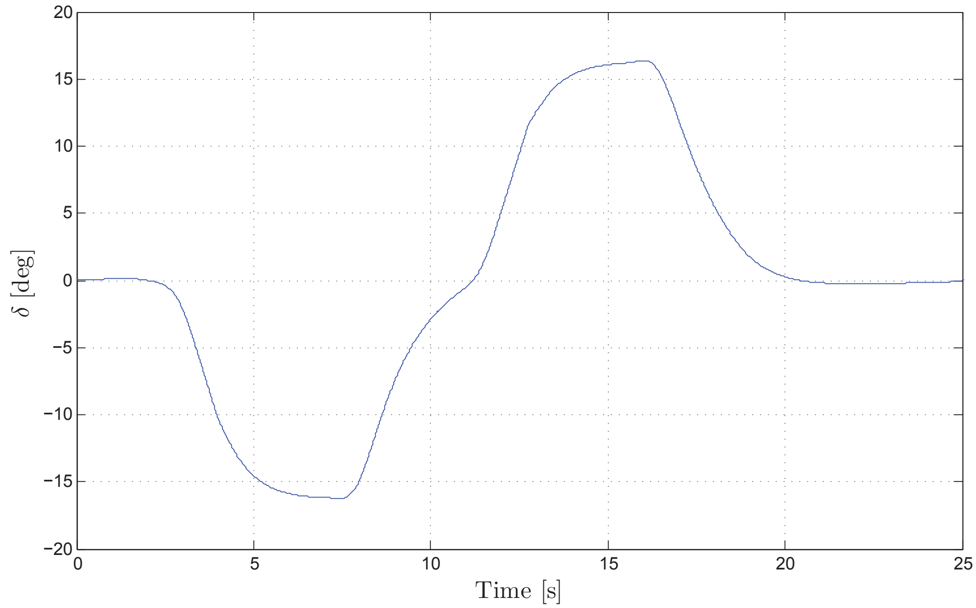

Figure 3.21: Urban Scenario Roadwheel Steering Angle, Five-Axle Model

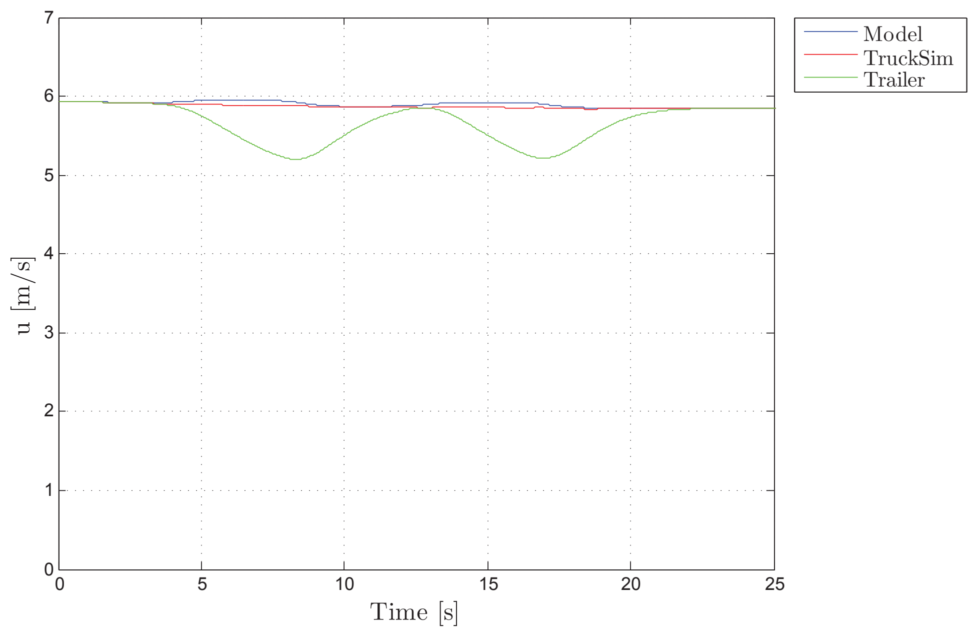

Figure 3.22: Urban Scenario Speed, Five-Axle Model

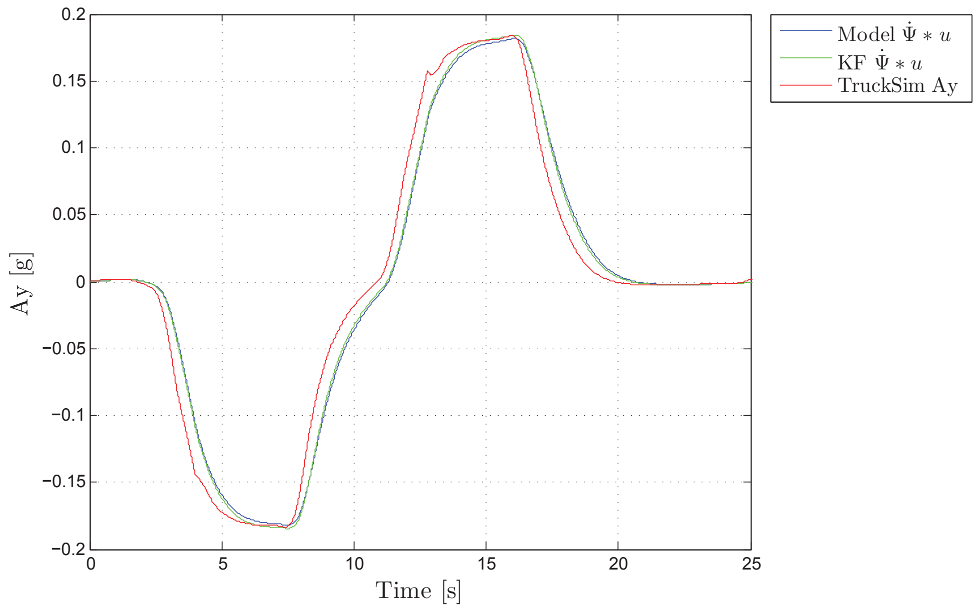

Figure 3.23: Urban Scenario Lateral Acceleration, Five-Axle Model

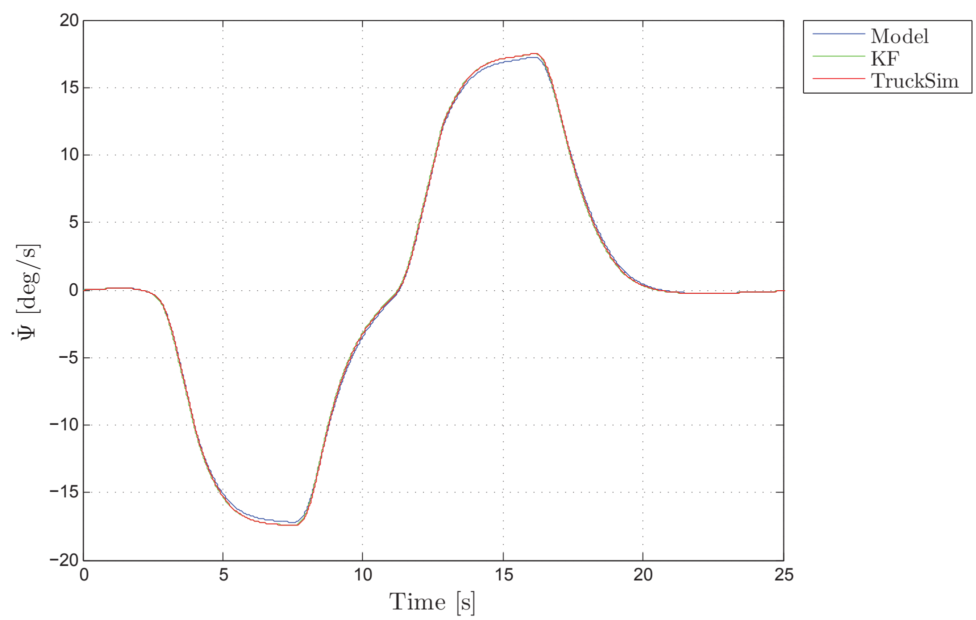

Figure 3.24: Urban Scenario Yaw Rate, Five-Axle Model

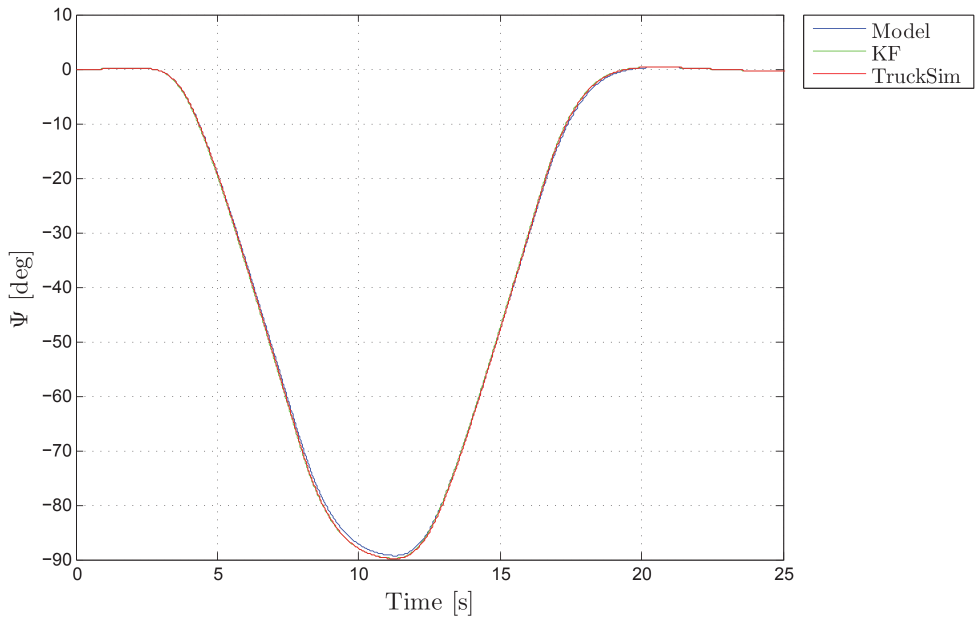

Figure 3.25: Urban Scenario Yaw Angle, Five-Axle Model

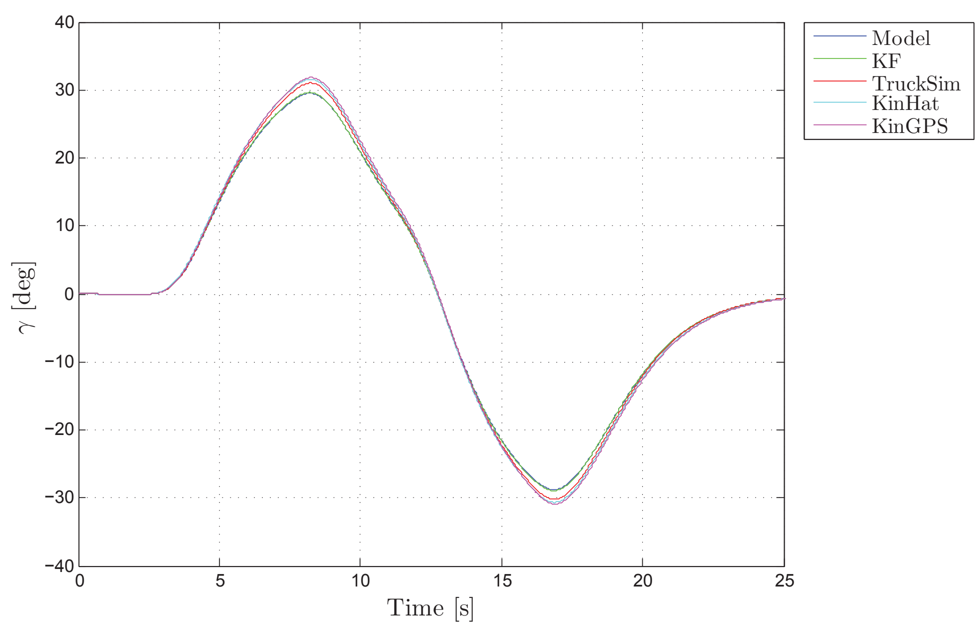

Figure 3.26: Urban Scenario Hitch Angle, Five-Axle Model

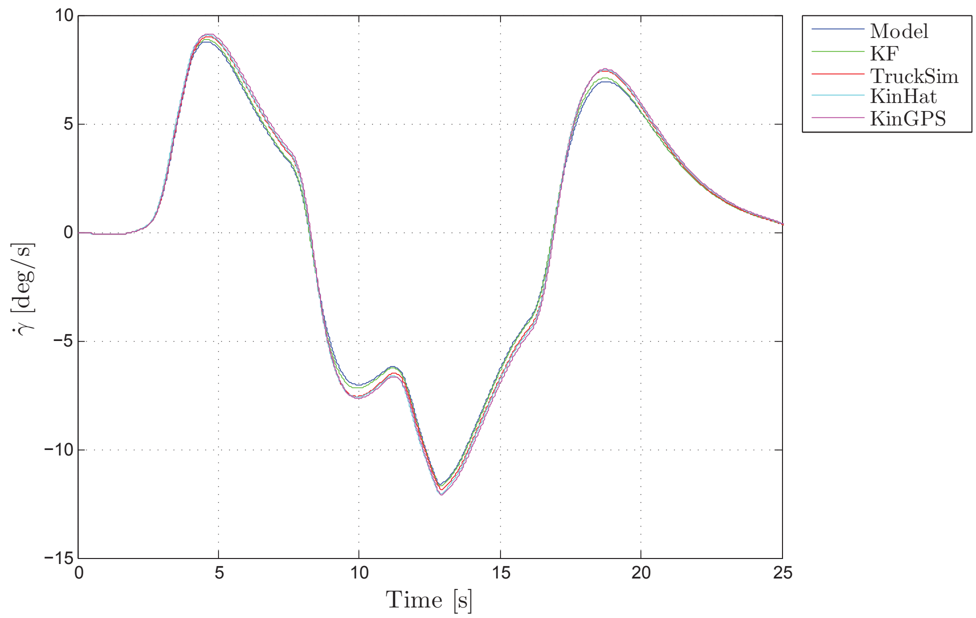

Figure 3.27: Urban Scenario Hitch Rate, Five-Axle Model

3.6 Conclusion

This chapter has presented the development and simulation-based validation of the five-axle lateral dynamic heavy truck model. The model's states and parameters were introduced and the derivation was explained using Lagrange's Equation. The effects of various assumptions embedded in the Lagrangian were examined and two feasible models were identified. A new method of estimating hitch angle, based on kinematics, was introduced and its equations were derived. A new method for the estimation of trailer tire cornering stiffness was proposed and a suitable measurement was identified via simulation. Finally, TruckSim was used to validate the model. The position estimate produced by the system was found to be acceptable as were both methods (kinematic and dynamic) of estimating articulation angle. The effects of using real truck data will be examined in the next chapter.

Chapter References

[1] W. Deng and X. Kang, "Parametric study on vehicle-trailer dynamics for stability control," *SAE*, no. 2006-01-1965, 2003.

[2] L. Perko, *Differential Equations and Dynamical Systems*. New York: Springer, 1996. Second edition.

[3] D. Simon, *Optimal State Estimation*. New Jersey: Wiley, 2006.

[4] W. Milliken and D. Milliken, *Race Car Vehicle Dynamics*. Warrendale, PA: SAE, 1995.

[5] D. Greenwood, *Principles of Dynamics*. New Jersey: Prentice Hall, 1987. Second edition.

[6] L. Chu, Y. Fang, M. Shang, J. Guo, and F. Zhou, "Estimation of articulation angle for tractor semi-trailer based on state observer," *International Conference on Measuring Technology and Mechatronics Automation*, 2010.

[7] A. Dunn, "Jacknife Stability of Articulated Ttractor Semitrailer Vehicles with High-Output Brakes and Jackknife Detection on Low Coefficient Surfaces." Doctoral Dissertation, The Ohio State University, 2003.

[8] S. Zhou, S. Zhang, and G. Zhao, "Jackknife control on tractor semi-trailer during emergency braking," *Advanced Materials Research*, vol. 299-300, no. 1303-1306, 2011.

[9] R. Anderson and D. Bevly, "Estimation of tire cornering stiffness using gps to improve model based estimation of vehicle states," *Proceedings of IEEE Intelligent Vehicles Symposium*, no. 801-806, 2005.

[10] W. Sienel, "Estimation of the tire cornering stiffness and its application to active car steering," *Proceedings of the 36th IEEE Conference on Decision and Control*, vol. 5, no. 4744-4749, 1997.

[11] D. Wesemeier and R. Isermann, "Identification of vehicle parameters using stationary driving maneuvers," *Control Engineering Practice*, vol. 17, no. 1426-1431, 2009.

[12] G. Baffet, A. Charara, and D. Lechner, "Estimation of vehicle sideslip, tire force and wheel cornering stiffness," *Control Engineering Practice*, vol. 17, no. 1255-1264, 2009.

[13] S. You, J. Hahn, and H. Lee, "New adaptive approaches to real-time estimation of vehicle sideslip angle," *Control Engineering Practice*, vol. 17, no. 1367-1379, 2009.

[14] L. Alexander, M. Donath, M. Hennessey, V. Morellas, and C. Shankwitz, "A lateral dynamic model of a tractor–trailer: Experimental validation." MN DOT Report, Contract 73168 TOC 174, November 1996.

[15] A. Hac, D. Fulk, and H. Chen, "Stability and control considerations of vehicle-trailer combination," *SAE*, no. 2008-01-1228, 2008.

CHAPTER 4

FIELD TESTING MODEL VALIDATION

4.1 Introduction

This chapter covers validation of the vehicle models introduced in Chapters 2 and 3. These models were developed using a high-fidelity TruckSim model created by Rao based on research conducted at NHTSA's Vehicle Research and Test Center (VRTC) [1]. The same vehicle was then used for physical testing, which was performed at the Transportation Research Center (TRC) in East Liberty, Ohio.

This chapter begins by detailing the equipment and facilities used in the testing. Following this is a validation of the three-axle model. Next, a more extensive validation of the five-axle model is presented. Finally, conclusions are drawn regarding the performance of the estimation system.

4.2 Equipment

4.2.1 Tractor

The tractor used for validation of both models was a 2006 Volvo 6x4 VNL64T630, VIN 4V4NC9GH16N441360. The tractor (with trailer attached) is pictured in Figure 4.1, where it is being weighed.

Figure 4.1: Volvo Tractor with Fruehauf Box Trailer

4.2.2 Trailer

The trailer used was a 53-foot Fruehauf box trailer (this was also modeled by Rao in [1]). It was loaded with concrete ballast blocks according to the diagram shown in Figure 4.2. The boxes containing an 'X' are welded steel frames which support the ballast blocks. The outriggers were not necessary for this testing and therefore were not used.

The lateral dynamic model originally used mass values taken from the TruckSim model, but these were adjusted slightly based on the measurements taken on the scale (shown in Figure 4.1). The small discrepancies arise from three sources: slightly different ballast blocks were used (e.g. a 4006 pound block was used in place of a 4000 pound block), the outriggers were not mounted on the trailer, and the weight of the

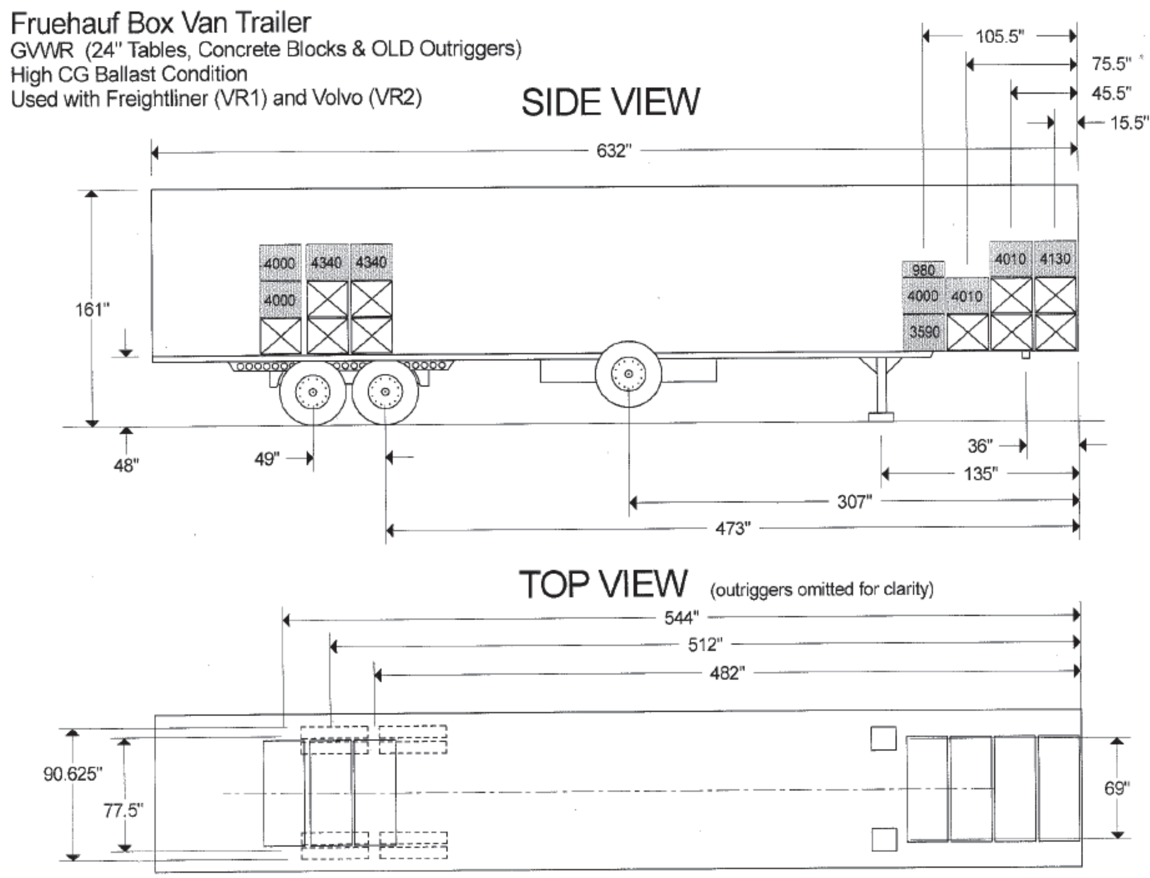

Figure 4.2: Fruehauf Box Trailer with High-CG Load

load frames were neglected in the original model. Figure 4.3 shows some of the ballast blocks used to load the trailer. Also visible attached to the ceiling is a mount for a GPS antenna (without antenna; directly above the kingpin).

Figure 4.3: Ballast in Fruehauf Box Trailer

4.2.3 Sensors

The vehicle was outfitted with a number of sensors for testing. A United Eletronic Industries (UEI) 'Cube' data acquisition system was installed to collect data from several sources. The J1939-standard truck CAN bus was monitored to collect vehicle-reported wheel-based vehicle speed, lateral acceleration, yaw rate, and handwheel steering angle [2]. Discrete sensors were also connected to the Cube, such as a string potentiometer used to measure handwheel steer angle. An RT3003 from Oxford Technical Solutions was also connected to the Cube to collect high-accuracy inertial measurements (lateral acceleration, yaw rate) and GPS-based speed.

In addition to the GPS antenna connected to the RT3003, three dual-frequency (L1/L2 band) Novatel GPS antennas were connected. The first antenna was mounted on the tractor, just aft of the cab on the vehicle centerline. The second antenna was mounted on the trailer, just under its fiberglass roof and directly above the kingpin. This point is common to both the tractor and trailer and thus served as a 'virtual sensor' for the tractor. The third antenna was mounted near the rear of the trailer just below its roof on the centerline. The first and second antenna (here acting as a 'virtual sensor') allowed the heading angle of the tractor to be calculated. By comparing this with the velocity heading (i.e. the direction in which the tractor is traveling), the body sideslip angle and sideslip velocity were also calculated. The second and third antenna allowed the heading angle of the trailer to be calculated. The difference between tractor and trailer heading is the hitch (articulation) angle.

Though handwheel steering angle was measured via CAN and a string potentiometer, road wheel steer angle is needed for the model. The steering gear ratio, i.e. the linear best fit of handwheel steer angle divided by road wheel steer angle, was reported by Rao as being 20.5 deg/deg (degree of handwheel angle per degree of road wheel angle) [1]. Thus the plots of road wheel steer angle in this chapter are in fact plots of handwheel steer angle divided by the steering gear ratio. This is the same signal that was provided to the estimator.

4.3 Facilities

4.3.1 Vehicle Dynamics Area (VDA)

The Vehicle Dynamics Area (VDA) at TRC is a wide, open expanse of asphalt approximately 50 acres in area. Adjacent to the VDA are two loops (the 'north loop' and 'south loop') that can be used to accelerate before entering the testing area. A drawing of the VDA can be found in Figure 4.4. The VDA was utilized for the ramp and hold maneuver as well as the urban driving scenario. For the ramp and hold maneuver, the tractor-trailer was driven out of the north (south) loop and turned to the right (left) at both 0.1 and 0.2 g. For the urban driving scenario, cones were set up near the north end of the VDA to mark low-speed left and right turns with radii of 20 m. A photograph of the urban driving scenario setup can be seen in Figure 4.5. The tire marks on the pavement are from the test vehicle, which can be seen at the far left of the frame.

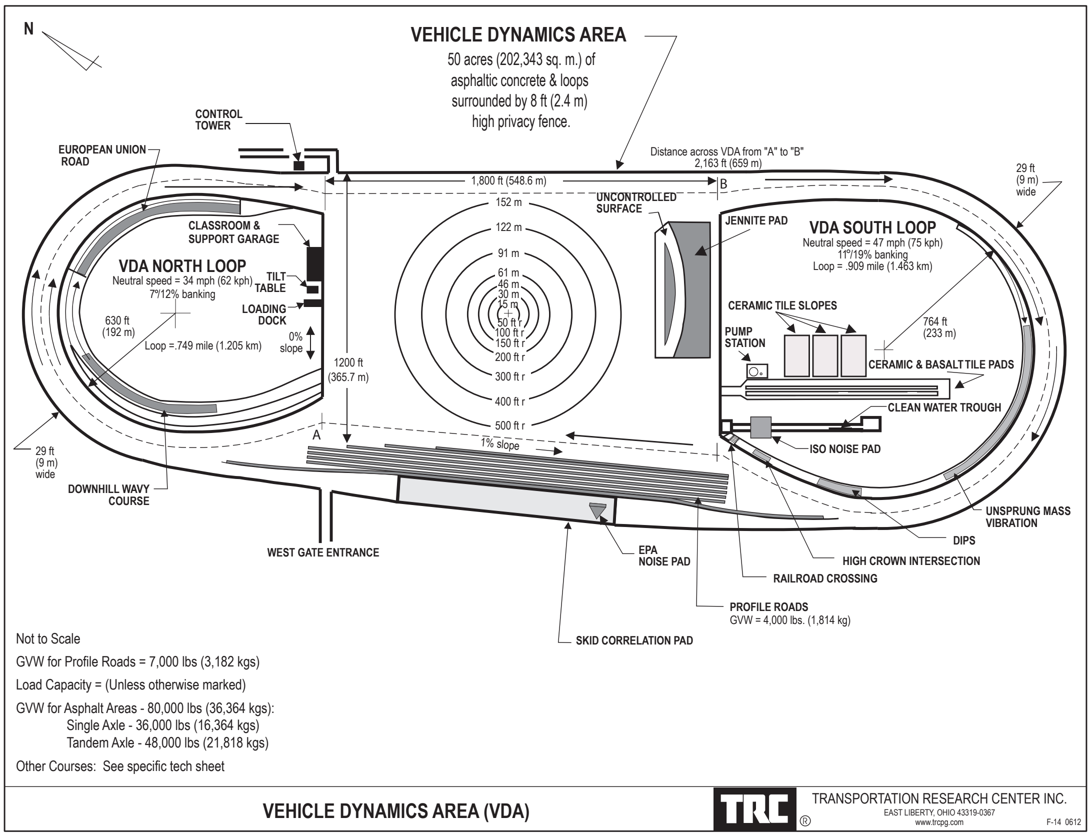

Figure 4.4: Vehicle Dynamics Area (VDA) at TRC

Figure 4.5: Experimental Setup for Urban Driving Scenario on VDA

4.3.2 7.5 Mile Test Track

TRC's 7.5-mile test track is a smooth, asphalt-paved track with banked lanes. Testing was conducted in Lane 0, which has the smallest amount of banking and the lowest minimum and maximum speeds (0 and 60 mph, respectively). A diagram of the track can be found in Figure 4.6. This test track was used to conduct the highway driving scenario tests.

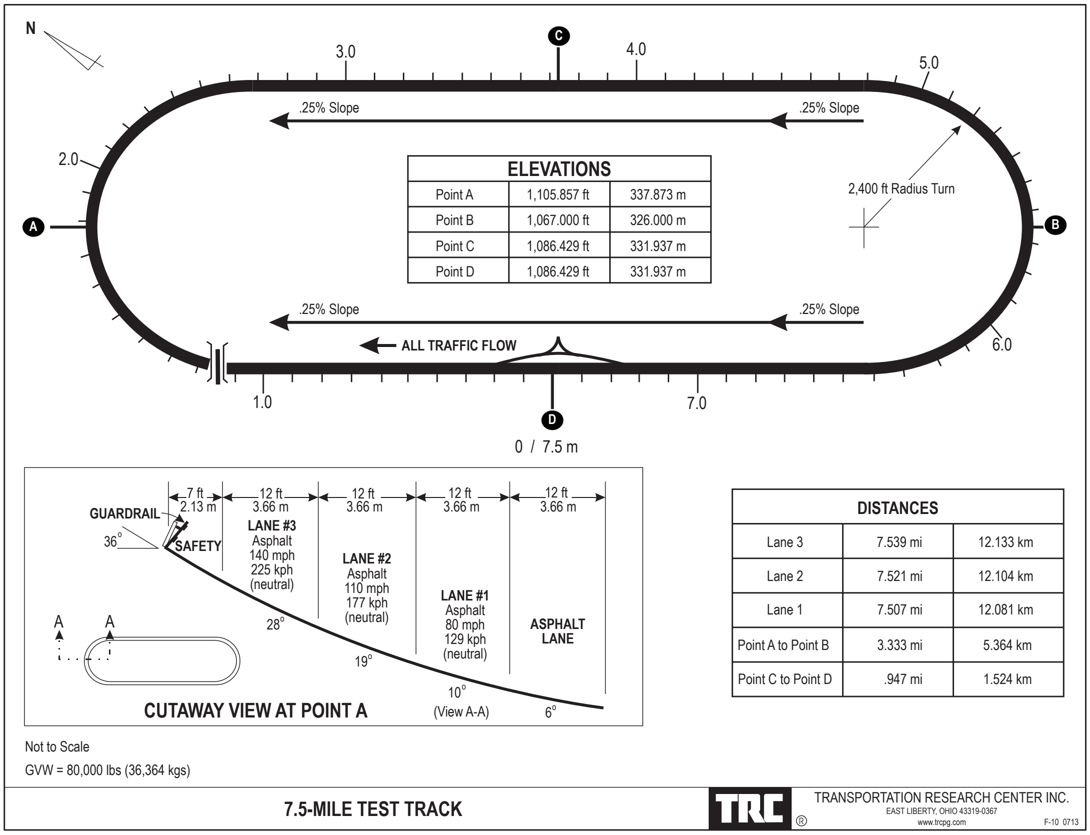

Figure 4.6: High-Speed 7.5 Mile Test Track at TRC, used for Highway Driving Scenario Testing

4.4 Three-Axle Model Validation

The National Highway Traffic Safety Administration's (NHTSA's) Vehicle Research and Test Laboratory (VRTC) is responsible for a wide range of vehicle testing. Because of VRTC's role in testing heavy truck ESC systems, large amounts of data are available. One of these tests was used to validate the three-axle model. Although these ESC test maneuvers are often severe, this provides 'worst-case' tests for the position estimator.

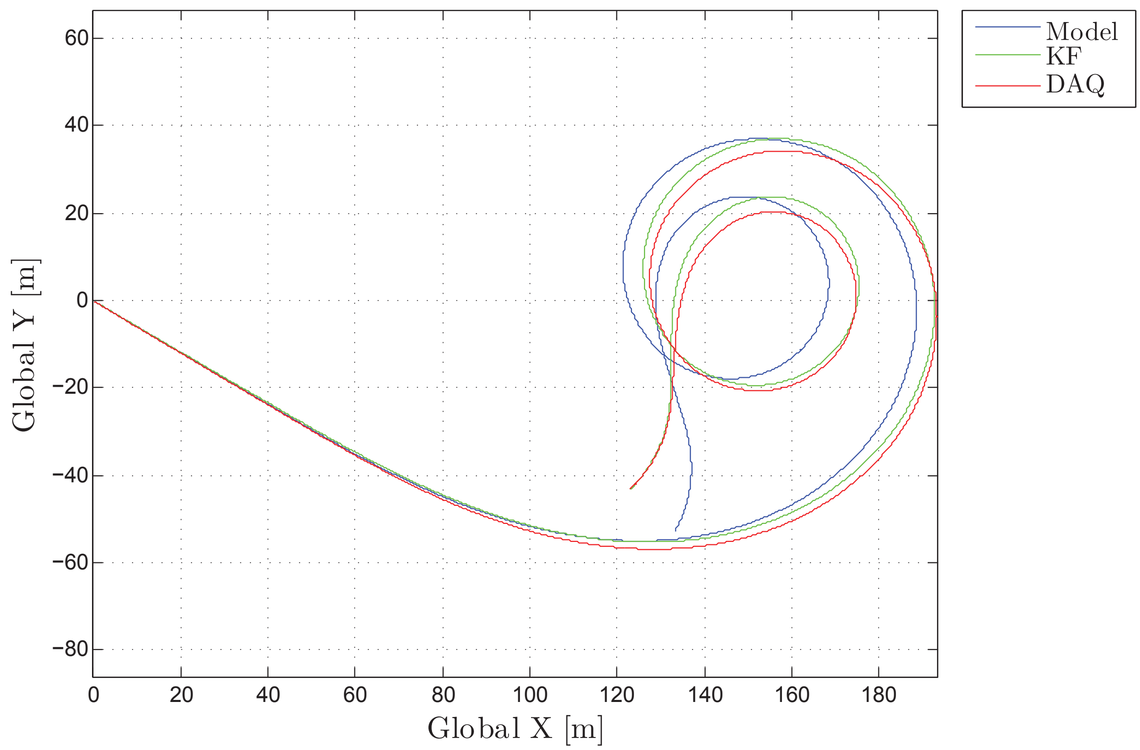

Figure 4.7: Path Prediction with Real Data, Three-Axle Model

Figure 4.7 shows the results of such a maneuver, which had a peak lateral acceleration of approximately 0.6 g. Figure 4.8 shows the position error corresponding to the open-loop and KF models. The maximum error for the KF model is about 4 m while the error of the open-loop model exceeds 15 m. Errors in $\hat{u}$ were found to be a significant source of error in the estimate of global position. While TruckSim wheel speeds are very close to the CG velocity, the measured wheel speeds were not as close. Figure 4.9 shows a plot of u for this same scenario. 'Model,' the speed used by the position estimator ($\hat{u}$), is estimated by averaging all six wheel speeds. 'DAQ' is taken directly from the recorded data. 'GPS Calc' is calculated using GPS Northings and Eastings velocity along with the GPS heading angle. Note that the 'Model' value exceeds the actual speed, especially during the period from 20 – 35 s. This could be

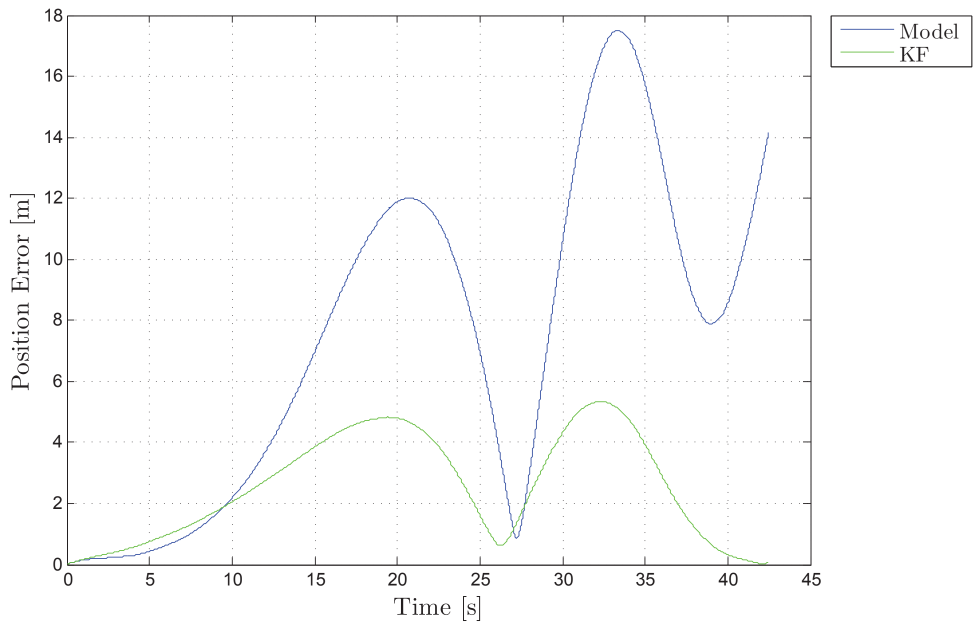

Figure 4.8: Global Position Error with Real Data, Three-Axle Model

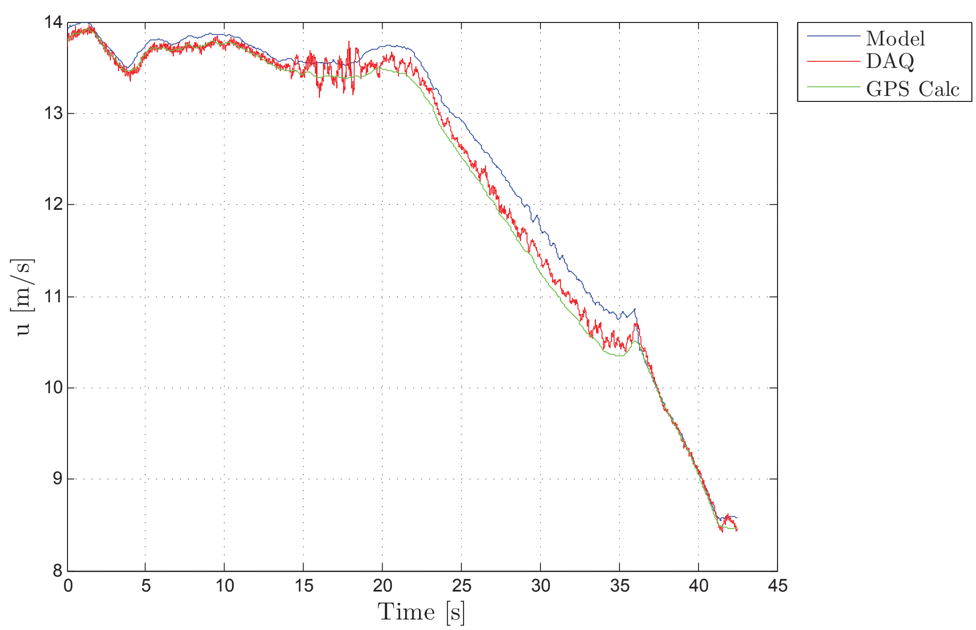

Figure 4.9: Vx with Real Data, Three-Axle Model

addressed in future work by better estimating the scale factor (effective loaded wheel radius) between wheel angular velocity and vehicle longitudinal velocity during times that GPS is available.

4.5 Five-Axle Model Validation

4.5.1 Ramp and Hold

Based on experience developing the tire cornering stiffness estimator using TruckSim, data was collected during several ramp and hold maneuvers. This involved driving the vehicle in a straight line for several seconds at approximately 70 kph and then linearly increasing steering angle until the desired lateral acceleration was reached. This level of lateral acceleration was then maintained for approximately 10 seconds. The vehicle was driven by a test driver (as opposed to a steer robot) because the tire cornering stiffness estimator should work despite natural driving behaviors (e.g. small steering oscillations) if it is to be feasible for a real embedded system. This test was repeated for left and right turns at nominal lateral accelerations of 0.1 and 0.2 g.

4.5.1.1 Ramp and Hold, Model Revision 4

Figures 4.10–4.18 show the results of ramp and hold maneuver #1338. This was a right-hand ramp at a nominal lateral acceleration of 0.2 g (in this case, 0.25–0.3 g). Figure 4.10 shows the tire cornering stiffness estimates generated by this run. For the purpose of tire cornering stiffness estimation, this scenario was initially processed using TruckSim values of tire cornering stiffness. The remainder of the plots were generated using estimated values of tire cornering stiffness. The estimates produced by y_2 (i.e. those appended with (2)) were found to be better, particularly because $C_{\alpha 1}(1)$ (generated using y_1) is estimated as being too high.

From Figure 4.12 we can see that the vehicle position estimator maintained lane-level positioning for approximately 7 s and road-level positioning for the duration of the run. This accuracy is achieved by having the Kalman filter highly 'trust' the CAN-based yaw rate measurement as can be seen in Figure 4.15. This is achieved through proper tuning of the $\mathbf{R}$ matrix, i.e. $\mathbf{R}(2,2)$ is set small, as explained in Section 2.4. As a result, the state estimate for heading angle is quite accurate, as can be seen in Figure 4.16.

Figure 4.17 shows that the estimate of hitch angle produced by the dynamic model (i.e. the trace labeled 'KF') is quite good, generally within about a tenth of a degree. Interestingly, here the kinematic model which results on estimated states ('KinHat') is actually more accurate than the kinematic model relying on GPS measurements ('KinGPS').

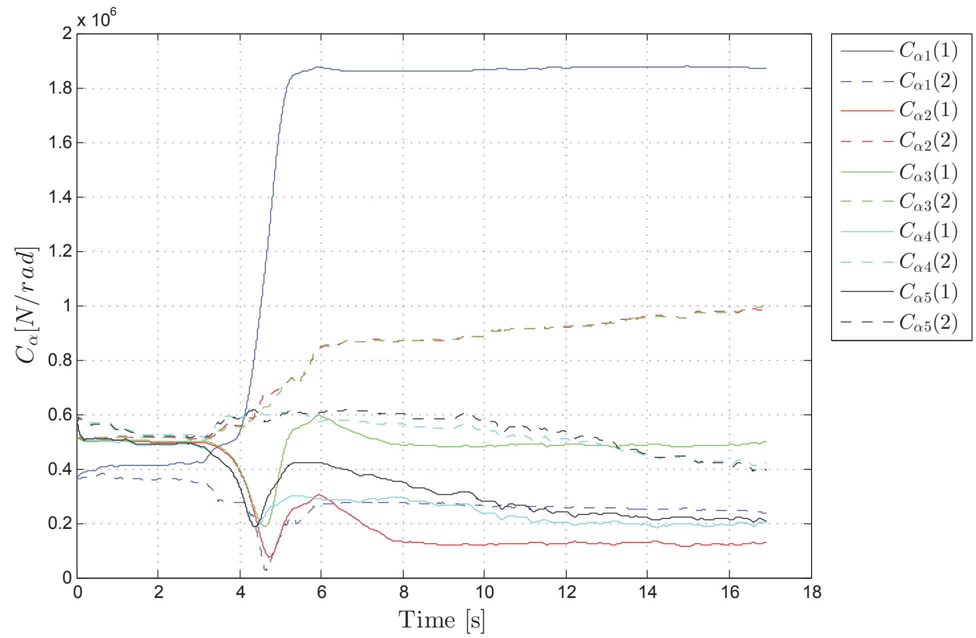

Figure 4.10: Ramp #1338 (Right, 0.2 g) Tire Cornering Stiffness Estimation, Five-Axle Model Revision 4

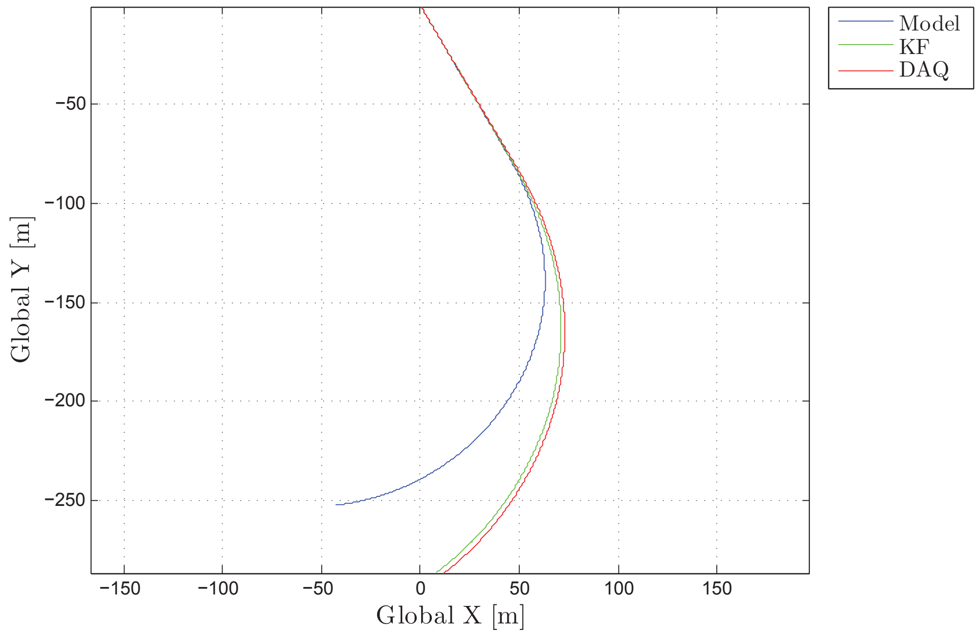

Figure 4.11: Ramp #1338 (Right, 0.2 g) Path Prediction, Five-Axle Model Revision 4

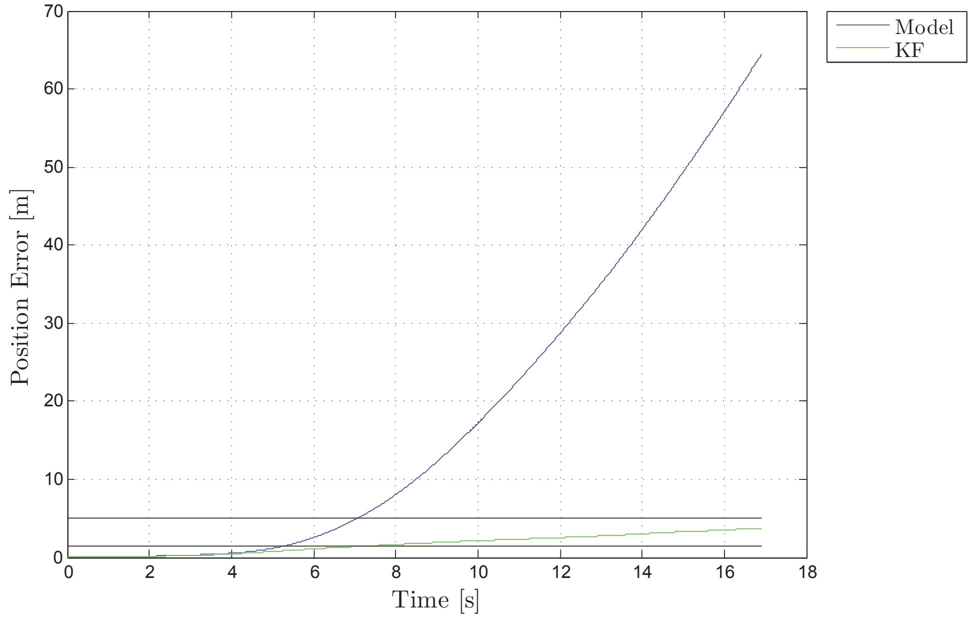

Figure 4.12: Ramp #1338 (Right, 0.2 g) Global Position Error, Five-Axle Model Revision 4

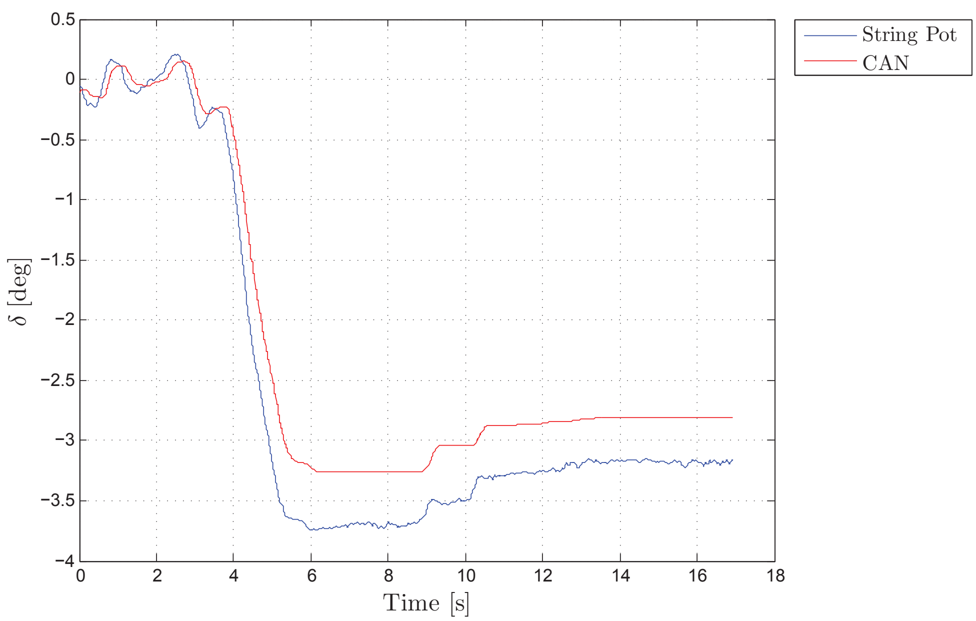

Figure 4.13: Ramp #1338 (Right, 0.2 g) Road Wheel Steering Angle, Five-Axle Model Revision 4

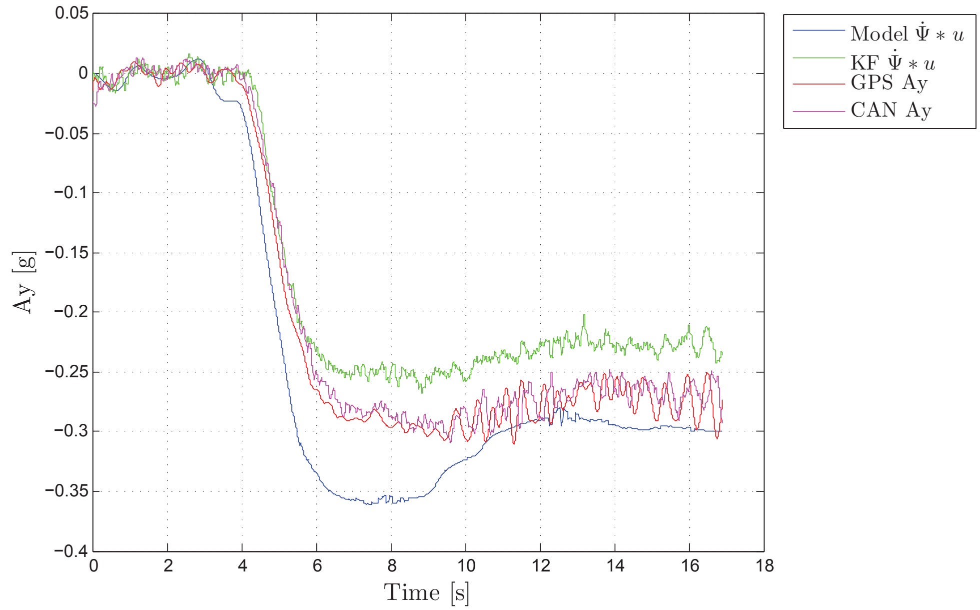

Figure 4.14: Ramp #1338 (Right, 0.2 g) Lateral Acceleration, Five-Axle Model Revision 4

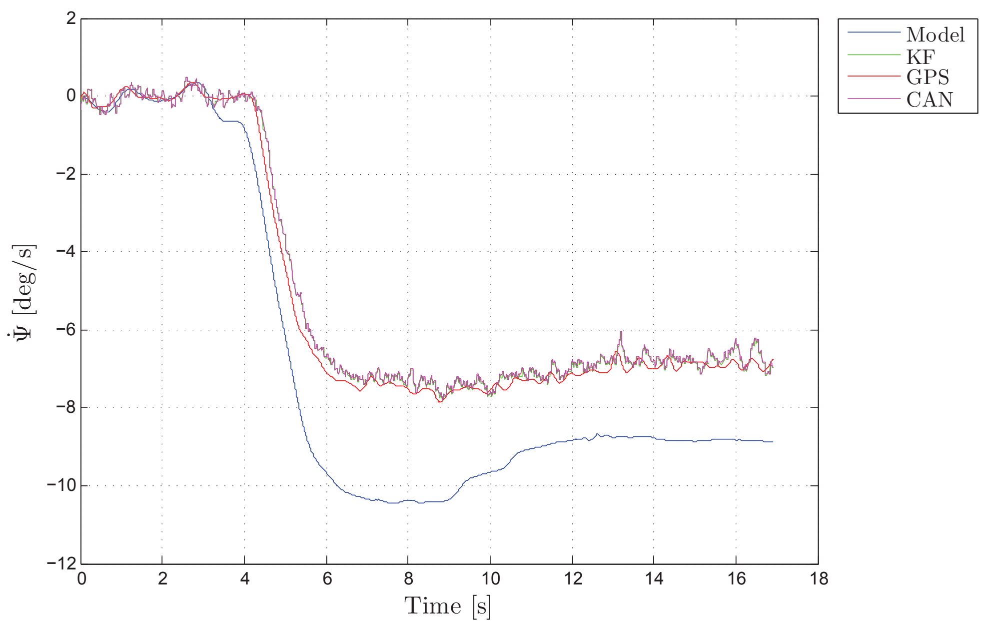

Figure 4.15: Ramp #1338 (Right, 0.2 g) Yaw Rate, Five-Axle Model Revision 4

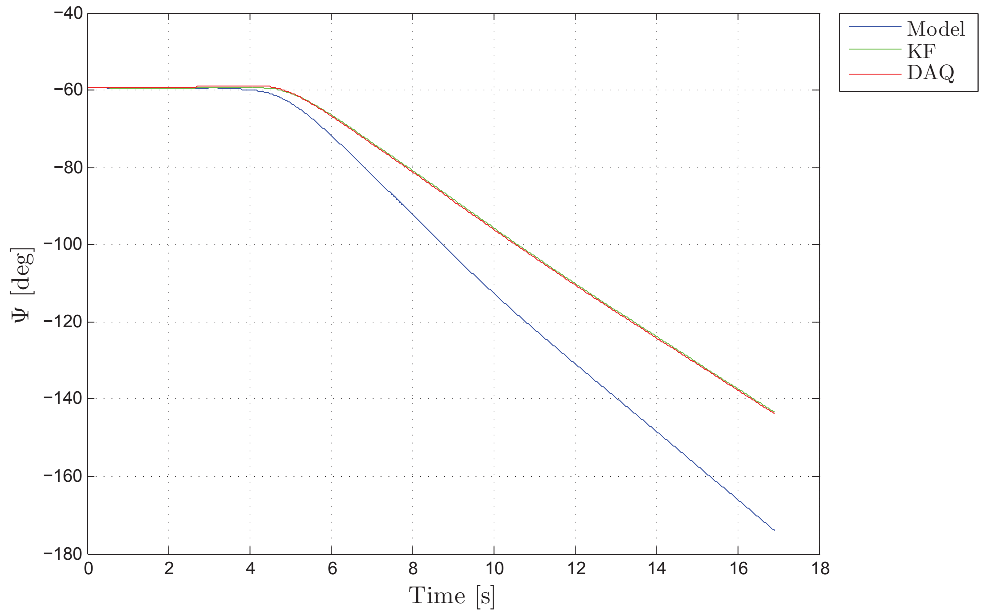

Figure 4.16: Ramp #1338 (Right, 0.2 g) Yaw Angle, Five-Axle Model Revision 4

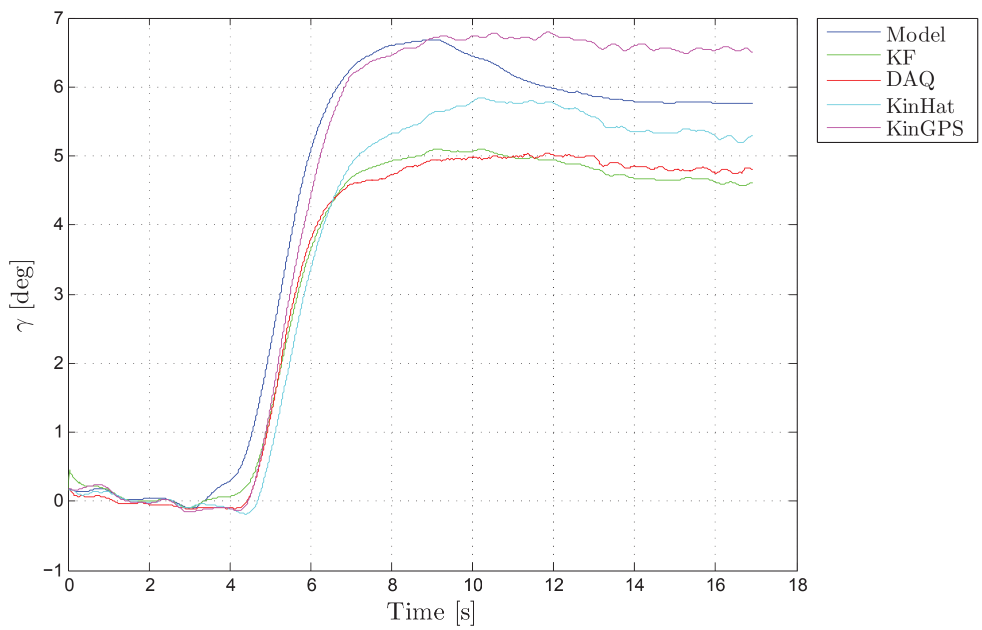

Figure 4.17: Ramp #1338 (Right, 0.2 g) Hitch Angle, Five-Axle Model Revision 4

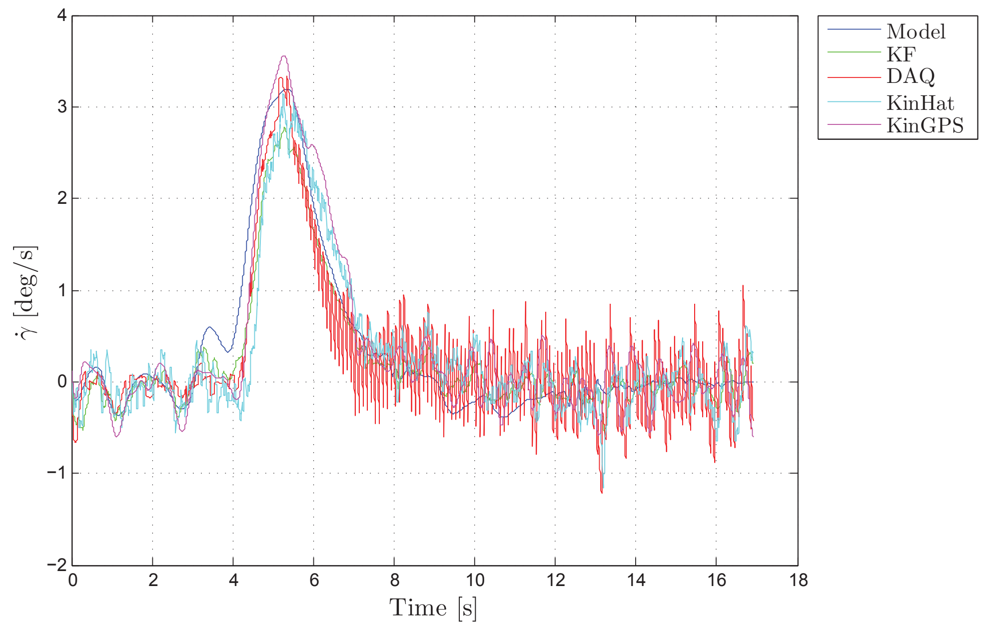

Figure 4.18: Ramp #1338 (Right, 0.2 g) Hitch Rate, Five-Axle Model Revision 4

Figures 4.19–4.27 show the results of ramp and hold maneuver #1342. This was a left-hand ramp at a nominal lateral acceleration of 0.1 g (in this case, about 0.11 g). Figure 4.19 shows the tire cornering stiffness estimates generated by this run. For the purpose of tire cornering stiffness estimation, this scenario was initially processed using TruckSim values of tire cornering stiffness. The remainder of the plots were generated using estimated values of tire cornering stiffness. The estimates produced by y_2 were again found to be better, because $C_{\alpha 1}(1)$ is estimated as being too high and $C_{\alpha 4}(1)$ is estimated as being nearly zero.

In this case, lane-level positioning was maintained for the entire duration of the run as can be seen in Figure 4.21. The estimates of hitch angle, shown in Figure 4.26, were also very good with the KF estimate generally being within a tenth of a degree. However, in steady state the kinematic model relying on estimated states ('KinHat') was more accurate than the dynamic model ('KF').

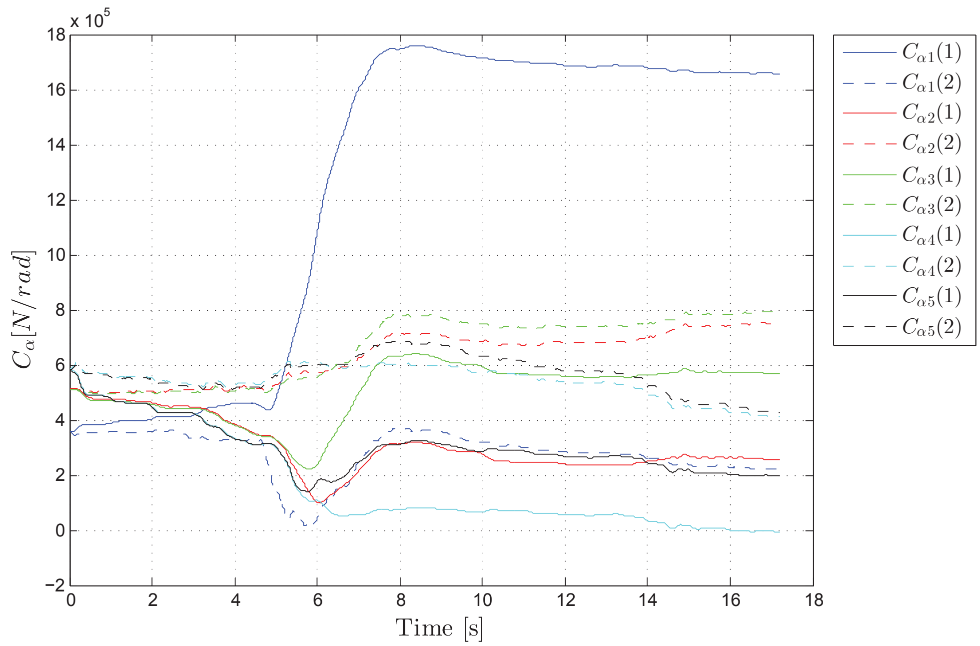

Figure 4.19: Ramp #1342 (Left, 0.1 g) Tire Cornering Stiffness Estimation, Five-Axle Model Revision 4

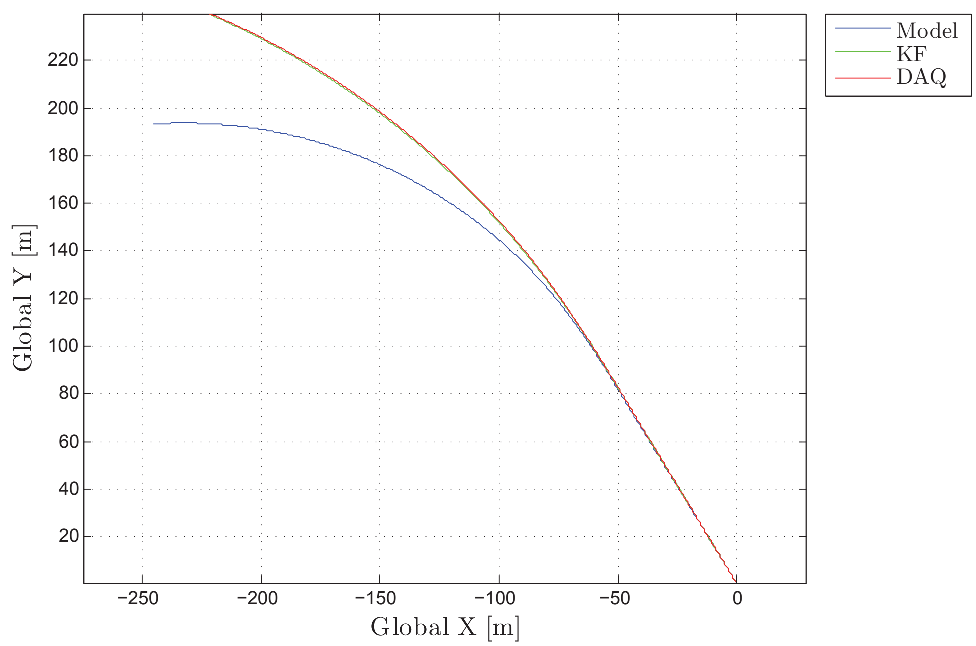

Figure 4.20: Ramp #1342 (Left, 0.1 g) Path Prediction, Five-Axle Model Revision 4

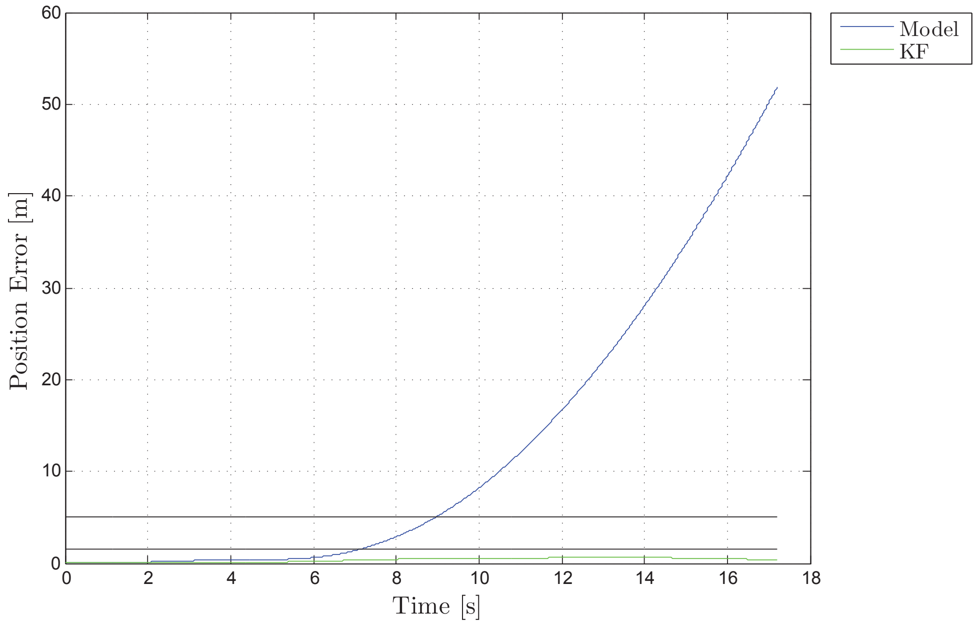

Figure 4.21: Ramp #1342 (Left, 0.1 g) Global Position Error, Five-Axle Model Revision 4

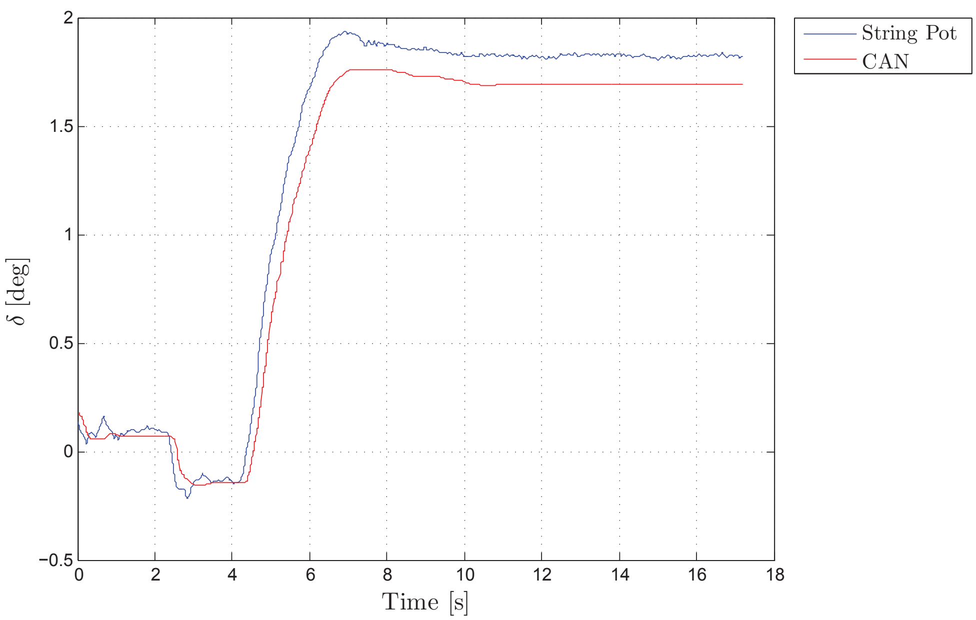

Figure 4.22: Ramp #1342 (Left, 0.1 g) Road Wheel Steering Angle, Five-Axle Model Revision 4

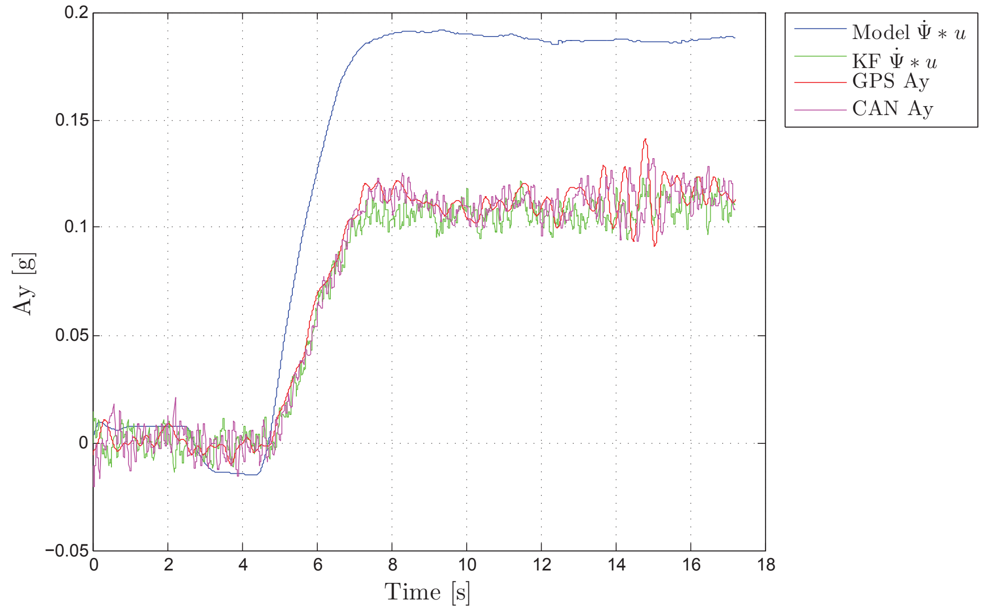

Figure 4.23: Ramp #1342 (Left, 0.1 g) Lateral Acceleration, Five-Axle Model Revision 4

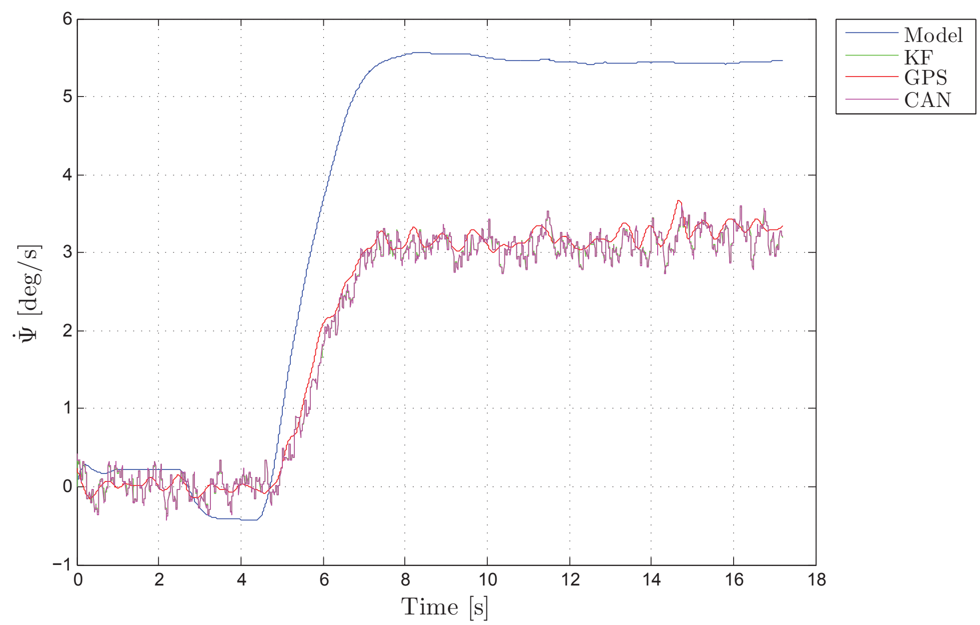

Figure 4.24: Ramp #1342 (Left, 0.1 g) Yaw Rate, Five-Axle Model Revision 4

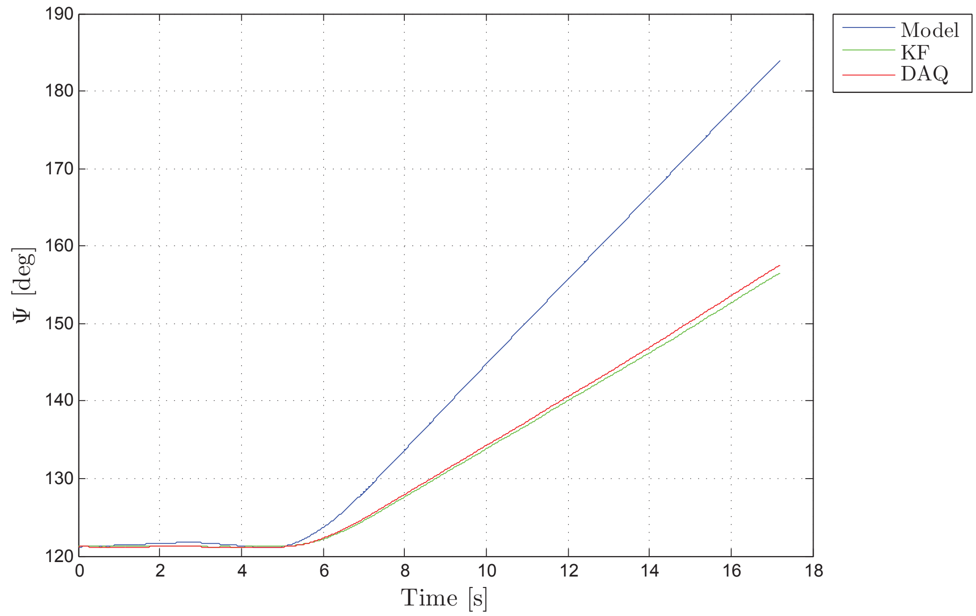

Figure 4.25: Ramp #1342 (Left, 0.1 g) Yaw Angle, Five-Axle Model Revision 4

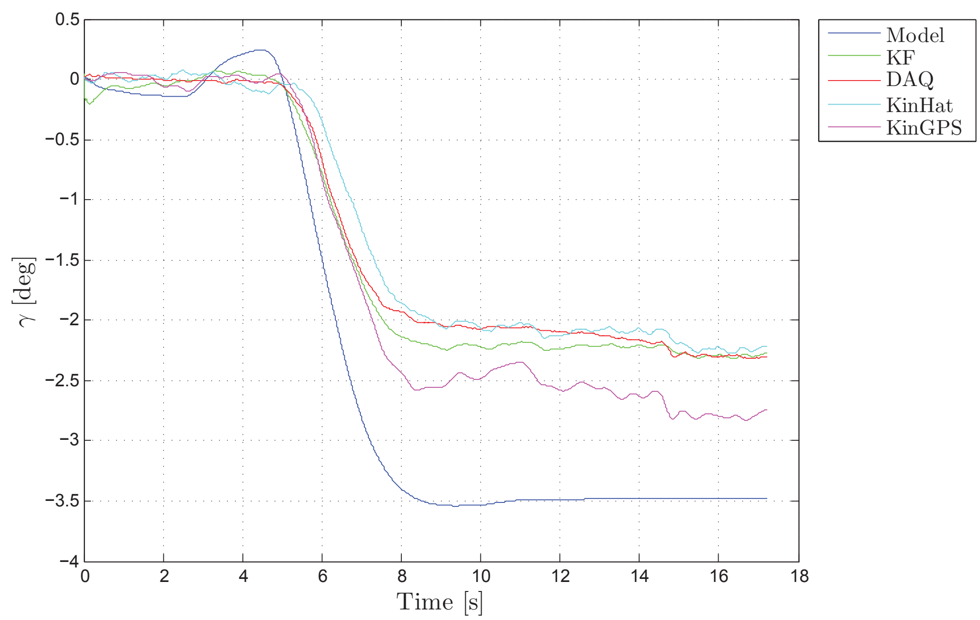

Figure 4.26: Ramp #1342 (Left, 0.1 g) Hitch Angle, Five-Axle Model Revision 4

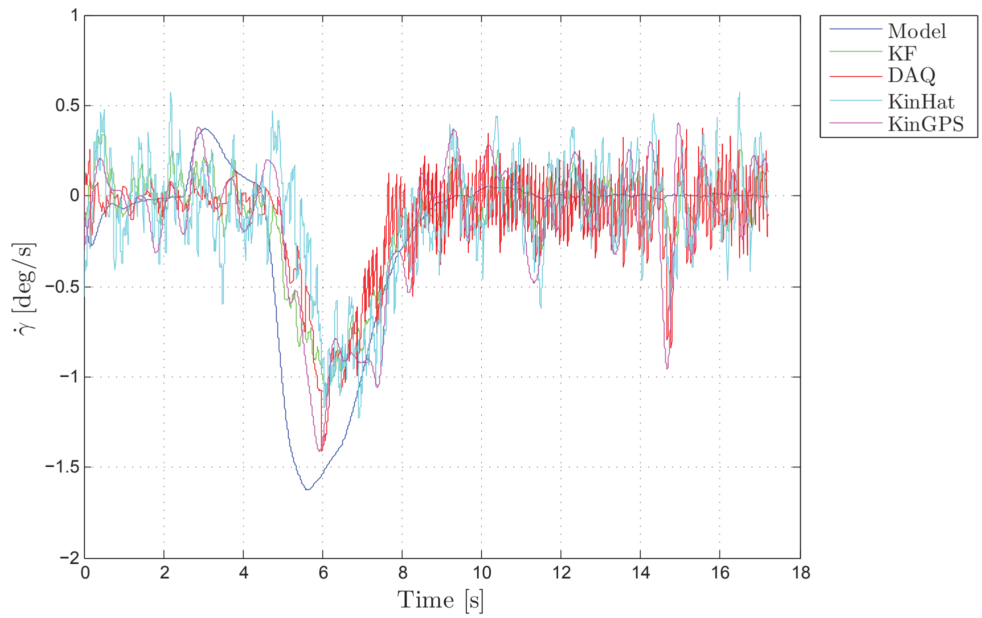

Figure 4.27: Ramp #1342 (Left, 0.1 g) Hitch Rate, Five-Axle Model Revision 4

4.5.1.2 Ramp and Hold, Model Revision 6

Figures 4.28–4.36 show the results using the Revision 6 model for ramp maneuver #1338. Figures 4.37–4.45 show the results using the Revision 6 model for ramp maneuver #1342. Close examination reveals that these curves are in fact distinct from those produced by the Revision 4 model, but no significant differences were observed.

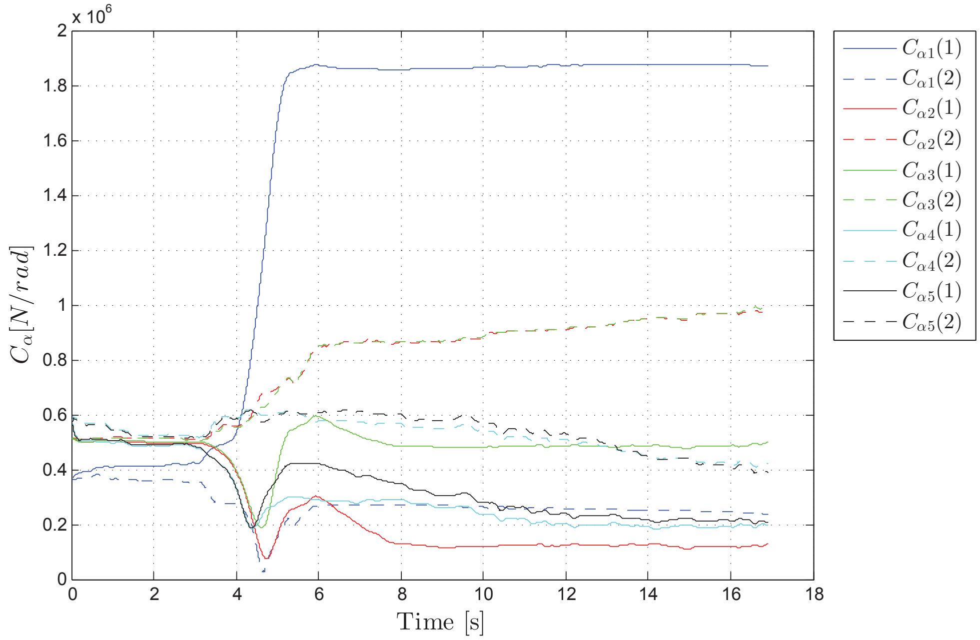

Figure 4.28: Ramp #1338 (Right, 0.2 g) Tire Cornering Stiffness Estimation, Five-Axle Model Revision 6

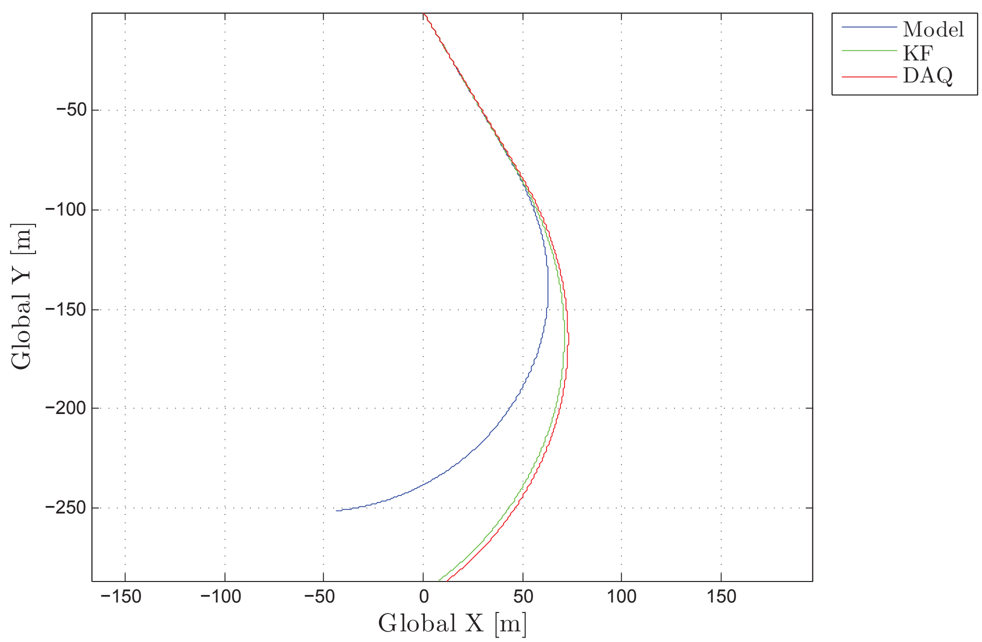

Figure 4.29: Ramp #1338 (Right, 0.2 g) Path Prediction, Five-Axle Model Revision 6

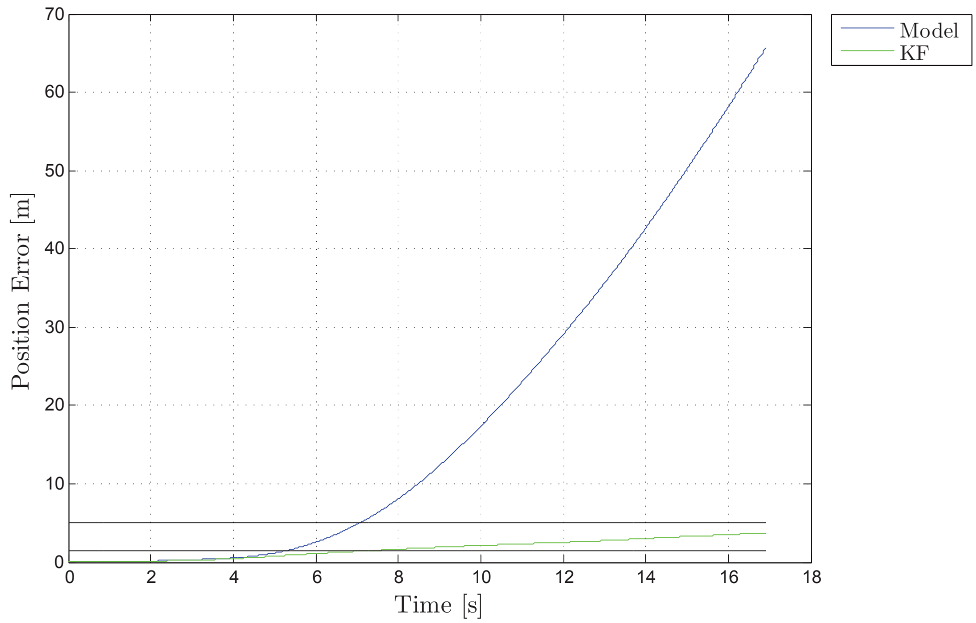

Figure 4.30: Ramp #1338 (Right, 0.2 g) Global Position Error, Five-Axle Model Revision 6

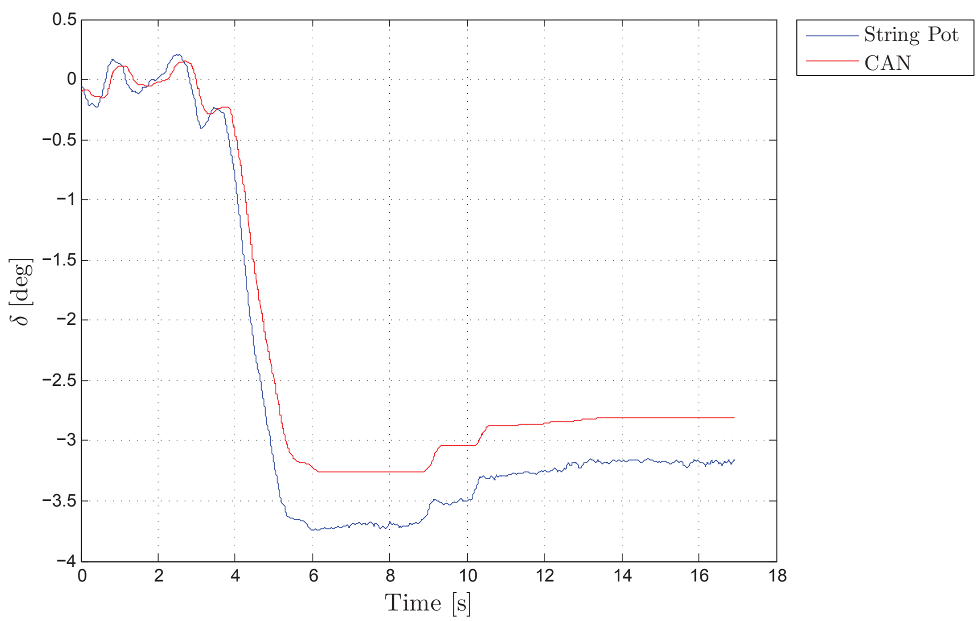

Figure 4.31: Ramp #1338 (Right, 0.2 g) Road Wheel Steering Angle, Five-Axle Model Revision 6

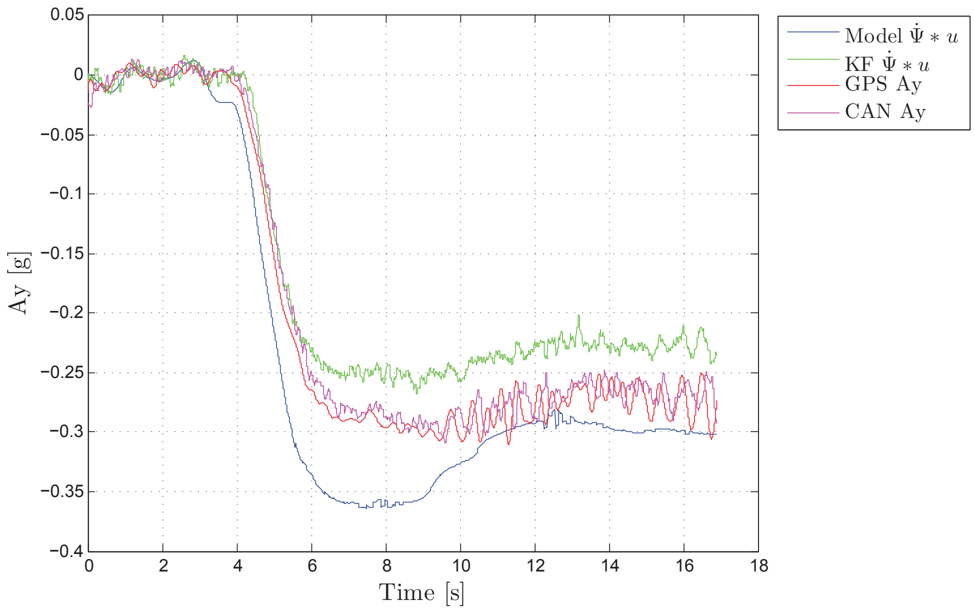

Figure 4.32: Ramp #1338 (Right, 0.2 g) Lateral Acceleration, Five-Axle Model Revision 6

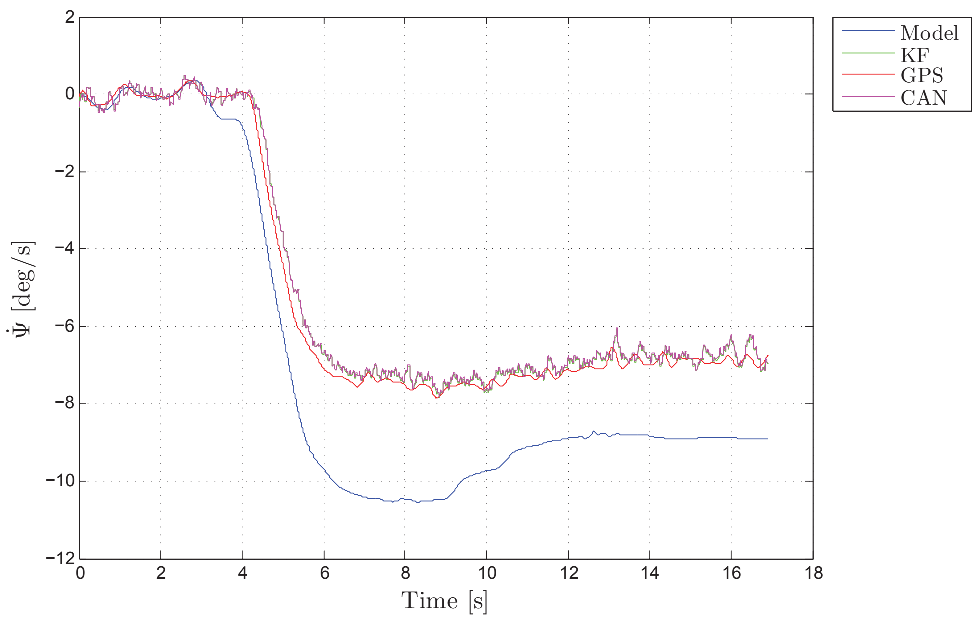

Figure 4.33: Ramp #1338 (Right, 0.2 g) Yaw Rate, Five-Axle Model Revision 6

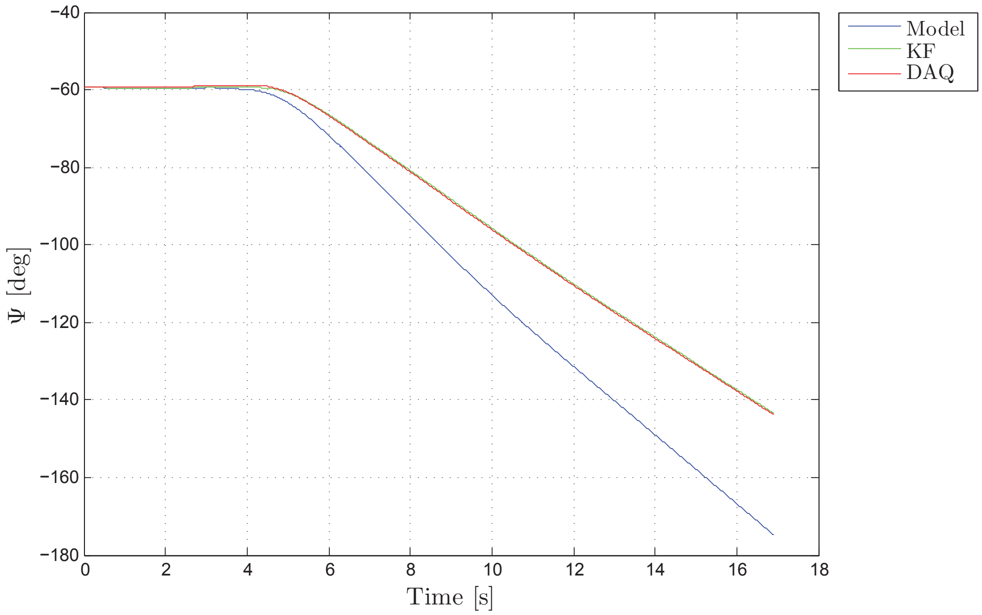

Figure 4.34: Ramp #1338 (Right, 0.2 g) Yaw Angle, Five-Axle Model Revision 6

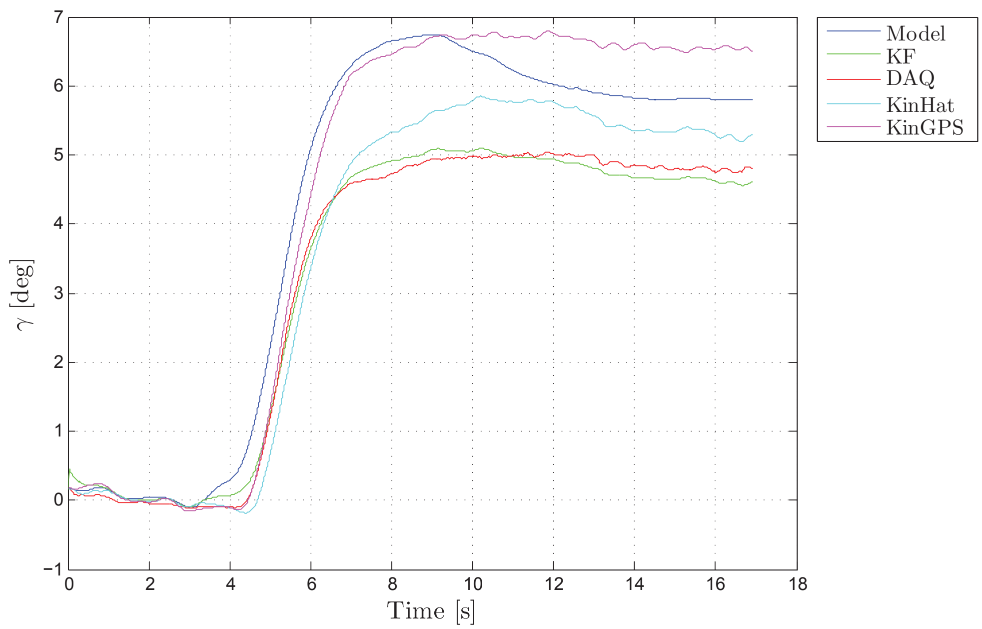

Figure 4.35: Ramp #1338 (Right, 0.2 g) Hitch Angle, Five-Axle Model Revision 6

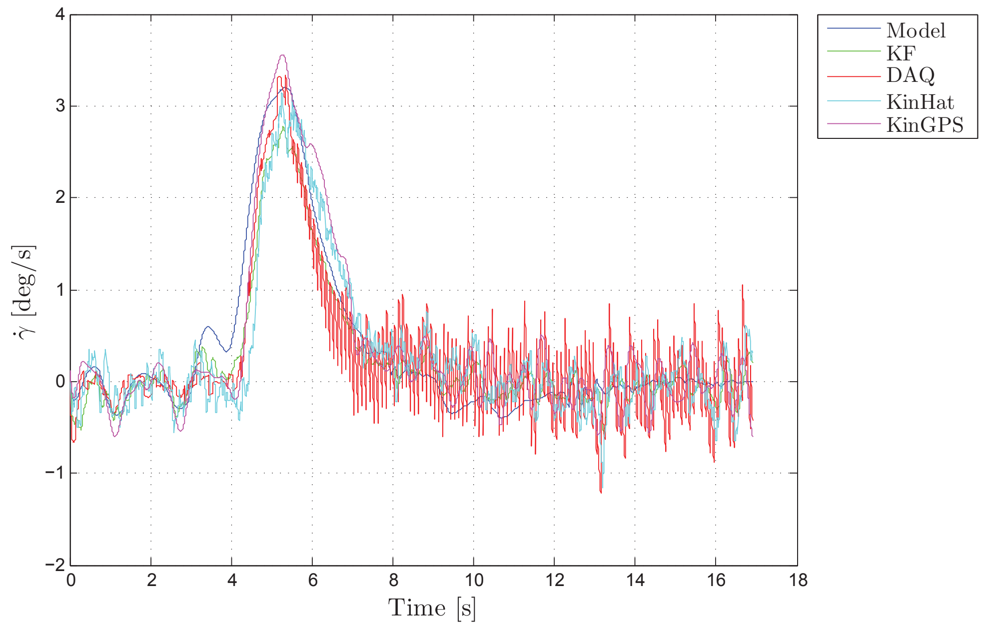

Figure 4.36: Ramp #1338 (Right, 0.2 g) Hitch Rate, Five-Axle Model Revision 6

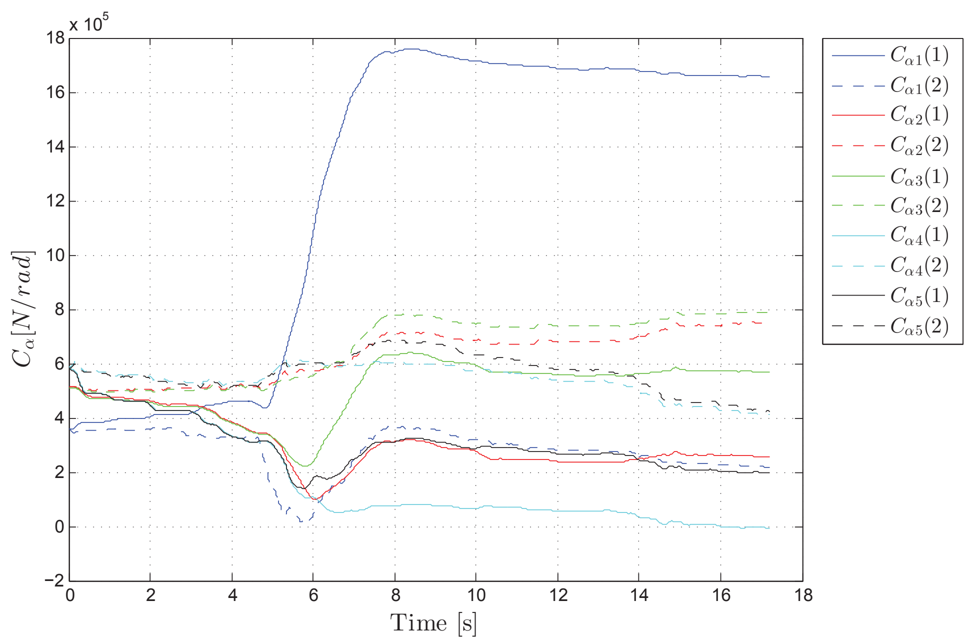

Figure 4.37: Ramp #1342 (Left, 0.1 g) Tire Cornering Stiffness Estimation, Five-Axle Model Revision 6

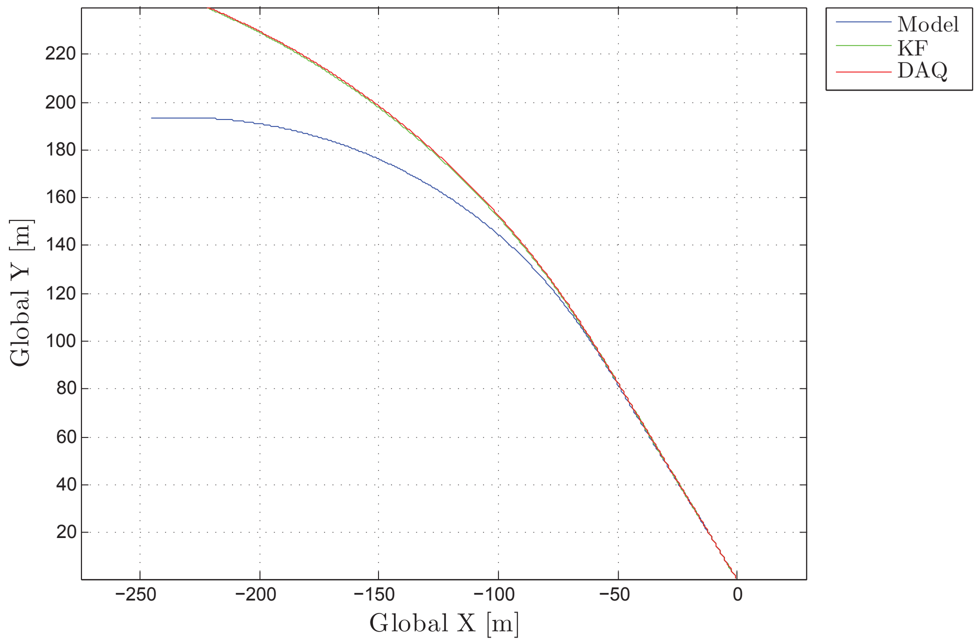

Figure 4.38: Ramp #1342 (Left, 0.1 g) Path Prediction, Five-Axle Model Revision 6

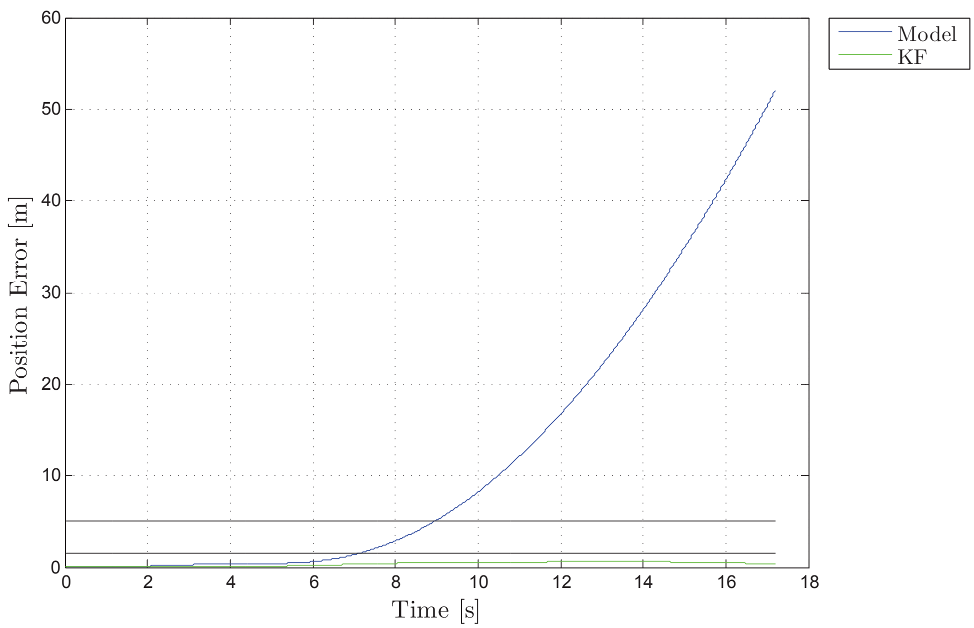

Figure 4.39: Ramp #1342 (Left, 0.1 g) Global Position Error, Five-Axle Model Revision 6

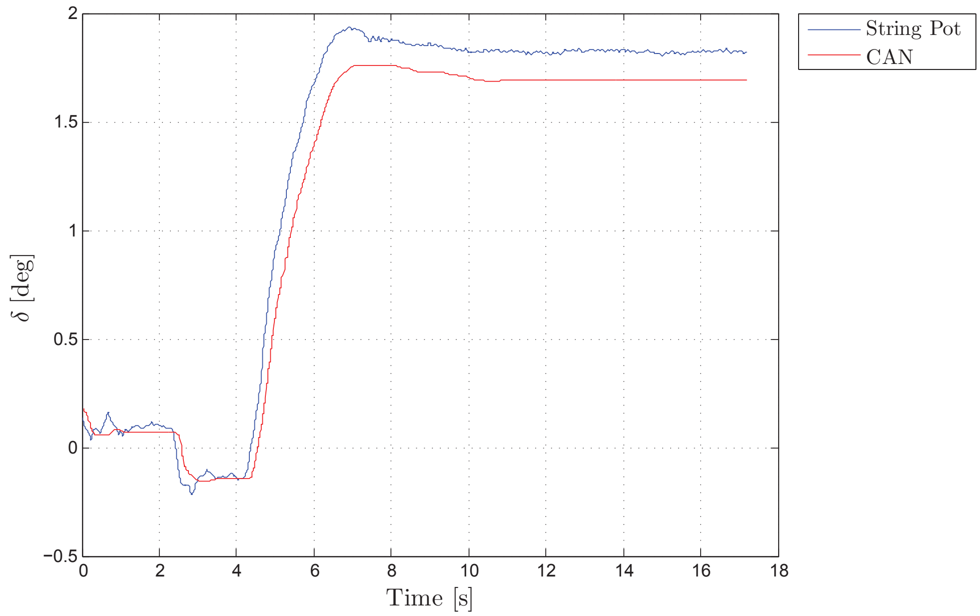

Figure 4.40: Ramp #1342 (Left, 0.1 g) Road Wheel Steering Angle, Five-Axle Model Revision 6

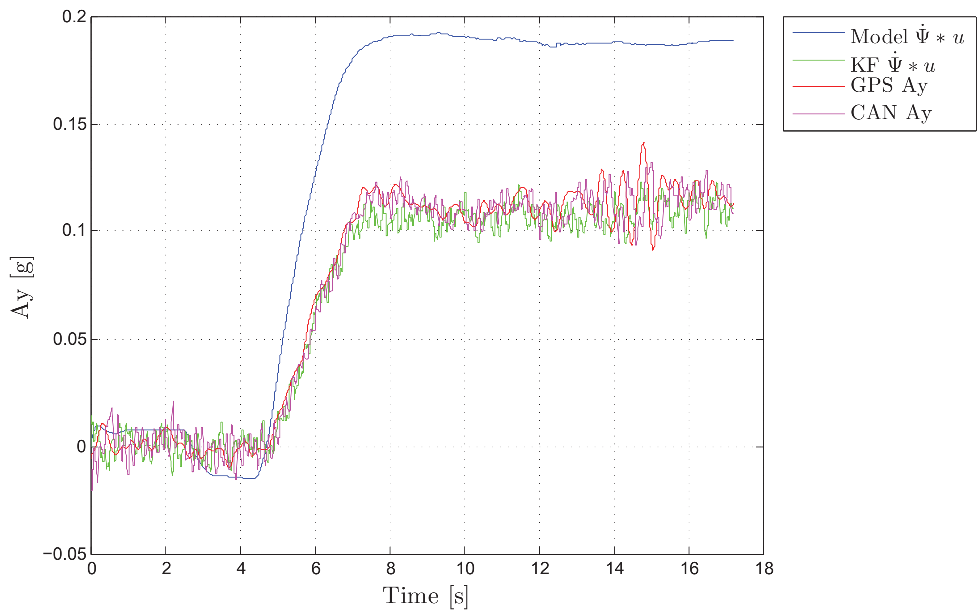

Figure 4.41: Ramp #1342 (Left, 0.1 g) Lateral Acceleration, Five-Axle Model Revision 6

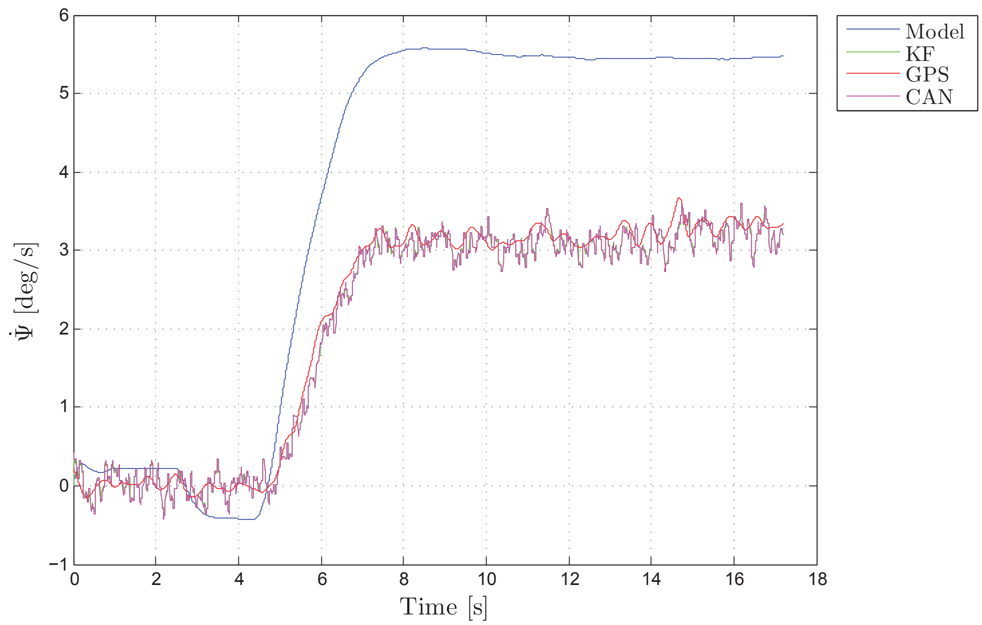

Figure 4.42: Ramp #1342 (Left, 0.1 g) Yaw Rate, Five-Axle Model Revision 6

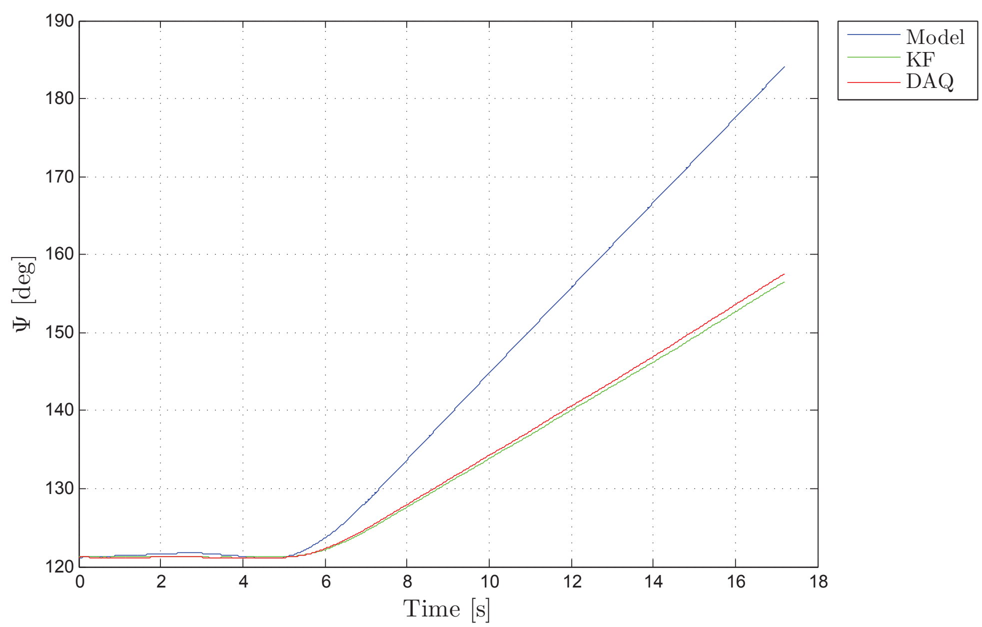

Figure 4.43: Ramp #1342 (Left, 0.1 g) Yaw Angle, Five-Axle Model Revision 6

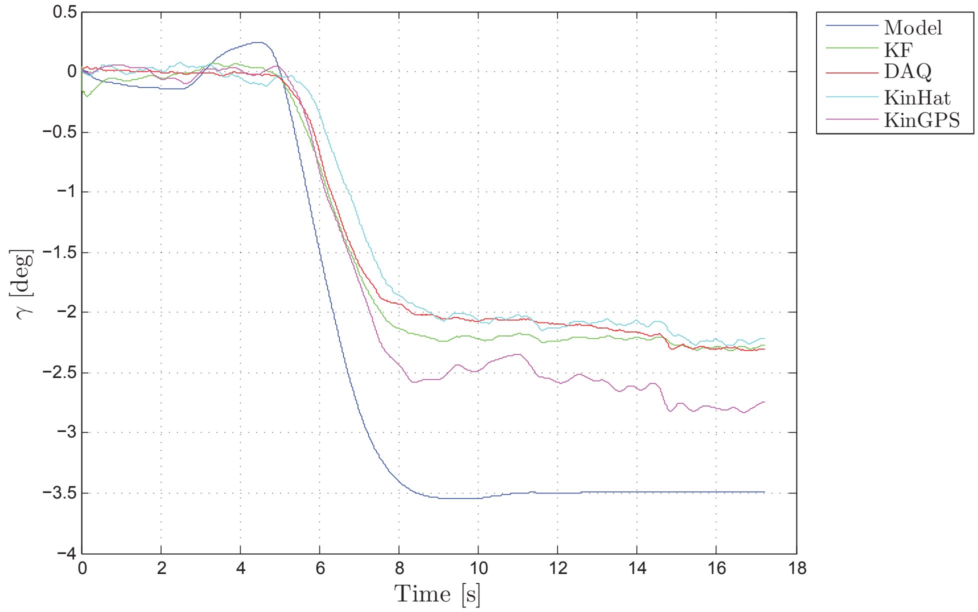

Figure 4.44: Ramp #1342 (Left, 0.1 g) Hitch Angle, Five-Axle Model Revision 6

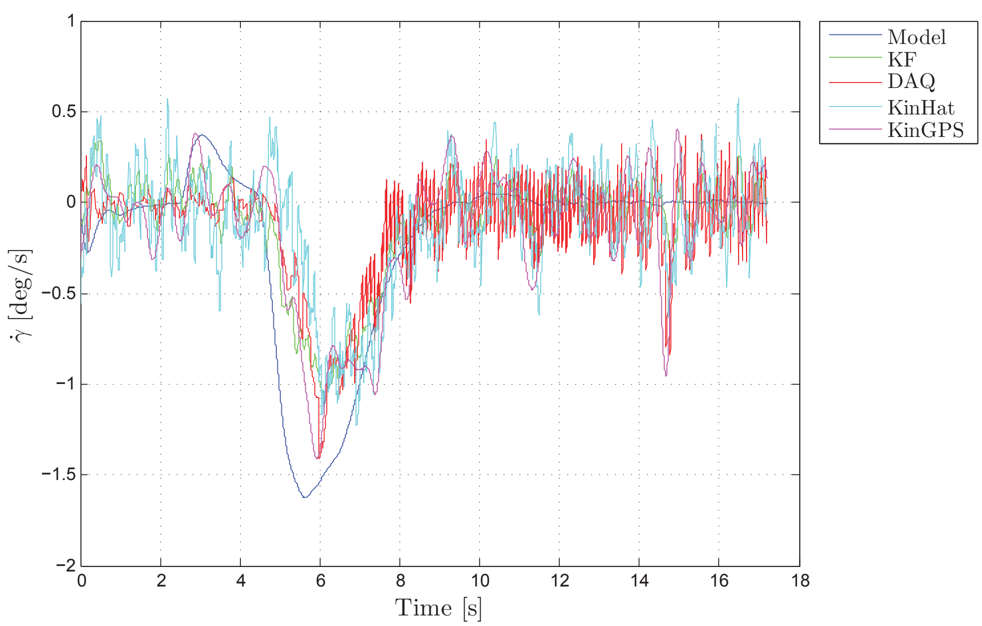

Figure 4.45: Ramp #1342 (Left, 0.1 g) Hitch Rate, Five-Axle Model Revision 6

4.5.2 Urban Driving Scenario

The urban driving scenario consists of straight driving; a 90-degree, 20 meter radius right turn; a 90-degree, 20 meter radius left turn; and then straight driving. The maneuver was run at two different speeds which were selected to produce nominal lateral accelerations of 0.1 and 0.2 g (16 and 22 kph respectively). This test was devised to test the ability of the system to locate the vehicle during GPS dropouts and accurately predict hitch angle during small radius (tight) turns. Urban environments are the most likely to lack GPS accuracy or even availability. They are also the most likely to have turns that result in high articulation angles. Accordingly, this is the location where this research may be most useful.

4.5.2.1 Urban Driving Scenario, Model Revision 4

Figures 4.46–4.53 show the results using the Revision 4 model for urban driving scenario #1325. This was a 0.1 g maneuver (16 kph). The algorithm was able to maintain lane-level positioning for the duration of the maneuver. As in other cases, the key to this accuracy is proper tracking of the heading angle shown in Figure 4.51. This is accomplished by having the Kalman filter trust the CAN-based yaw rate signal as seen in Figure 4.50. Error still accumulates, though, largely because this measurement is imperfect. The estimates of hitch angle for this maneuver can be seen in Figure 4.52. The estimate produced by the Kalman filter model is within 1.5 deg of the measured angle. The kinematic model is nearly perfect when using measured states and within about a tenth of a degree when using estimated states (from the Kalman filter).

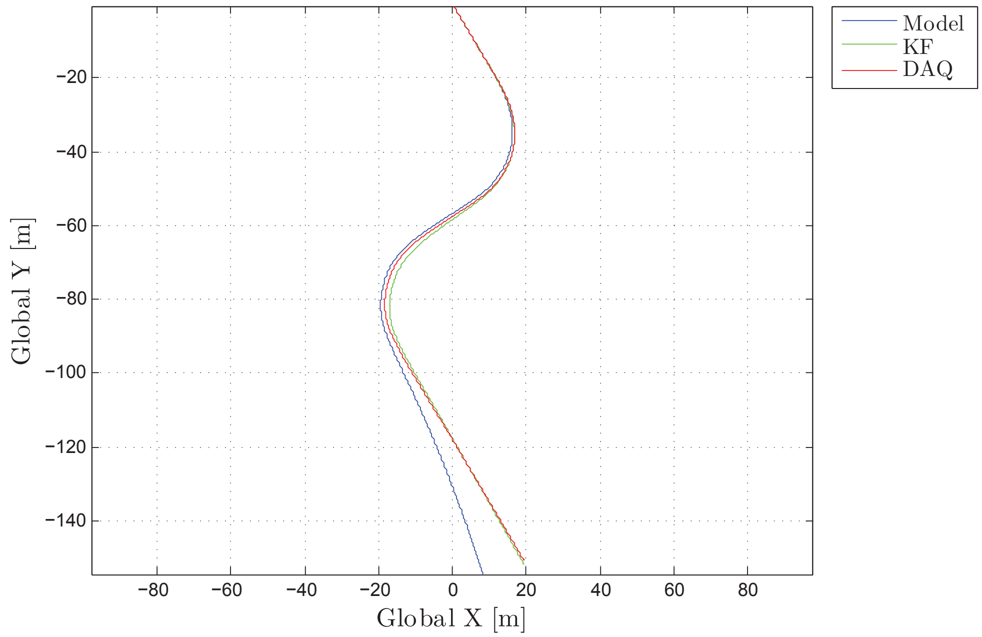

Figure 4.46: Urban Driving Scenario #1325 (0.1 g) Path Prediction, Five-Axle Model Revision 4

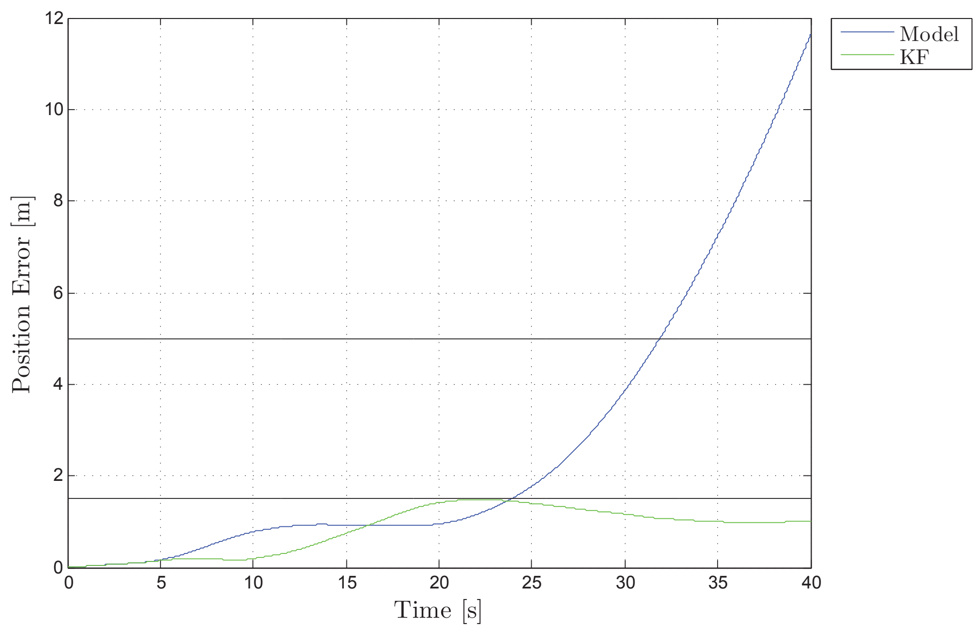

Figure 4.47: Urban Driving Scenario #1325 (0.1 g) Global Position Error, Five-Axle Model Revision 4

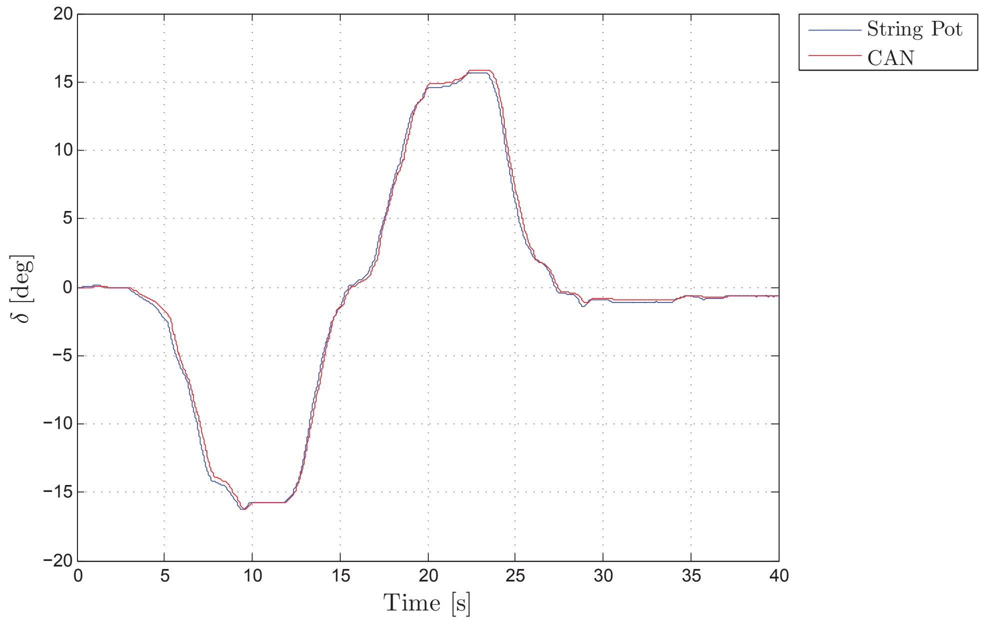

Figure 4.48: Urban Driving Scenario #1325 (0.1 g) Road Wheel Steering Angle, Five-Axle Model Revision 4

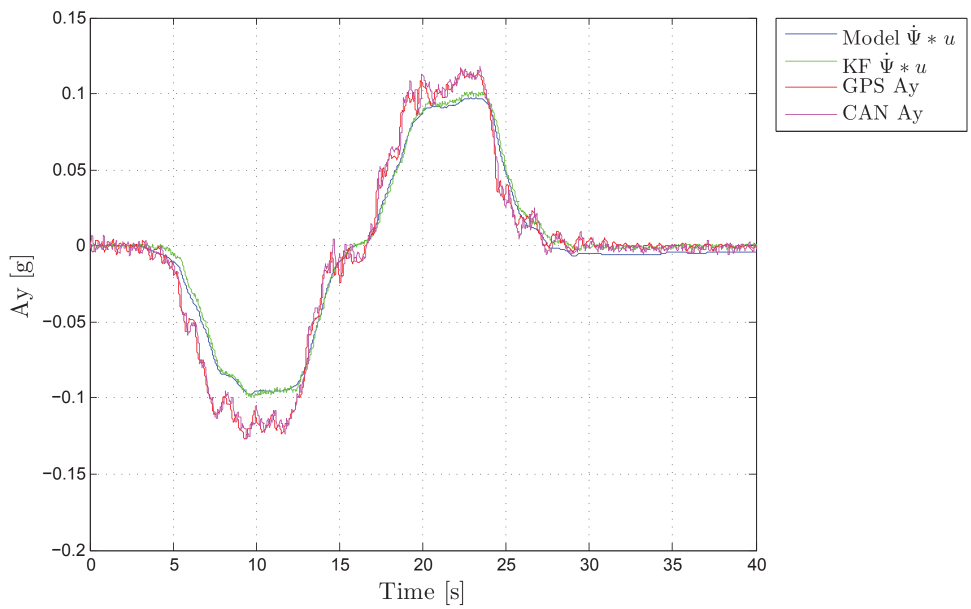

Figure 4.49: Urban Driving Scenario #1325 (0.1 g) Lateral Acceleration, Five-Axle Model Revision 4

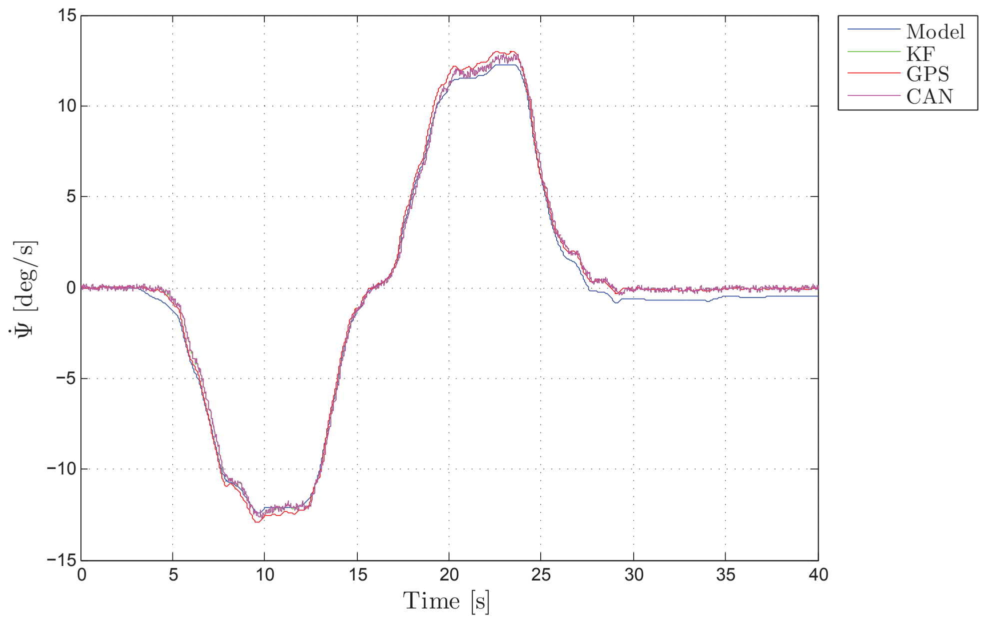

Figure 4.50: Urban Driving Scenario #1325 (0.1 g) Yaw Rate, Five-Axle Model Revision 4

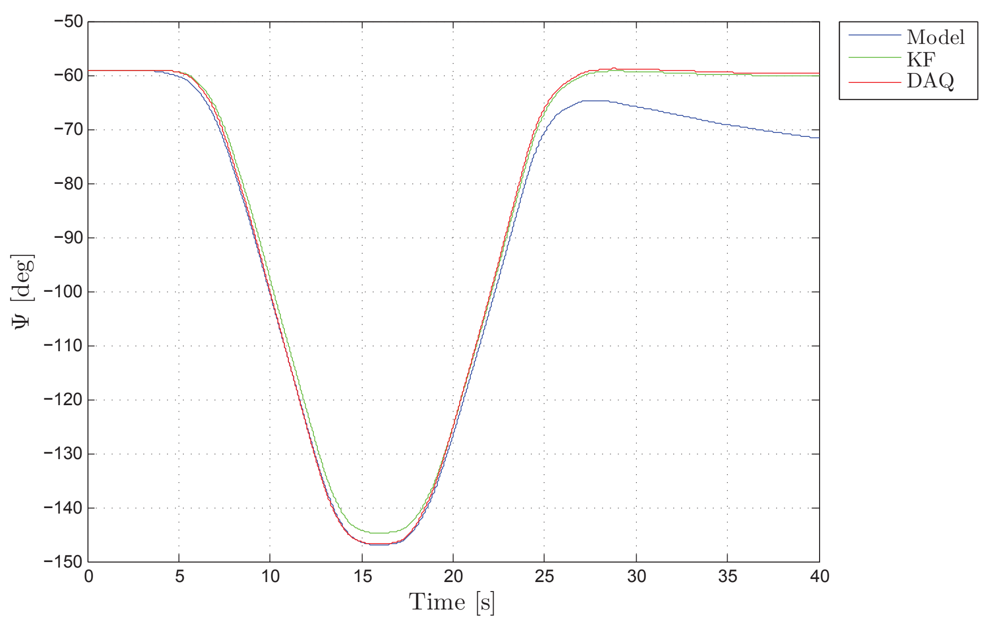

Figure 4.51: Urban Driving Scenario #1325 (0.1 g) Yaw Angle, Five-Axle Model Revision 4

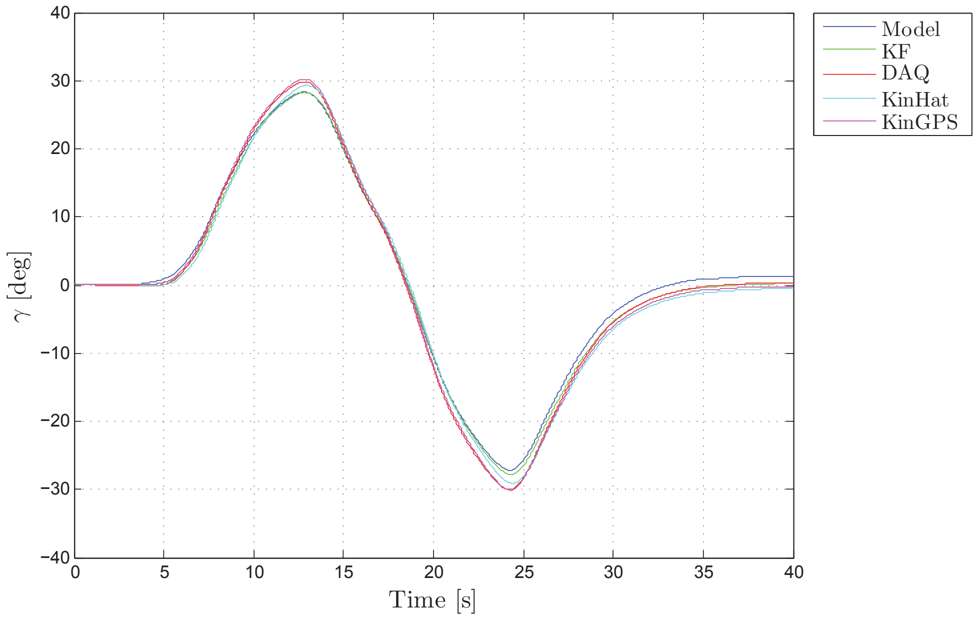

Figure 4.52: Urban Driving Scenario #1325 (0.1 g) Hitch Angle, Five-Axle Model Revision 4

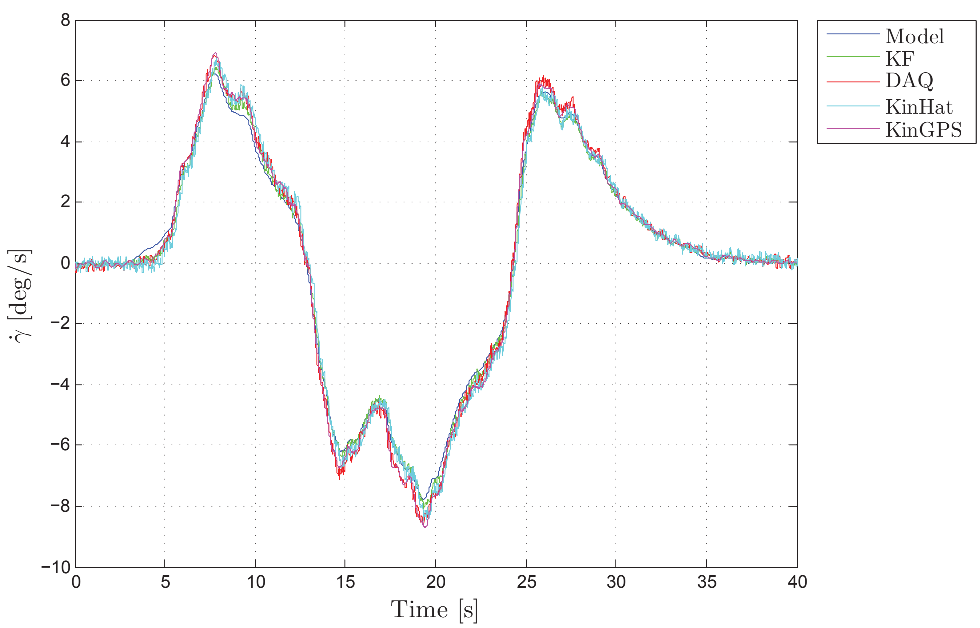

Figure 4.53: Urban Driving Scenario #1325 (0.1 g) Hitch Rate, Five-Axle Model Revision 4

Figures 4.54–4.61 show the results using the Revision 4 model for urban driving scenario #1329. This was a 0.2 g maneuver (22 kph). The algorithm was able to maintain lane-level positioning for the duration of the maneuver. The estimates of hitch angle for this maneuver can be seen in Figure 4.60. The estimate produced by the Kalman filter model is off by up to 2.4 deg, but the kinematic model (using estimated states) is within half of a degree. When using measured states, the kinematic model is nearly perfect.

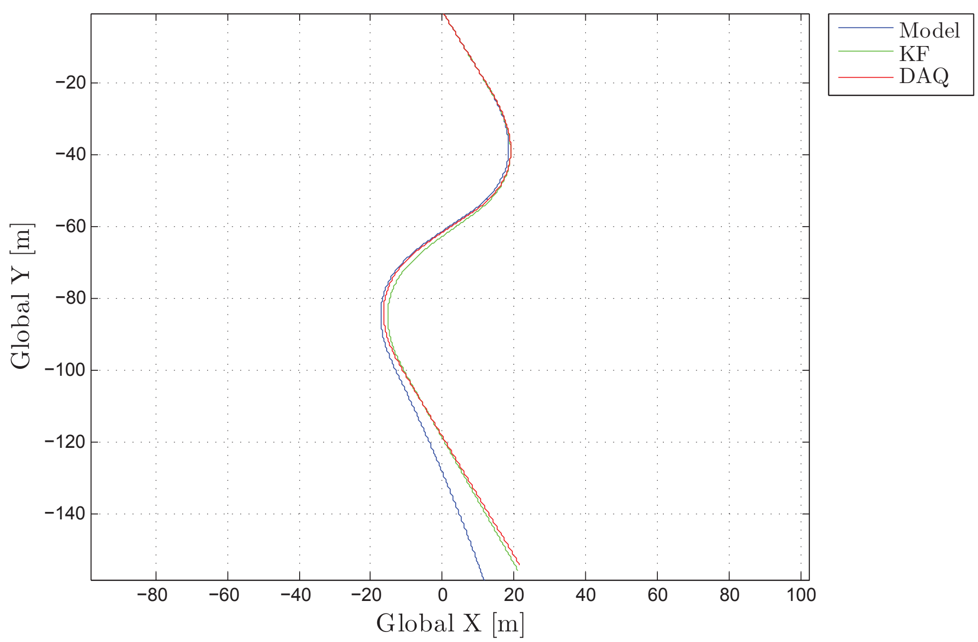

Figure 4.54: Urban Driving Scenario #1329 (0.2 g) Path Prediction, Five-Axle Model Revision 4

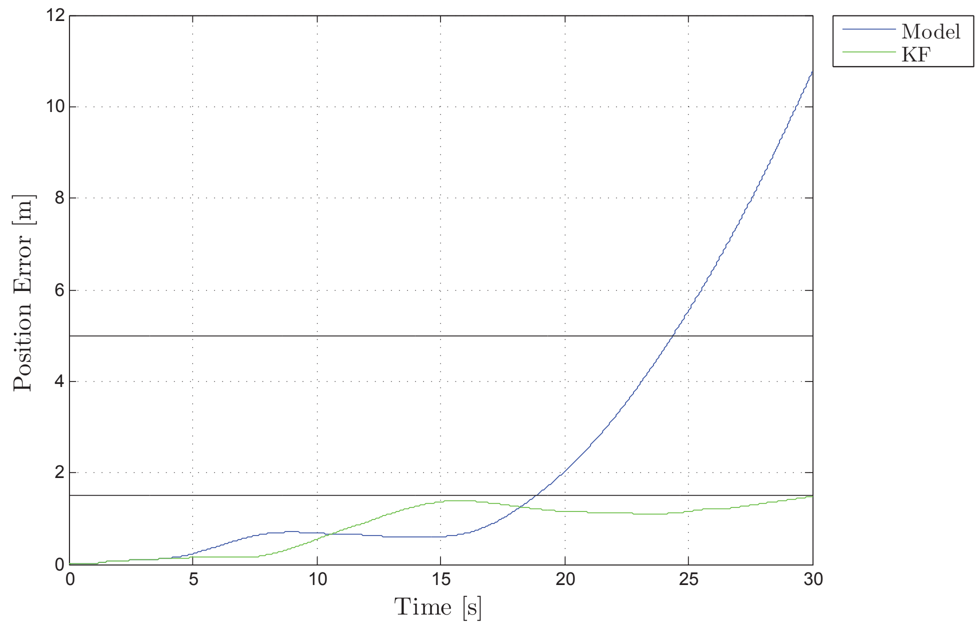

Figure 4.55: Urban Driving Scenario #1329 (0.2 g) Global Position Error, Five-Axle Model Revision 4

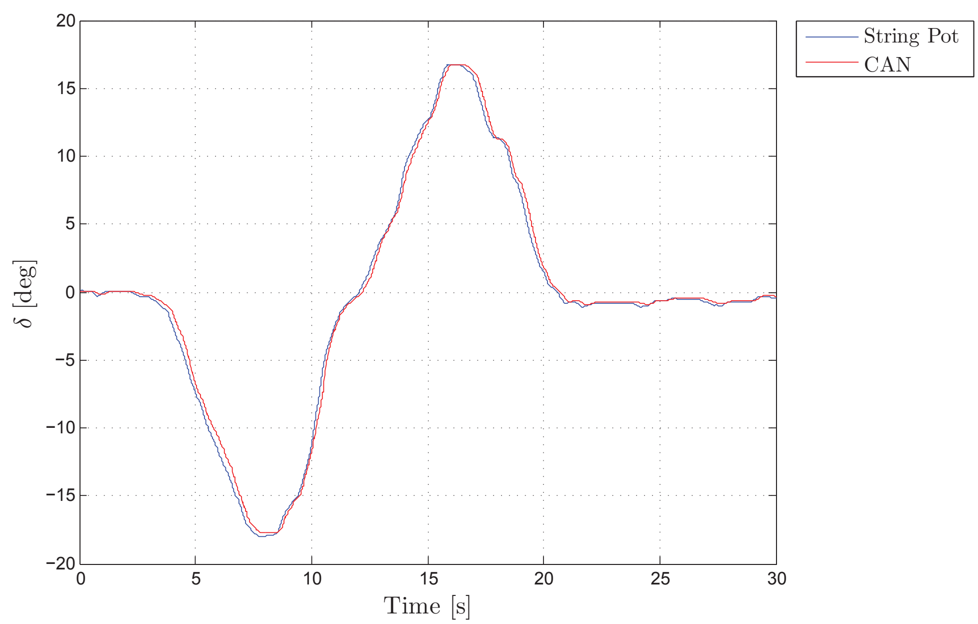

Figure 4.56: Urban Driving Scenario #1329 (0.2 g) Road Wheel Steering Angle, Five-Axle Model Revision 4

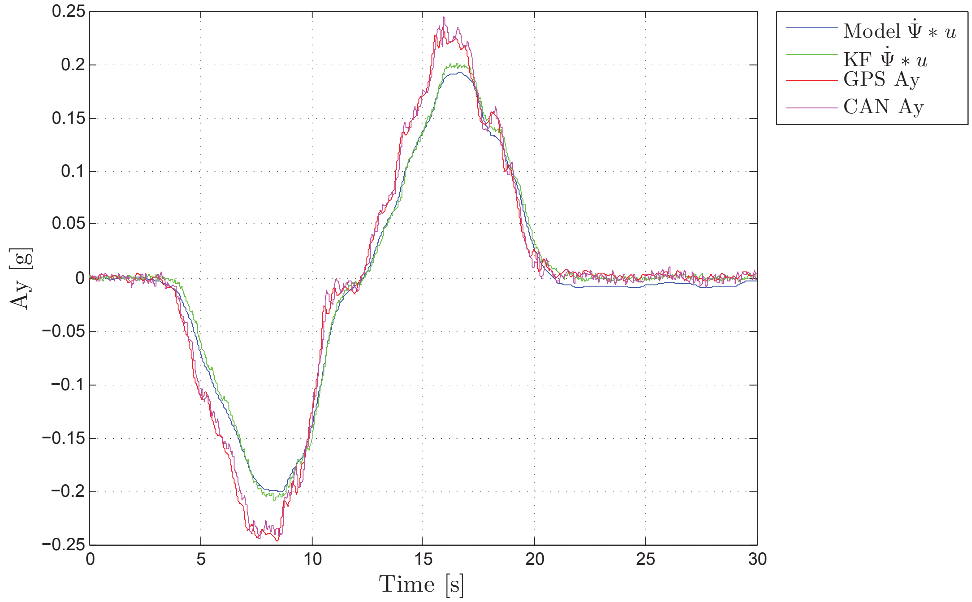

Figure 4.57: Urban Driving Scenario #1329 (0.2 g) Lateral Acceleration, Five-Axle Model Revision 4

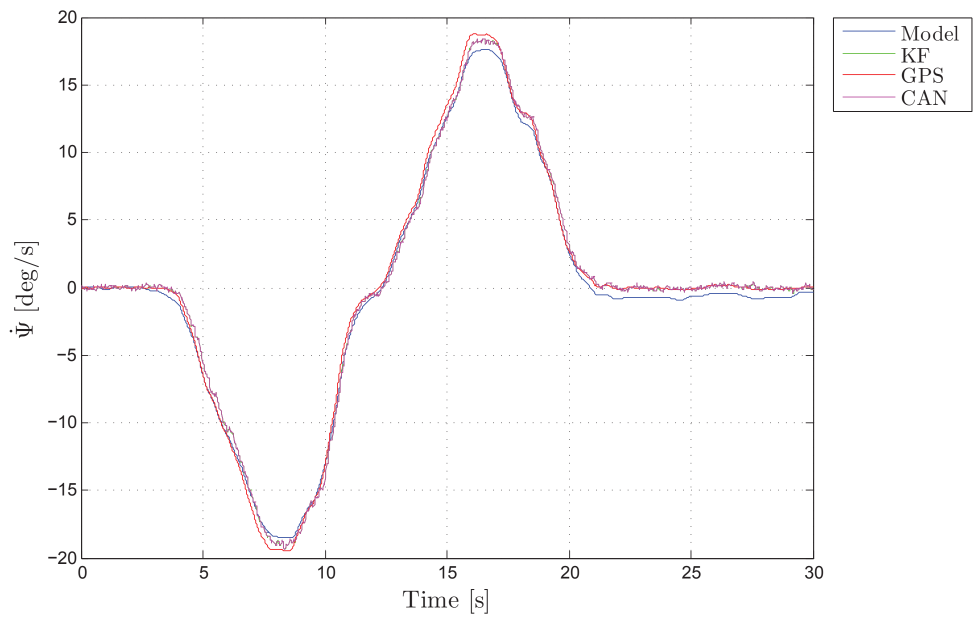

Figure 4.58: Urban Driving Scenario #1329 (0.2 g) Yaw Rate, Five-Axle Model Revision 4

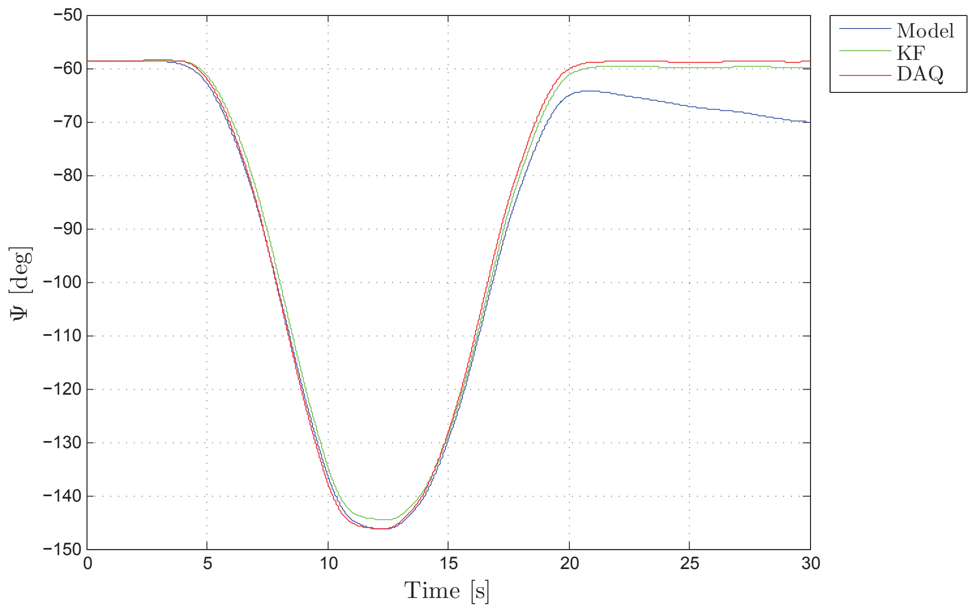

Figure 4.59: Urban Driving Scenario #1329 (0.2 g) Yaw Angle, Five-Axle Model Revision 4

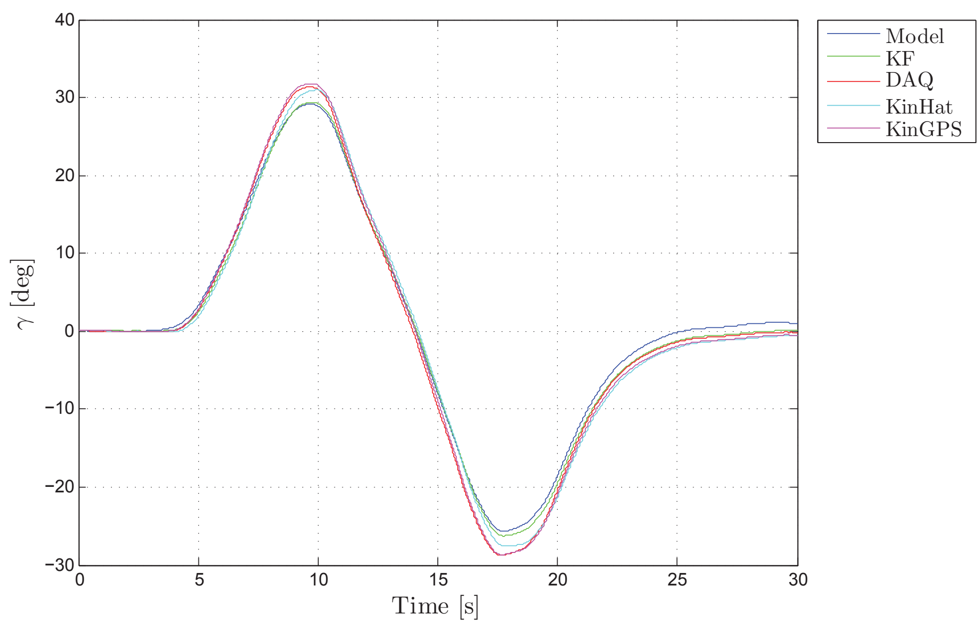

Figure 4.60: Urban Driving Scenario #1329 (0.2 g) Hitch Angle, Five-Axle Model Revision 4

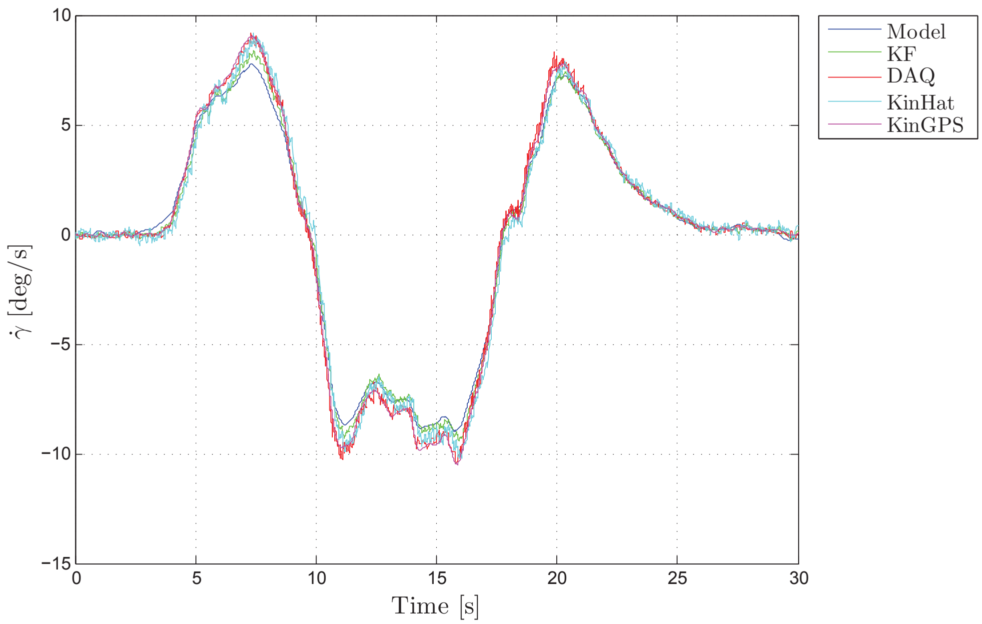

Figure 4.61: Urban Driving Scenario #1329 (0.2 g) Hitch Rate, Five-Axle Model Revision 4

4.5.2.2 Urban Driving Scenario, Model Revision 6

Figures 4.62–4.69 show the results using the Revision 6 model for urban driving scenario #1325. The positioning accuracy is unaffected by the model change, but the hitch angle prediction is worsened. Figure 4.68 shows that the hitch angle estimated by the Kalman filter model is about three and a half degrees less than the measured hitch angle at the second peak (although the kinematic models remain within one degree of the measured hitch angle). In contrast, the hitch angle estimate produced by the Kalman filter of the Revision 4 model was only off by 1.5 deg.

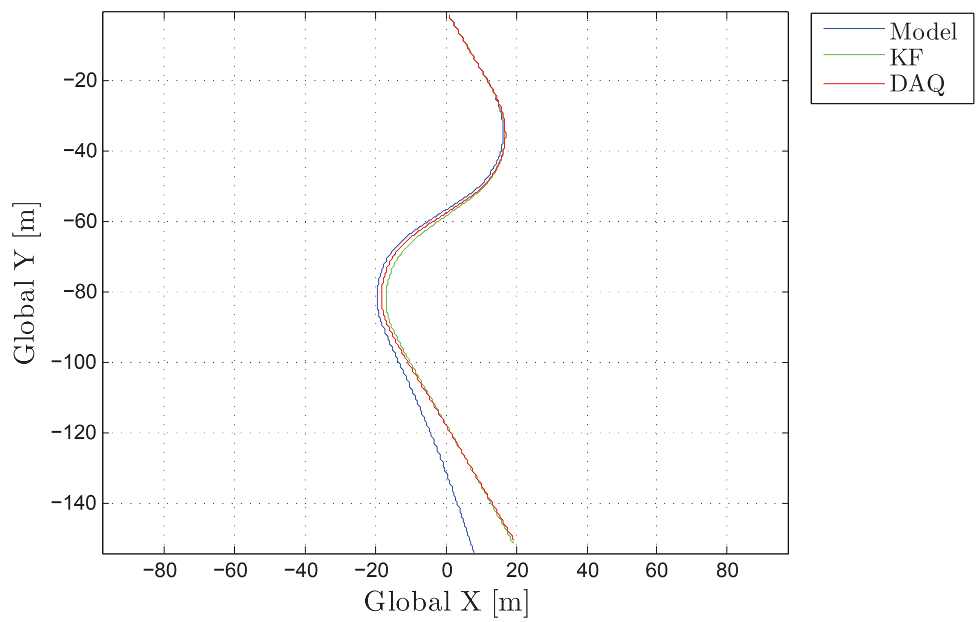

Figure 4.62: Urban Driving Scenario #1325 (0.1 g) Path Prediction, Five-Axle Model Revision 6

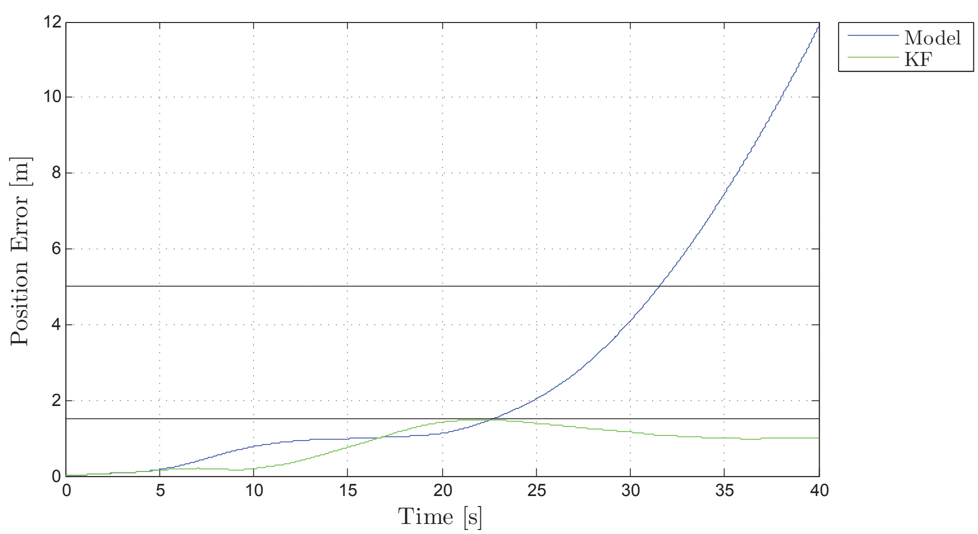

Figure 4.63: Urban Driving Scenario #1325 (0.1 g) Global Position Error, Five-Axle Model Revision 6

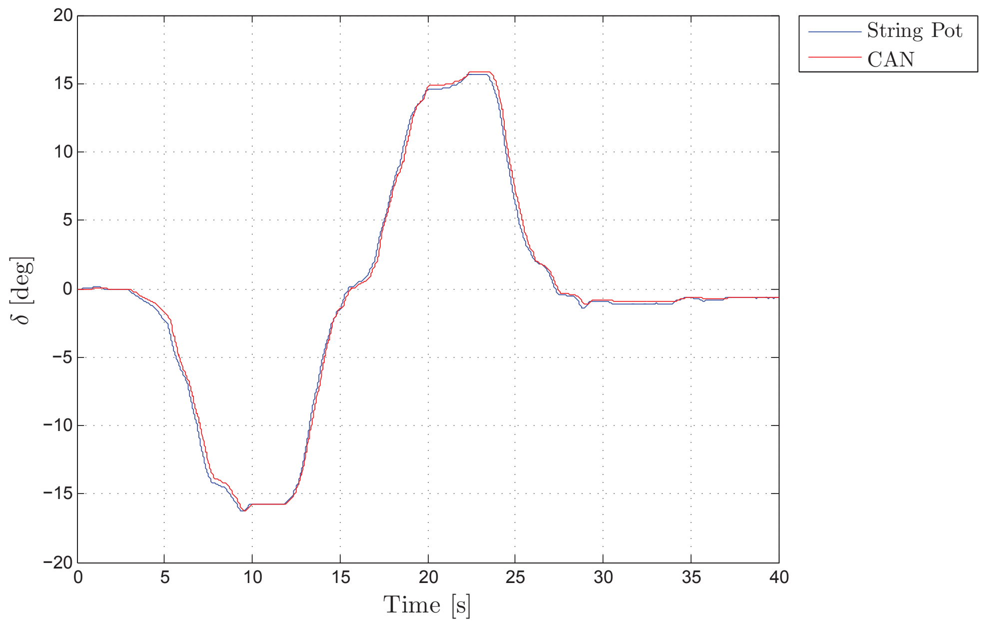

Figure 4.64: Urban Driving Scenario #1325 (0.1 g) Road Wheel Steering Angle, Five-Axle Model Revision 6

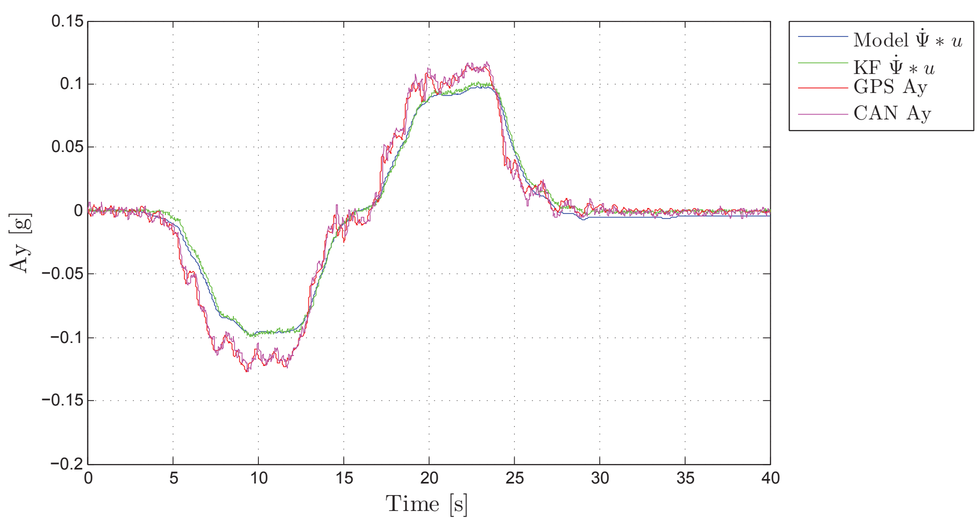

Figure 4.65: Urban Driving Scenario #1325 (0.1 g) Lateral Acceleration, Five-Axle Model Revision 6

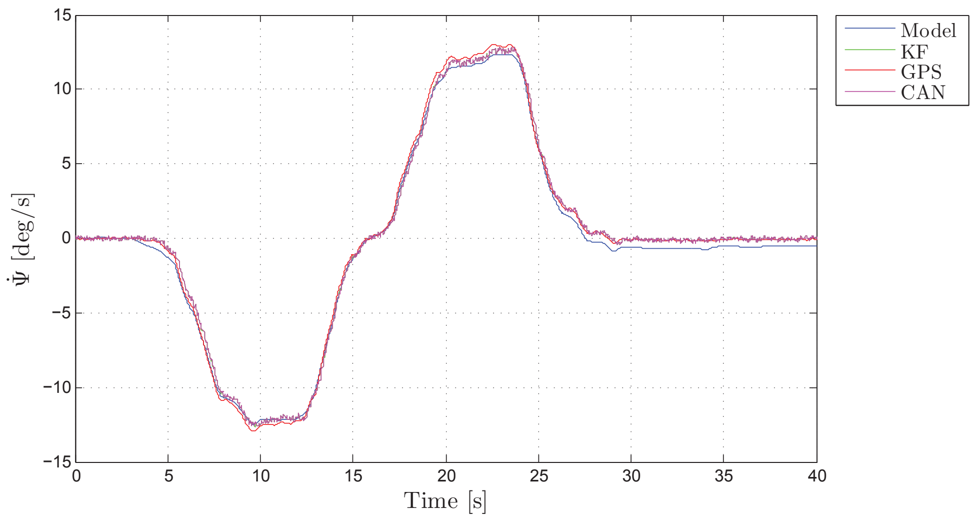

Figure 4.66: Urban Driving Scenario #1325 (0.1 g) Yaw Rate, Five-Axle Model Revision 6

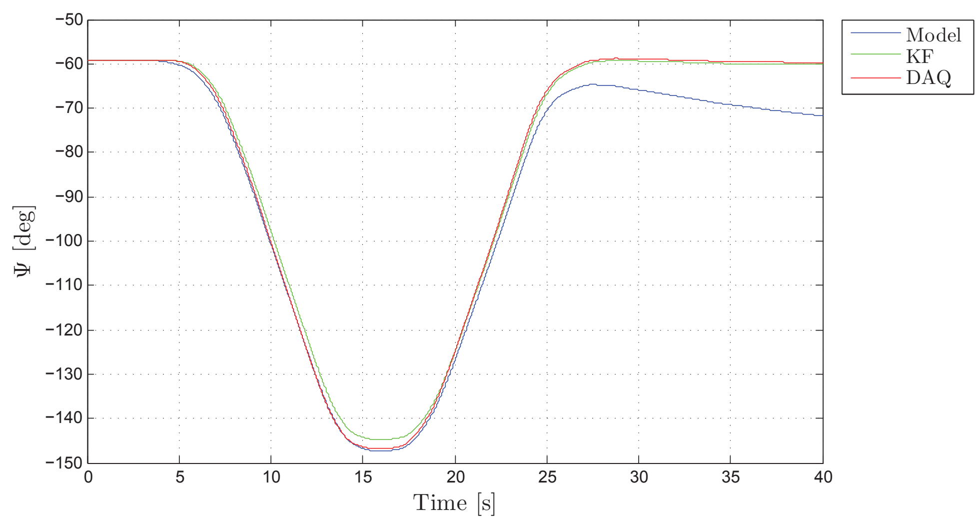

Figure 4.67: Urban Driving Scenario #1325 (0.1 g) Yaw Angle, Five-Axle Model Revision 6

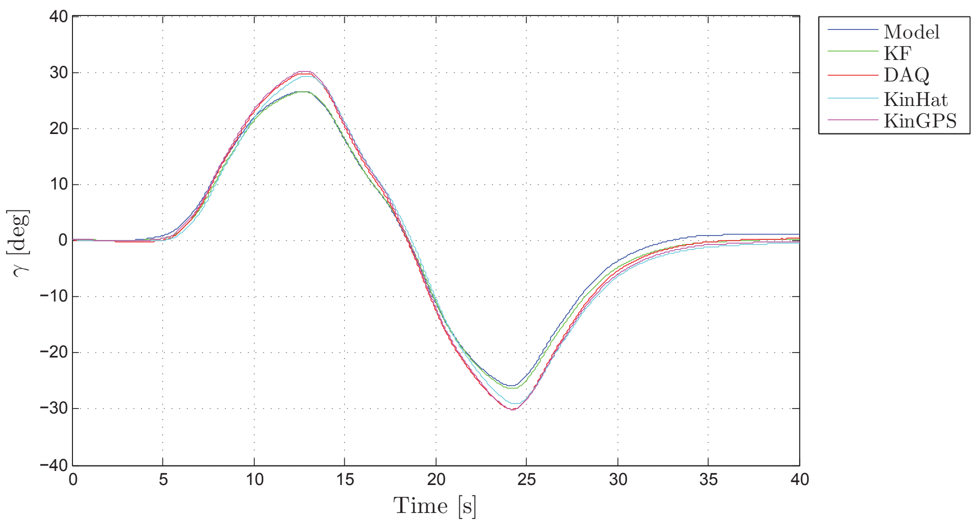

Figure 4.68: Urban Driving Scenario #1325 (0.1 g) Hitch Angle, Five-Axle Model Revision 6

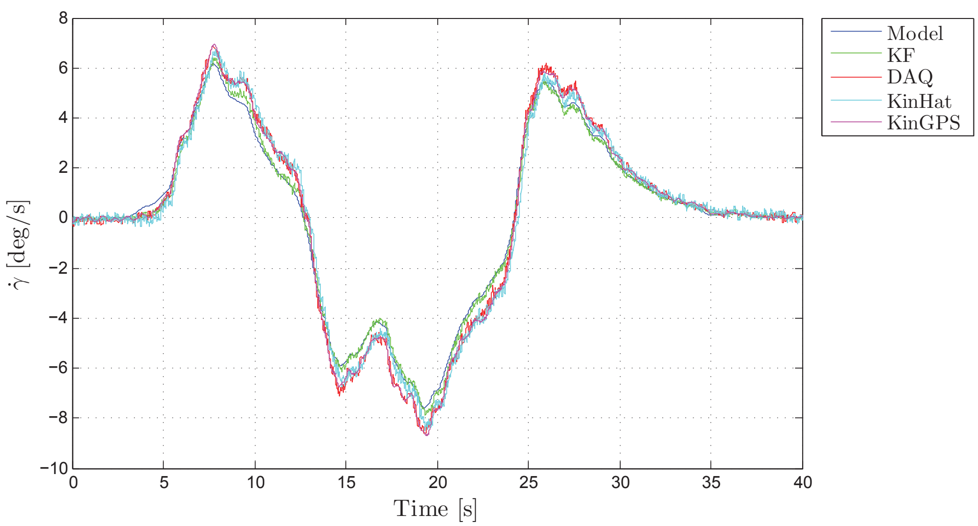

Figure 4.69: Urban Driving Scenario #1325 (0.1 g) Hitch Rate, Five-Axle Model Revision 6

Figures 4.70–4.77 show the results using the Revision 6 model for urban driving scenario #1329. Results were similar to using the Revision 6 model on the previous scenario (#1325), i.e. lane-level positioning accuracy was maintained for the duration of the scenario, but hitch angle prediction using the dynamic model ('KF') was up to four degrees off of the measured value. The hitch angle estimated by the kinematic model using estimated states ('KinHat') was relatively unaffected.

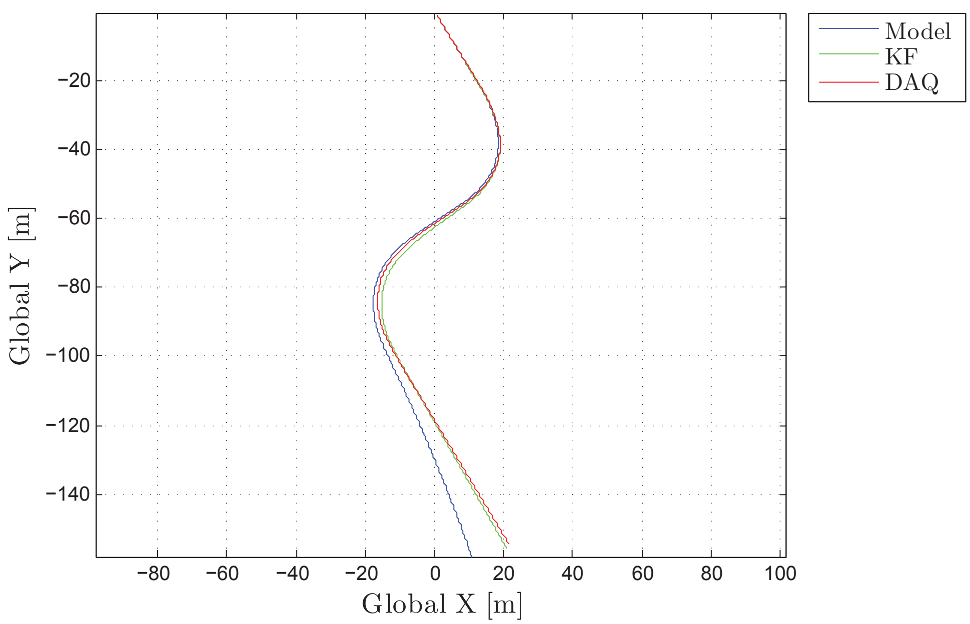

Figure 4.70: Urban Driving Scenario #1329 (0.2 g) Path Prediction, Five-Axle Model Revision 6

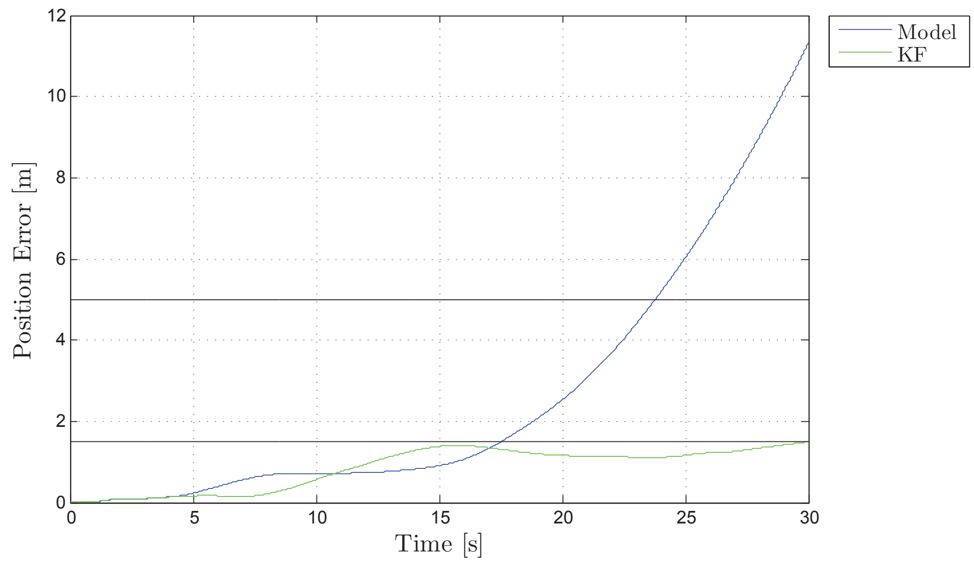

Figure 4.71: Urban Driving Scenario #1329 (0.2 g) Global Position Error, Five-Axle Model Revision 6

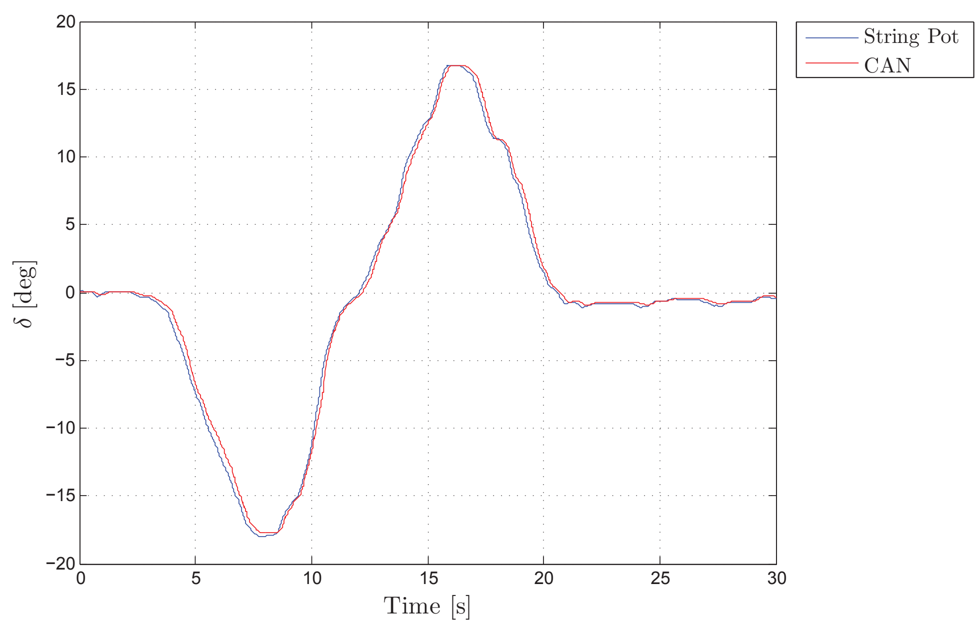

Figure 4.72: Urban Driving Scenario #1329 (0.2 g) Road Wheel Steering Angle, Five-Axle Model Revision 6

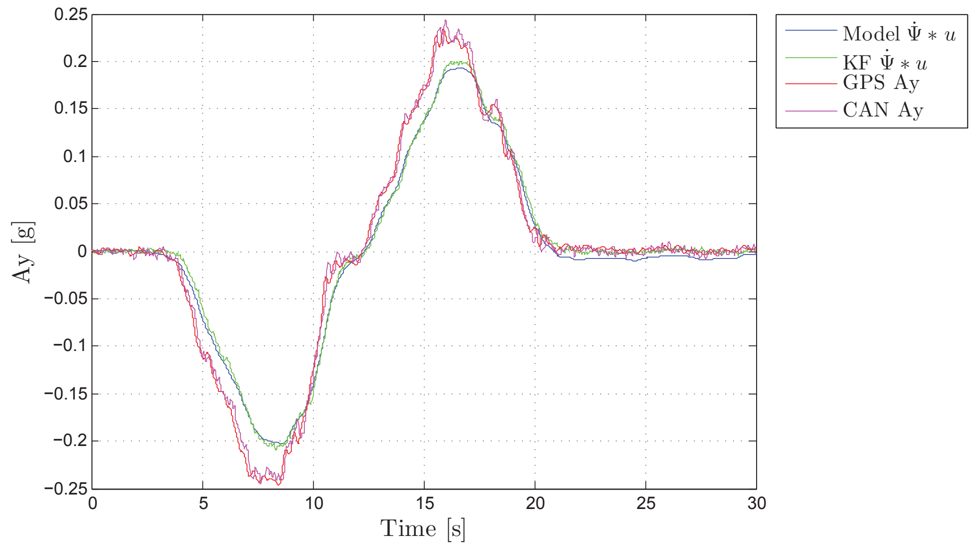

Figure 4.73: Urban Driving Scenario #1329 (0.2 g) Lateral Acceleration, Five-Axle Model Revision 6

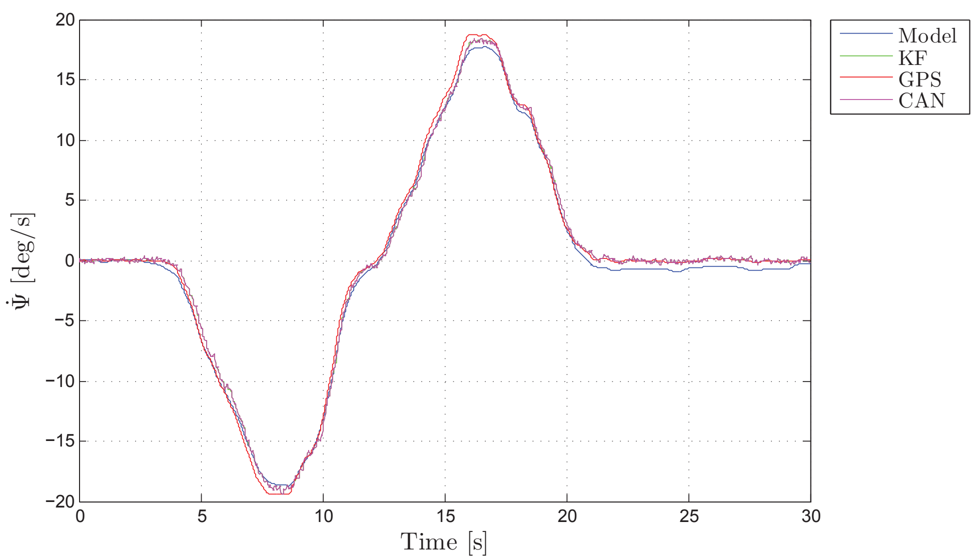

Figure 4.74: Urban Driving Scenario #1329 (0.2 g) Yaw Rate, Five-Axle Model Revision 6

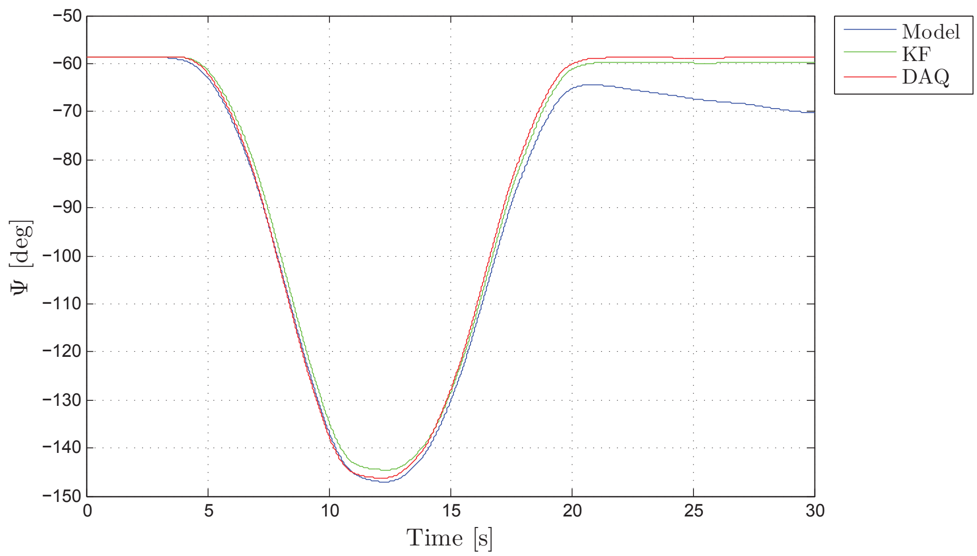

Figure 4.75: Urban Driving Scenario #1329 (0.2 g) Yaw Angle, Five-Axle Model Revision 6

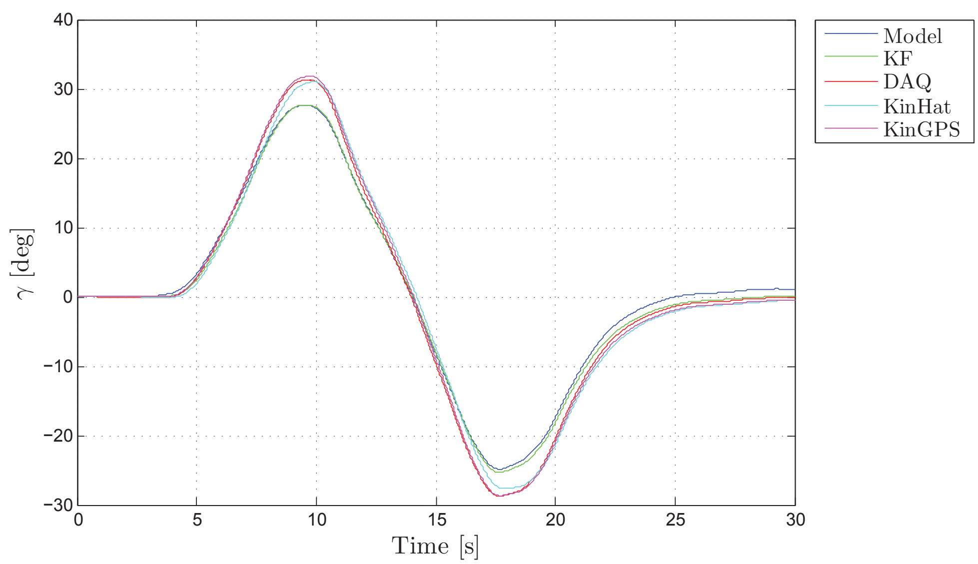

Figure 4.76: Urban Driving Scenario #1329 (0.2 g) Hitch Angle, Five-Axle Model Revision 6

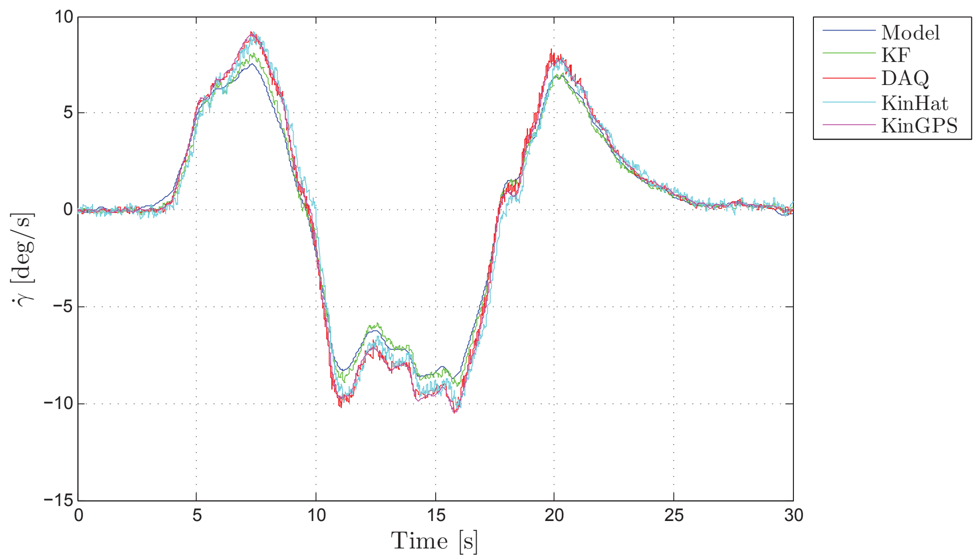

Figure 4.77: Urban Driving Scenario #1329 (0.2 g) Hitch Rate, Five-Axle Model Revision 6

4.5.3 Highway Driving Scenario

The highway driving scenario consists of straight driving; a 180-degree, 732 meter (2400 ft) radius right turn; and straight driving. The speed for this maneuver was 100 kph. GPS visibility is usually quite good during highway driving. However, a single GPS on the tractor cannot measure the articulation angle of the heavy truck. Therefore, the purpose of this test is primarily to test the ability of the estimator to accurately estimate small hitch angles during highway driving.

Although data for several runs were collected, only one trial was found usable after post-processing. As seen in Figure 4.6, there is a bridge crossing the track near the 1.0 mile marker. Passing underneath this bridge caused a lack of satellite visibility, and as a result the data taken from the north end of this loop were useless. Additionally, slow-moving test vehicles caused the driver to abort some of of the maneuvers from the south end of the track, leaving one ‘good’ run.

4.5.3.1 Highway Driving Scenario, Model Revision 4

Figures 4.78–4.86 show the results of the highway driving scenario using the Revision 4 model. It is clear from Figures 4.78 and 4.79 that the positioning accuracy is not suitable for locating the vehicle for the duration of the maneuver. Figure 4.80 shows that the position estimate is lane-level accurate for approximately 20 s and road-level accurate for approximately 28 s.

This maneuver highlights some of the challenges of modeling a real vehicle during highway driving. Figure 4.81 shows how ‘noisy’ the steer angle tends to be. Since this plot shows two independent measurements, we can surmise that this is actual driver behavior and not the defect of a sensor. However, the behavior of the vehicle is not reflective of this noisy input. By comparing the steering input to the open-loop model lateral acceleration trace in Figure 4.82, we can see that the model is predicting larger variations in lateral acceleration than those experienced by the vehicle. (The fact that the measured lateral acceleration is altogether lower than the estimated lateral acceleration is due to the bank angle the vehicle is traveling on.) Variations in yaw rate, Figure 4.83 exhibit a similar trend, i.e. lower variation than what the change in steer angle would cause one to expect. The lack of response by the vehicle suggests that though these variations are really occurring in the *handwheel* steer angle, they are not really present in the *road wheel* steer angle. This is because moving the steering through the lash in the steering gear box will change the handwheel steer angle without changing the road wheel steer angle. This will cause significant variations in hand wheel steer angle to be present in the data even during straight line driving. Figure 4.83 shows how the Kalman filter is able to cope with this problem. Another possible solution would be to measure the road wheel steer angle (i.e. tierod movement) as opposed to hand wheel angle.

Figure 4.85 shows the estimates of hitch angle for this maneuver. Due to the high speed, this was only about 1.5 deg. Surprisingly, the kinematic model that relies on estimated signals is significantly more accurate than the model relying on measured signals. The 'KinHat' model is within a few tenths of a degree, and the Kalman filter model is within about half of a degree. It is worth noting that the goal for accuracy of hitch angle estimation was ±2 deg, which is satisfied by zero (straight-truck assumption).

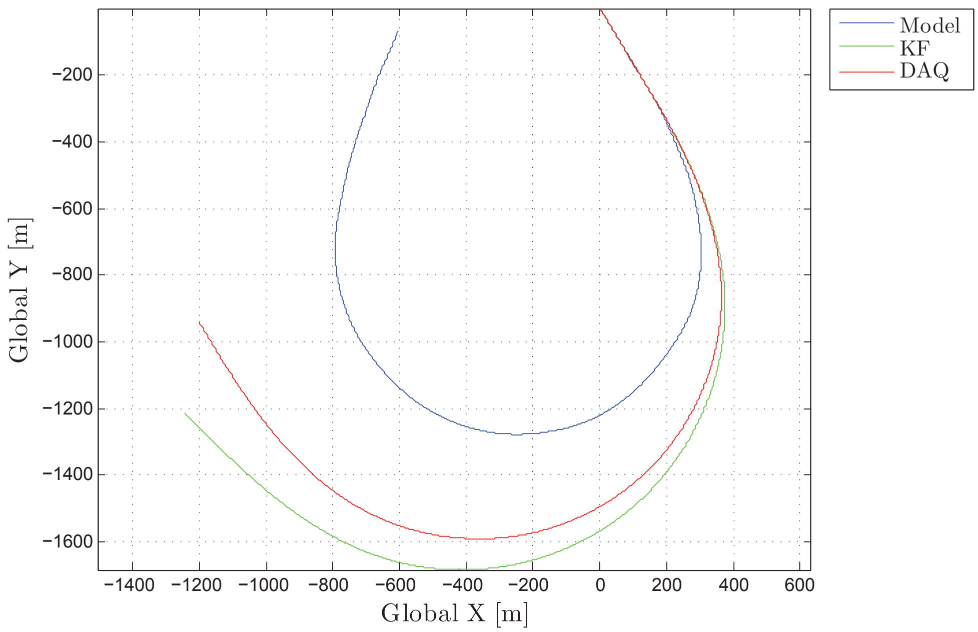

Figure 4.78: Highway Driving Scenario Path Prediction, Five-Axle Model Revision 4

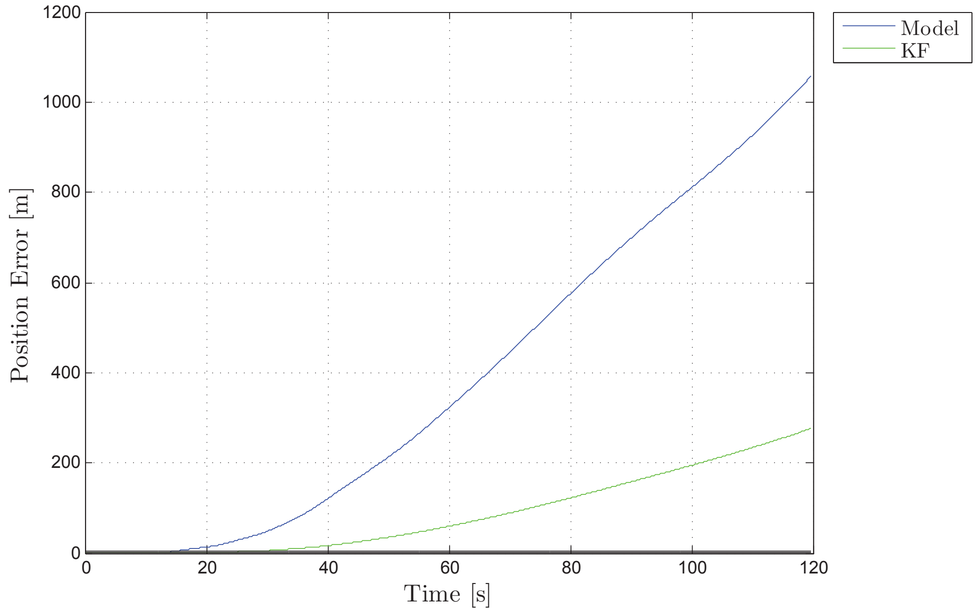

Figure 4.79: Highway Driving Scenario Global Position Error, Five-Axle Model Revision 4

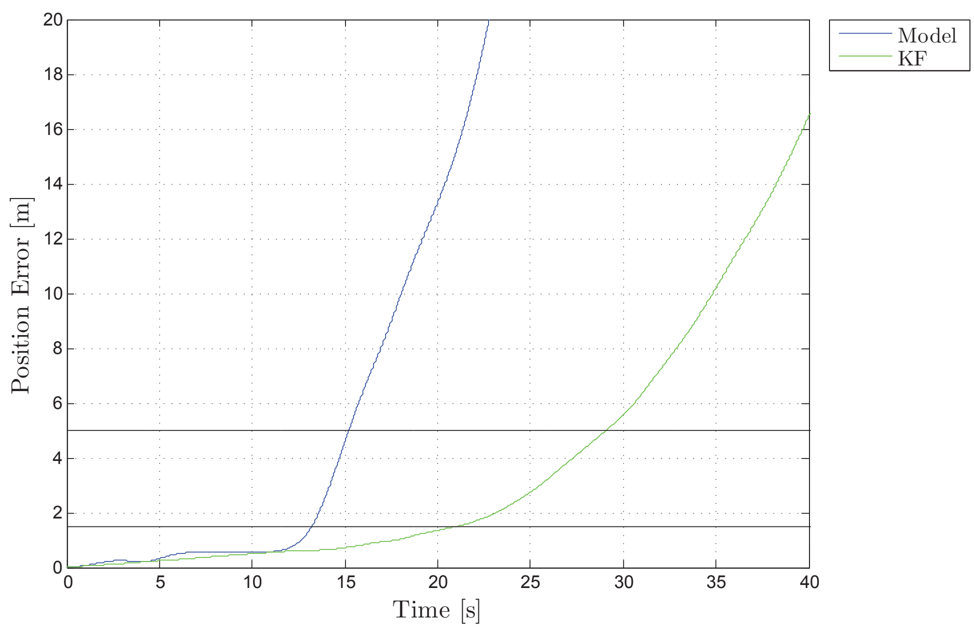

Figure 4.80: Highway Driving Scenario Global Position Error (scale smaller), Five-Axle Model Revision 4

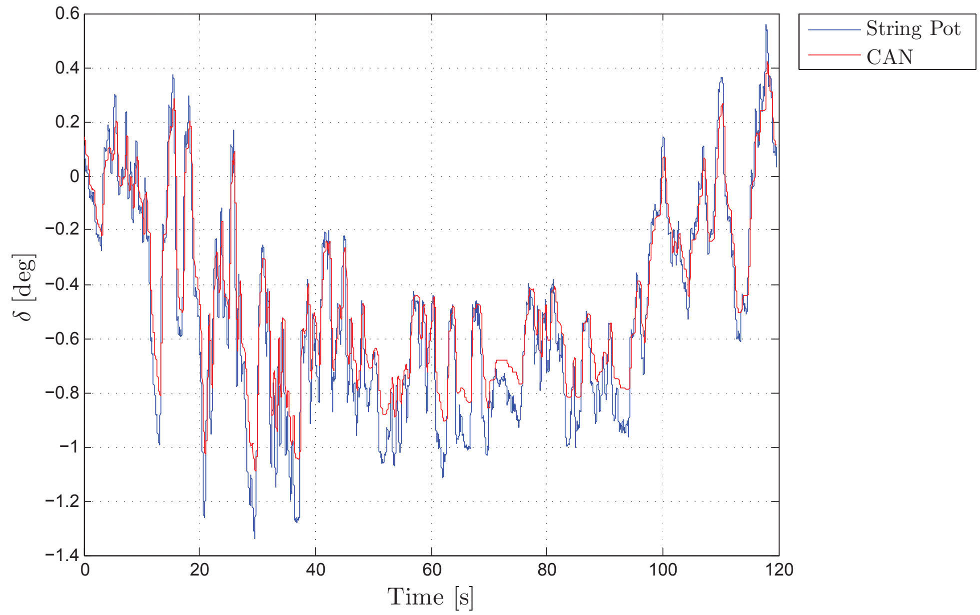

Figure 4.81: Highway Driving Scenario Road Wheel Steering Angle, Five-Axle Model Revision 4

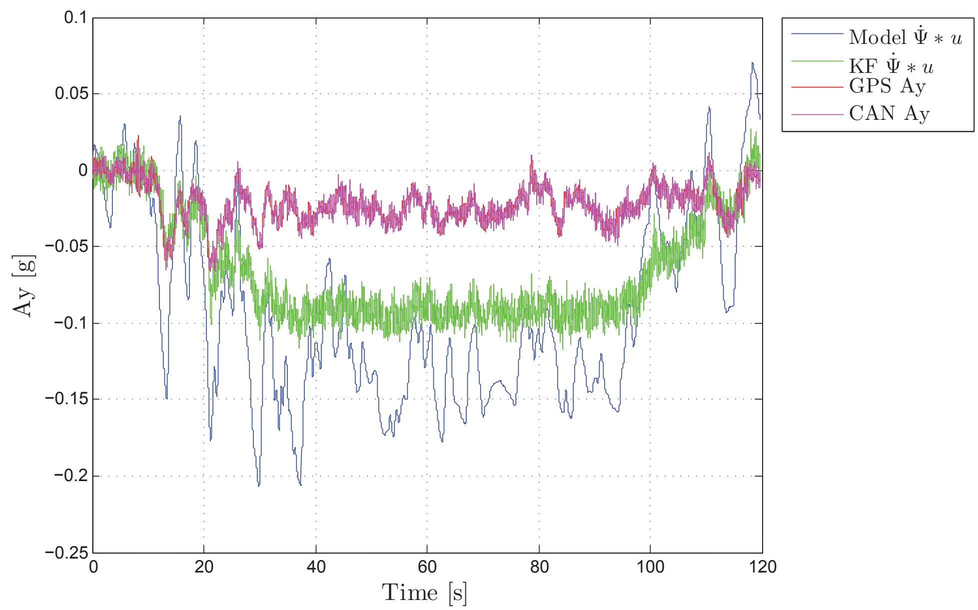

Figure 4.82: Highway Driving Scenario Lateral Acceleration, Five-Axle Model Revision 4

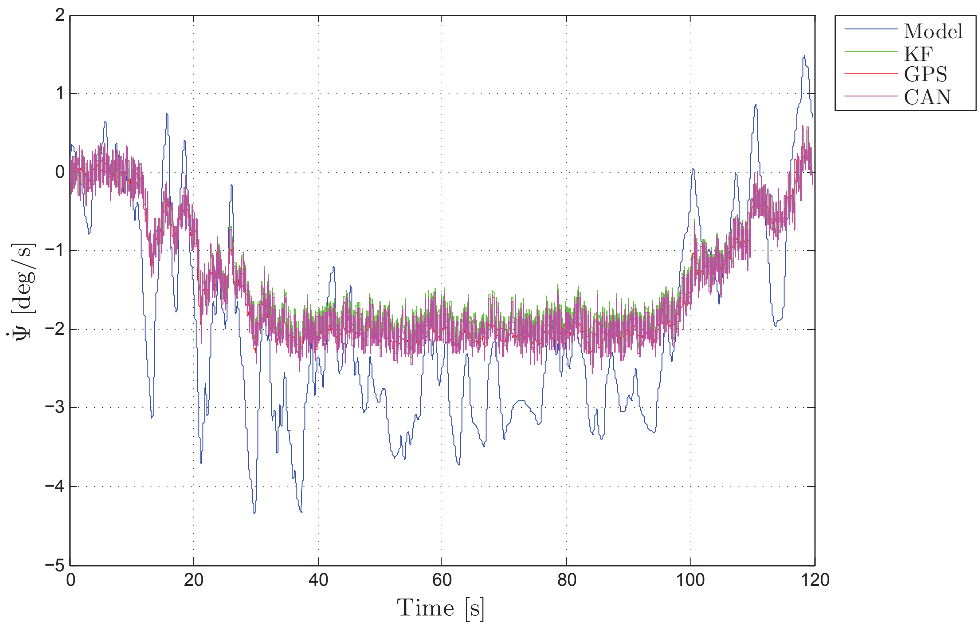

Figure 4.83: Highway Driving Scenario Yaw Rate, Five-Axle Model Revision 4

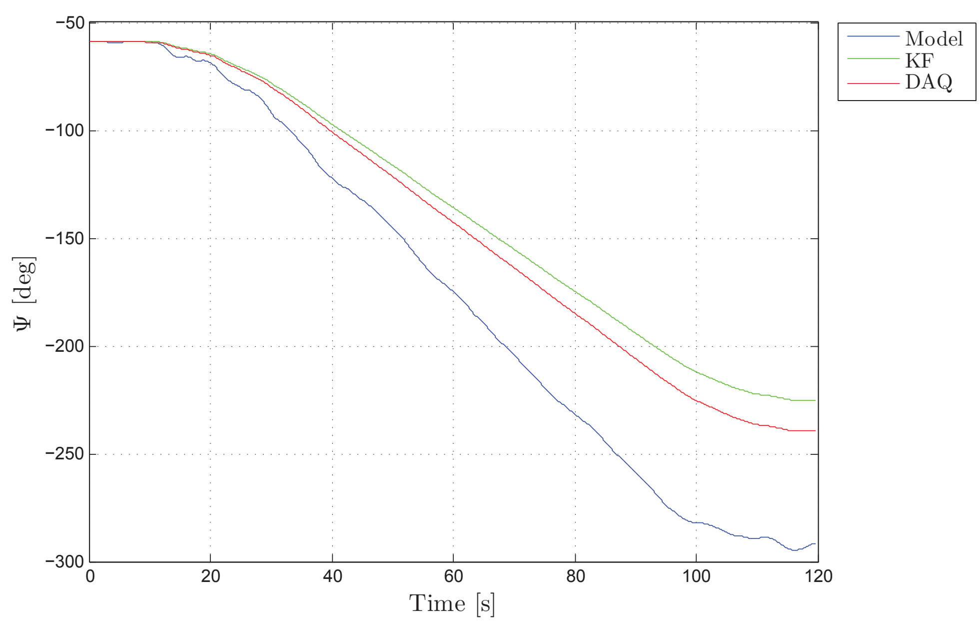

Figure 4.84: Highway Driving Scenario Yaw Angle, Five-Axle Model Revision 4

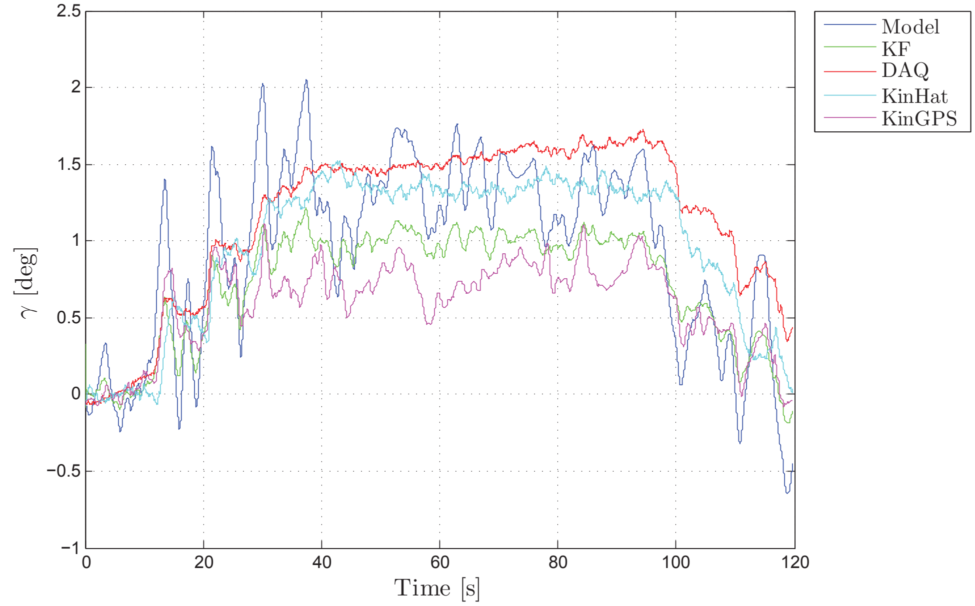

Figure 4.85: Highway Driving Scenario Hitch Angle, Five-Axle Model Revision 4

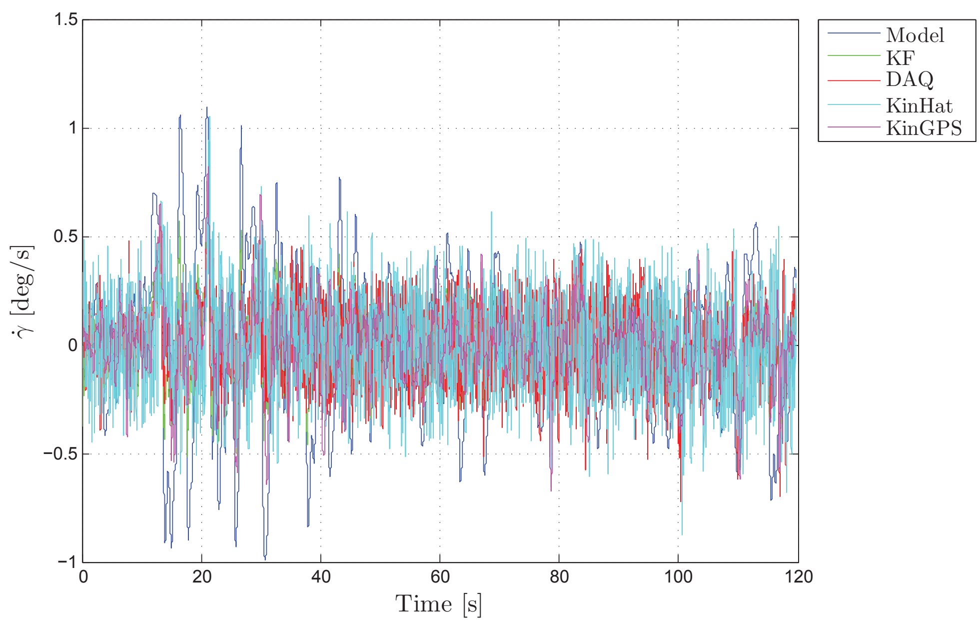

Figure 4.86: Highway Driving Scenario Hitch Rate, Five-Axle Model Revision 4

4.5.3.2 Highway Driving Scenario, Model Revision 6

Figures 4.87–4.95 show the results of the highway driving scenario using the Revision 6 model. No significant differences were observed as compared to the Revision 4 model.

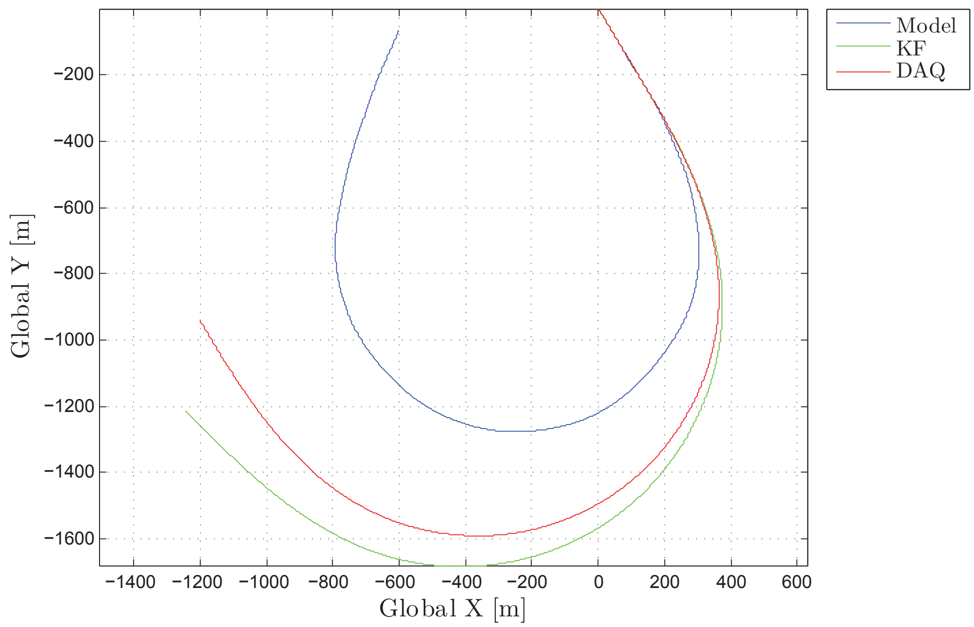

Figure 4.87: Highway Driving Scenario Path Prediction, Five-Axle Model Revision 6

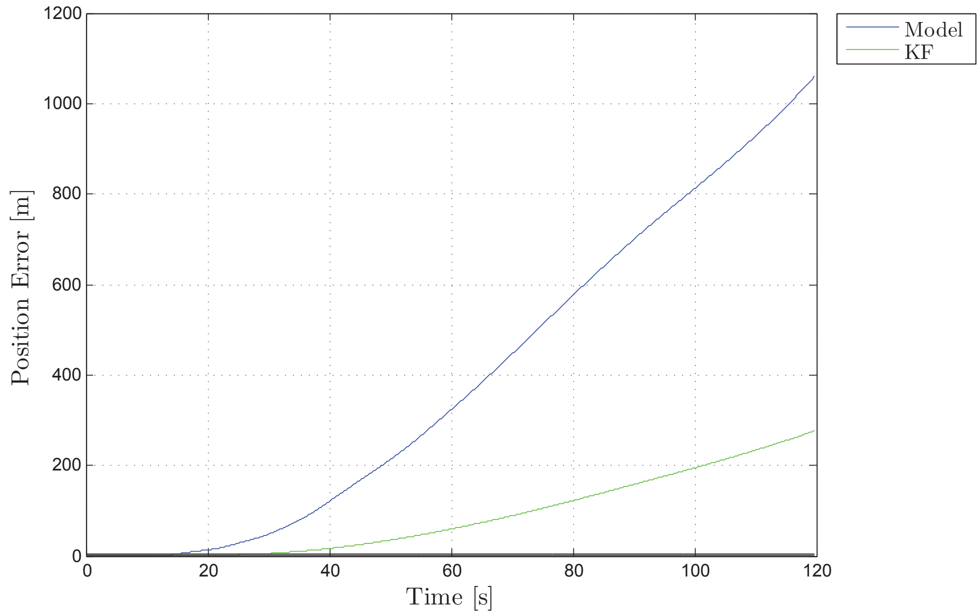

Figure 4.88: Highway Driving Scenario Global Position Error, Five-Axle Model Revision 6

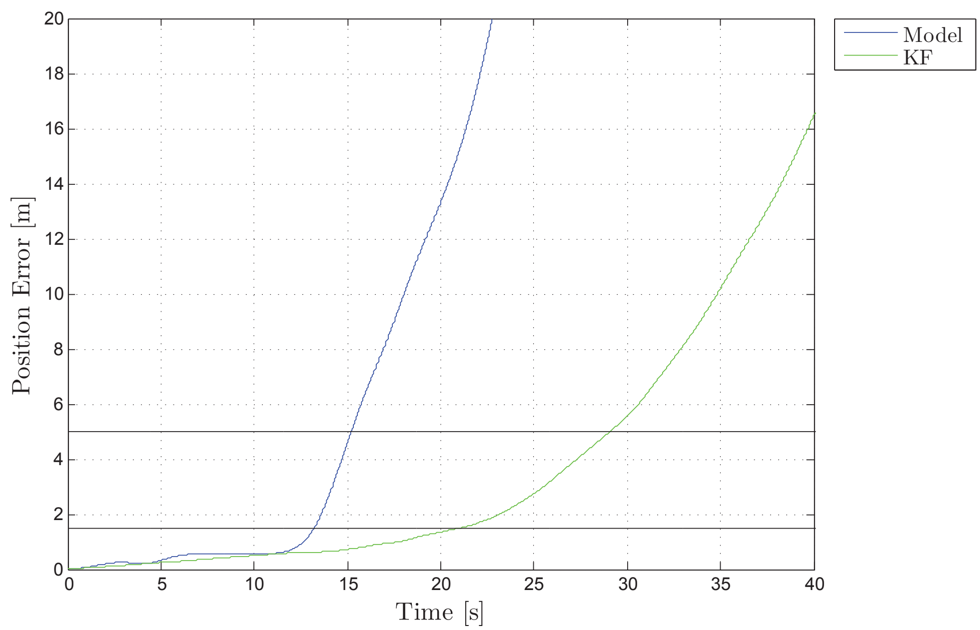

Figure 4.89: Highway Driving Scenario Global Position Error (scale smaller), Five-Axle Model Revision 6

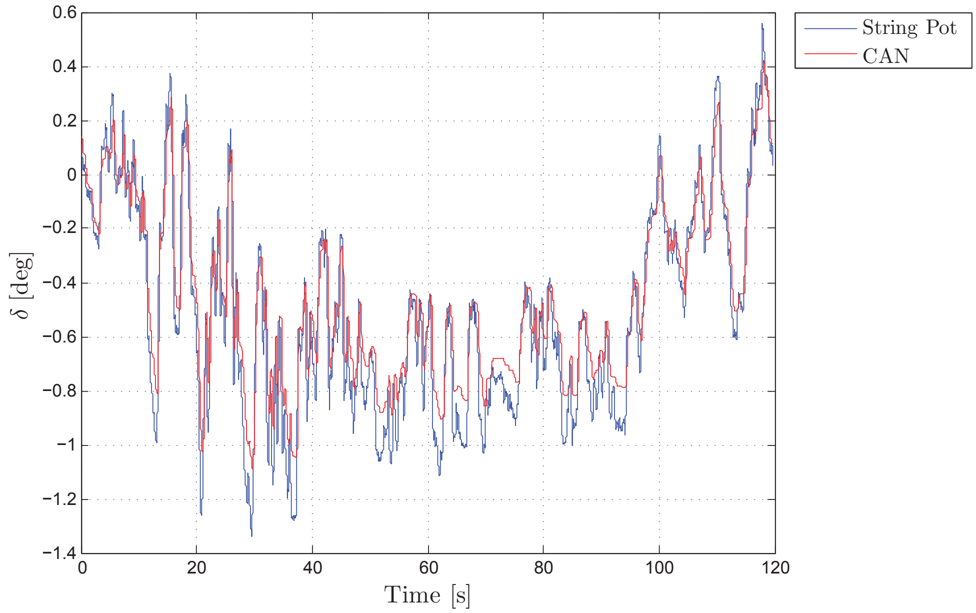

Figure 4.90: Highway Driving Scenario Road Wheel Steering Angle, Five-Axle Model Revision 6

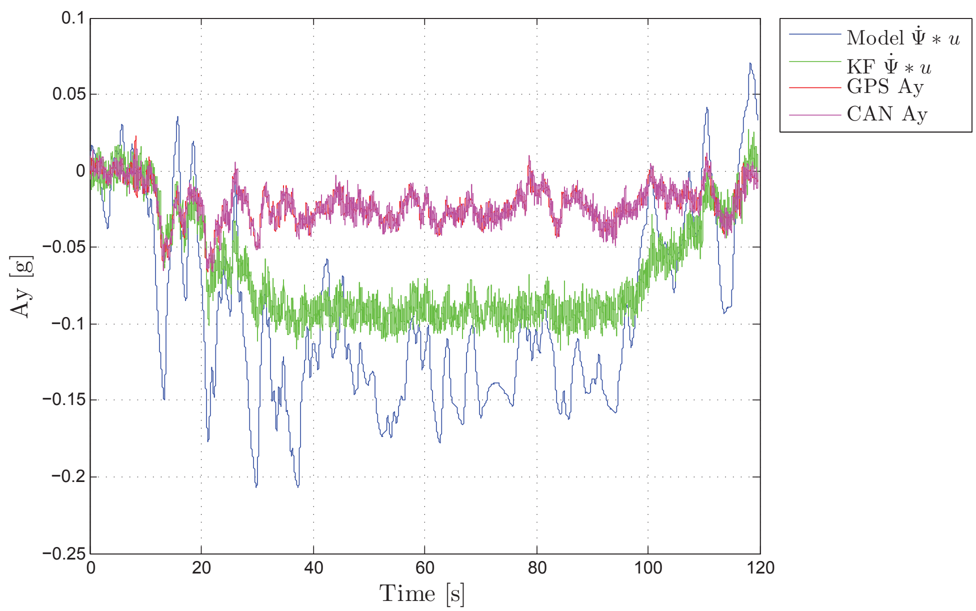

Figure 4.91: Highway Driving Scenario Lateral Acceleration, Five-Axle Model Revision 6

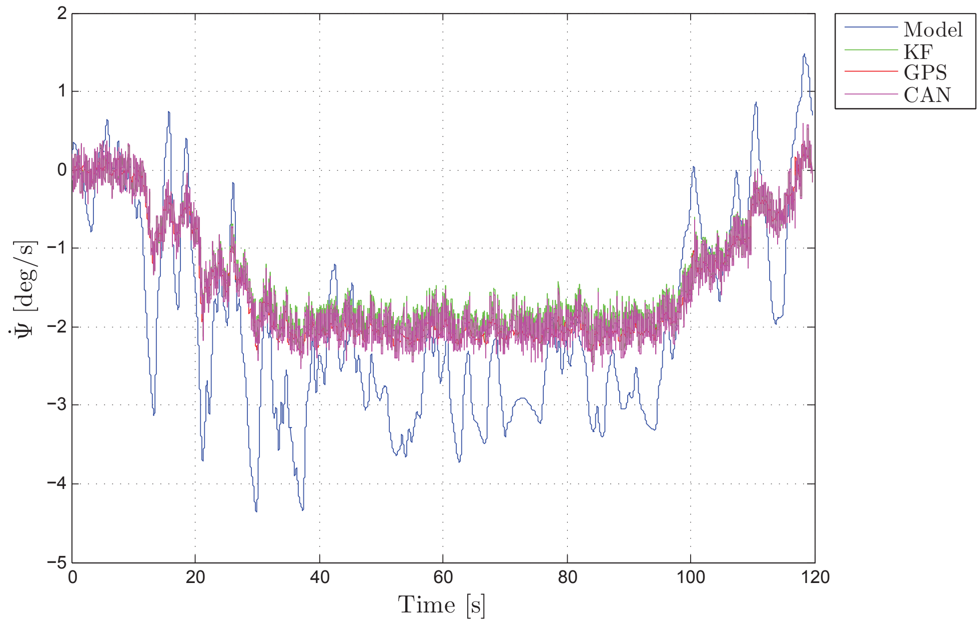

Figure 4.92: Highway Driving Scenario Yaw Rate, Five-Axle Model Revision 6

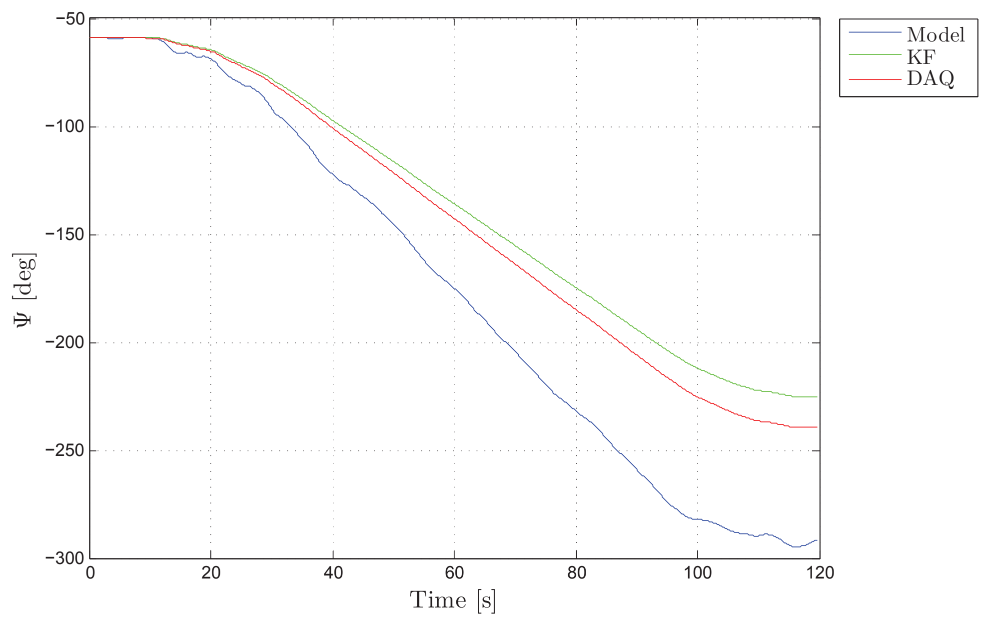

Figure 4.93: Highway Driving Scenario Yaw Angle, Five-Axle Model Revision 6

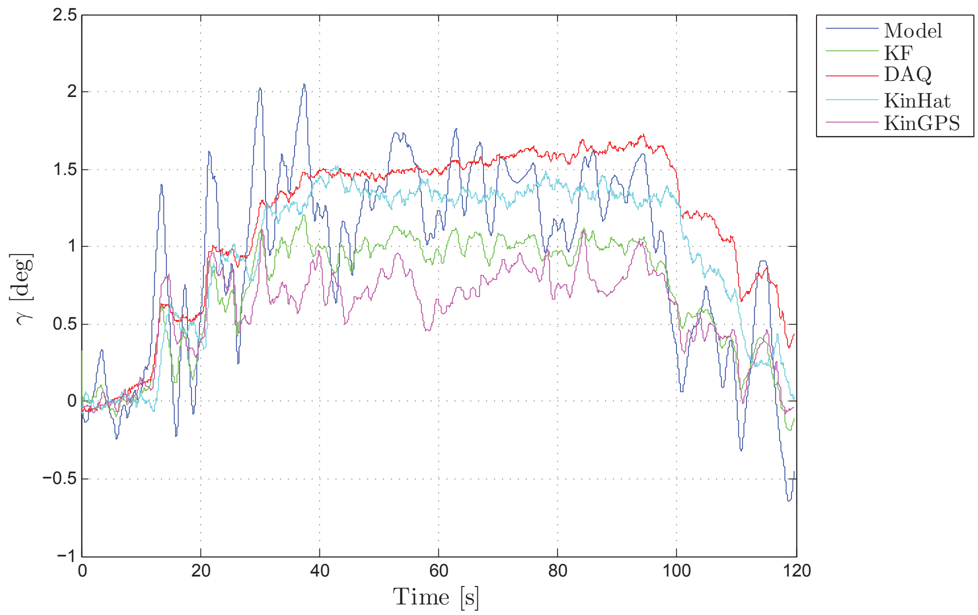

Figure 4.94: Highway Driving Scenario Hitch Angle, Five-Axle Model Revision 6

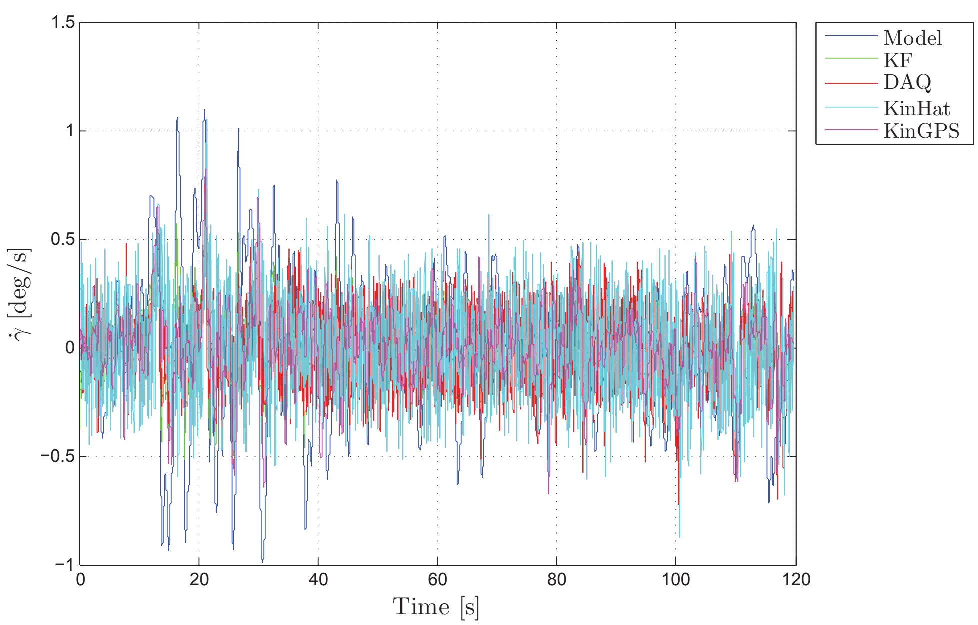

Figure 4.95: Highway Driving Scenario Hitch Rate, Five-Axle Model Revision 6

4.6 Conclusion

This chapter has presented a physical validation of the overall estimation system. The chapter began by highlighting the vehicle, trailer, instrumentation, and facilities used in testing. The maneuvers were explained and data from various trials were analyzed. Careful analysis of such data should answer the following three questions:

1. Did the system function using real data?

The first question presents a very basic hurdle. An estimation system which works well in a simulation environment cannot be assumed to work well in a physical environment. Sensor biases and inaccuracies, for example, could potentially hobble a system with weak excitation. This was a very real risk in this research due to the fact that the models and estimation schemes were developed entirely using high-accuracy, low-noise TruckSim signals. The system passed this test in that it worked (qualitatively speaking).

2. Did the performance of the system meet the research goals?

The research goals, as laid out in Section 1.2.1, were as follows: maintain lane-level (1.5 m RMS) vehicle positioning accuracy for up to 20 s, road-level (5 m RMS) vehicle positioning accuracy for up to 70 s, and hitch angle accuracy of ± 2 deg for all time. For the ramp maneuvers (about 17 s in duration at 70 kph), lane-level positioning was maintained the entire time in one trial but only 7 s in the second trial (road-level positioning was maintained for the duration). For the urban driving scenario trials (30–40 s in duration at 16–22 kph), lane-level positioning was maintained for the entire duration. Owing to its high speed (100 kph), lane-level and road-level positioning accuracy were only maintained for about 20 and 28 s respectively in the highway driving scenario.

Hitch angle estimation was very promising, with the kinematic model based on estimated signals ('KinHat') tracking the measured hitch angle very well in all maneuvers. Although the dynamic ('KF') model was able to best the kinematic model in hitch angle estimation during ramp maneuvers, the dynamic model failed to meet the accuracy target during the extreme articulation angles encountered in the urban driving scenario. Additionally, the 'KinHat' model performed best during the highway driving scenario.

3. What was learned about the system as a result of the experimental validation?

The diversity of maneuvers indicate that this estimation system has the greatest chance of proving beneficial in urban environments. This is due to a number of factors. First, the high speeds encountered outside of urban environments quickly render the positioning accuracy of the system unacceptable. Second, deep urban environments typically only have GPS accuracy of about 10 m RMS, if GPS is available at all – they are the environment where a non-GPS, CAN-based localization scheme is needed most [3]. Third, the high articulation angles caused by the low speed, tight turns common to urban environments (e.g. intersection) also suggest that these areas most need such a system.

Physical testing also revealed the slight superiority of the Revision 4 model to the Revision 6 model. Differences were only observed at high articulation angles, which is to be expected since the difference is updating the value of $\cos\gamma$ (Revision 6) versus assuming it is unity (Revision 4). It is unclear, however, why Revision 4 outperformed Revision 6.

Chapter References

[1] S. Rao, "Development of a Hardware in the Loop Simulation System for Heavy Truck ESC Evaluation and Trailer Parameter and State Estimation." Doctoral Dissertation, The Ohio State University, 2013.

[2] Truck Bus Control And Communications Network Committee, "Serial control and communications heavy duty vehicle network," *SAE Standard J1939*, August 2013.

[3] Crash Avoidance Metrics Partnership, "Vehicle Safety Communications - Applications (VSC-A) Final Report." DOT DTNH22-05-H-01277, May 2011. Appendix E.

CHAPTER 5

CONCLUSIONS AND FUTURE RESEARCH

5.1 Introduction

This chapter details the contributions of the research described in this dissertation as well as its limitations. It is expected that application of this research will allow for enhanced reliability and performance of V2V systems without adding hardware costs. Future research and integration work is required, though, and some limitations may require user acceptance (e.g. the user might have to manually enter data).

5.2 Contributions

5.2.1 Modeling

Several models that existed prior to this research were discussed in Chapters 1 and 3. Accordingly, it is not claimed that the lateral dynamic model presented in this text represents new art. Rather, the new contribution to the field is the validation of a complete lateral dynamic model – position estimator – parameter estimator – Kalman filter system which possesses the following attributes:

- Linear (quasi-linear)
- Feasible for on-line implementation
- Recursive in nature

- Simple enough to run at 100 Hz
- Accurate enough positioning to fill in GPS outages
- Receives input and feedback from extant CAN signals
- Estimates cornering stiffness of all tires without additional sensors
- Estimates hitch angle without additional sensors
- Validated with a physical vehicle and CAN signals

This research represents an important contribution to the estimation of trailer states and parameters. Some other prior models have estimated hitch angle, but not as accurately, as well validated, or without the requirement to fit additional sensors to the system [1],[2]. Much of this work had been done for jackknife detection and prevention, where it may not be necessary to estimate hitch angle as accurately. It is the first known recursive, on-line method for the estimation of trailer cornering stiffness which does not rely on any signals not available on the CAN bus.

5.2.2 V2V

V2V safety systems hold great promise for mitigating collisions and saving lives, but the current state of the art is immature. The primary issue stems from the inherently unreliable nature of GPS. Because it requires a clear view of the sky, accuracy and availability suffer when the view is obstructed. Accuracy of 1.0–1.5 m RMS is required to enable lane-level positioning while 5–10 m is good enough for road-level positioning [3]. Typical driving situations such as a city center or tree-lined street cause accuracy to drop below what is required for V2V systems, and techniques that enable greater relative positioning accuracy, i.e. RTK approach, increase the length of dropouts [4]. This research allows lane-level positioning in urban environments, enhancing the performance of V2V systems in situations with degraded GPS.

Another issue arises from the implicit assumption that articulated trucks are straight at all times [5]. At high articulation angles, this can lead to false positives and missed warnings. Even at low articulation angles this degrades performance because other vehicles will improperly judge the location of the rear of the trailer. This research shows that a kinematic model (fed with state estimates from a dynamic model) can accurately estimate the tractor-trailer articulation angle, generally within half of a degree or less. Providing an accurate estimate of hitch angle fixes this issue, enhancing the performance of the V2V system.

This research also helps NHTSA to achieve its regulatory mission with regards to V2V collision avoidance systems. Demonstration of a validated method for predicting hitch angle, for example, allows them to understand how OEMs might overcome such challenges. The work regarding position estimation enhances their knowledge of how GPS limitations might be overcome and introduces issues that may arise in the future (e.g. a need to measure road wheel steer angle instead of handwheel steer angle).

5.3 Future Research

This research holds promise for the enhancement of V2V functionality, but additional work is required to integrate the algorithms into the onboard hardware. First, a procedure must be developed to initialize the model. The model would definitely be required once the number of observed satellites falls below the necessary four, but it might also be used during times when positioning is available but at degraded accuracy. GPS sensor models can calculate dilution of precision (DOP) based on satellite geometry. If pseudorange errors are known, this can be converted to RMS positioning accuracy at the ground, often termed user-equivalent range error or UERE [6]. Once GPS is determined to be inaccurate or unavailable, the model can be initialized from the last known good position. In practice, this might require that a buffer of model inputs be stored so that the model can 'catch up' to real time (because GPS positioning is not likely to instantaneously transition from excellent to poor and be detected immediately).

A formalized procedure would also need to be developed for updating tire cornering stiffnesses. Based on this research, it appears that some excitations (such as steady lateral acceleration) are better than others for estimating tire properties. This supervisory program would be two-fold: first, it would detect that a suitable excitation is present and begin estimating cornering stiffnesses. Next, it would test if the new estimate was better than the old. This is readily accomplished because GPS is available most of the time. The supervisory program could run two instances of the model in parallel, one with the old cornering stiffness estimate and one with the new. The cornering stiffness estimate would be updated if the new outperformed the old based on some metric or set of metrics, such as maximum positioning error.

Additional validation of hitch angle prediction should be performed with different tractors, trailers, and loading conditions. This would help elucidate differences in performance between the kinematic and dynamic methods for estimating articulation rate and angle. Integrators of V2V systems might use a single model, fuse the models, or switch models depending on regime of operation. Parametric uncertainties might also affect the relative performance. While the dynamic model requires more parameters, the kinematic model may be more sensitive to errors in trailer wheelbase. Since the kinematic model relies on the dynamic model for some signals (most notably side-slip velocity), it should be investigated how parametric uncertainties in the dynamic model filter into the kinematic model.

5.4 Limitations

A number of parameters are required for the dynamic model and V2V systems in general. Some of these are known to the manufacturer, some can be estimated, and still others must be manually entered by the user.

First, the V2V system must determine whether or not a trailer is connected. This can be accomplished by comparing the ECU's mass estimate (available via CAN [7]) to the assumed known mass of the tractor. If the mass estimate is significantly greater than the tractor mass, the system can conclude that a trailer is attached (the driver weighs comparatively little and even fuel load is available via CAN [7]). Trailer inertia is required for the dynamic model and remains unknown, but could be estimated from the trailer mass (total mass minus tractor mass) and some assumptions about load distribution.

Next, the system needs to know how long the trailer is (from kingpin to the rear bumper). This information is required even in the current V2V implementation that assumes the truck is straight. The driver could manually enter this information, making it subject to human transcription error or forgetfulness. Another possibility is to place low-cost radio frequency identification (RFID) tags on trailers, containing such information as physical dimensions and empty weight. The V2V system on the tractor would then need an RFID reader. RFID devices are already used for other Intelligent Transportation System (ITS) applications. New York City uses the ubiquitous RFID-based E-ZPass toll tags to estimate vehicle volume for adaptive traffic signaling [8]. Bermuda uses RFID readers at major junctions to ensure vehicles are properly licensed [9].

The load distribution of the trailer remains to be determined, i.e. the location of CG_2, which is parameter d in Figure A.1. This can be calculated if the axle loads are known. The SAE J1939 standard includes a standardized message for axle loads, but it is unclear what proportion of vehicles broadcast this signal [7]. There are several commercial systems that calculate axle loads by measuring suspension airbag pressures. Examples include systems from WABCO [10], Vishay Precision Group [11], and Air Weigh [12].

Some parameters can also be adjusted by the user and would need to be manually entered. The location of the kingpin (parameter c in Figure A.1) can be moved on the tractor to adjust axle weighting. This complicates things not only for the dynamic model, but indeed for even the current V2V implementation as this changes the effective length of the articulated vehicle. The location of the rear axles (parameters f_1 and f_2) can also be adjusted by the user. This is irrelevant for the current V2V implementation (straight truck assumption) but is a required parameter for both the dynamic and kinematic models that predict articulation angle and rate.

Tractor parameters are a comparatively simple matter. Since the integrator of the V2V system is likely to be the manufacturer of the tractor (or a closely-related supplier), basic geometric and weight information is readily available. Although fuel load and driver weight will affect the mass and CG_1 location, these variations are small relative to those of the trailer. Tractor inertia may not be measured, but could be readily estimated from a CAD model.

5.5 Conclusion

This chapter has summarized the important contributions of this dissertation to the field of vehicle modeling and estimation. More importantly, it has examined how these contributions might be used to increase the feasibility, reliability, and effectiveness of V2V collision avoidance systems. However, there are issues (particularly related to the availability of parameters) that must be addressed before implementation is to be successful.

Chapter References

[1] L. Chu, Y. Fang, M. Shang, J. Guo, and F. Zhou, "Estimation of articulation angle for tractor semi-trailer based on state observer," *International Conference on Measuring Technology and Mechatronics Automation*, 2010.

[2] A. Dunn, "Jacknife Stability of Articulated Ttractor Semitrailer Vehicles with High-Output Brakes and Jackknife Detection on Low Coefficient Surfaces." Doctoral Dissertation, The Ohio State University, 2003.

[3] Crash Avoidance Metrics Partnership, "Enhanced Digital Mapping Project Final Report." DOT DTFH61-01-X-00014, November 2004.

[4] Crash Avoidance Metrics Partnership, "Vehicle Safety Communications - Applications (VSC-A) Final Report." DOT DTNH22-05-H-01277, May 2011. Appendix E.

[5] D. S. R. C. Technical Committee, "Dedicated Short Range Communications (DSRC) Message Set Dictionary," *SAE Standard J2735*, November 2009.

[6] J. Farrell, *Aided Navigation: GPS with High Rate Sensors*. New York: McGraw-Hill, 2008.

[7] Truck Bus Control And Communications Network Committee, "Serial control and communications heavy duty vehicle network," *SAE Standard J1939*, August 2013.

[8] ITS International, "New york's award-winning traffic control system," January 2013. Online; accessed May 15, 2014.

[9] R. Wessel, "Bermuda's rfid vehicle registration system could save 2 million per year," *RFID Journal*, May 2007. Online; accessed May 15, 2014.

[10] WABCO, "Product brochure: Electronically controlled air suspension." `http://www.wabco-auto.com/uploads/media/Product_Brochure-Trucks-Buses.pdf`. Online; accessed May 15, 2014.

[11] Vishay Precision Group, "Product brochure: Air suspension weighing system." `http://www.vishaypg.com/docs/32001/airscale.pdf`. Online; accessed May 15, 2014.

[12] Air Weigh, "Product brochure: Quickload tractor scale." `http://www.air-weighscales.com/Content/AirWeigh/Uploads/QLT_brochure_Website_.pdf`. Online; accessed May 15, 2014.

REFERENCES

[1] Highway Loss Data Institute, "Mercedes-Benz collision avoidance features: initial results." Bulletin, Vol. 29, No. 7, April 2012.

[2] National Highway Traffic Safety Administration, "Traffic Safety Facts, 2012 Data, Large Trucks." DOT HS 811 868, `http://www-nrd.nhtsa.dot.gov/Pubs/811868.pdf`, May 2014. Online; accessed June 10, 2014.

[3] F. S. Barickman, "NHTSA VRTC HV Forward Collision Avoidance and Mitigation Research." Government/Industry Brake Research Presentation, 2012.

[4] W. Najm, J. Koopmann, J. Smith, and J. Brewer, "Frequency of Target Crashes for Intellidrive Safety Systems." DOT HS 811 381, 2010.

[5] C. Weiss, "V2x communication in Europe – from research projects towards standardization and field testing of vehicle communication technology," *ComNet (Computer Networks)*, vol. 55, no. 3103-3119, 2011.

[6] Crash Avoidance Metrics Partnership, "Enhanced Digital Mapping Project Final Report." DOT DTFH61-01-X-00014, November 2004.

[7] Crash Avoidance Metrics Partnership, "Vehicle Safety Communications - Applications (VSC-A) Final Report." DOT DTNH22-05-H-01277, May 2011. Appendix E.

[8] Sage Wolfe, "Integration of CarSim into a Custom Cosimulation Program for Automotive Safety." Master's Thesis, The Ohio State University, 2011.

[9] D. S. R. C. Technical Committee, "Dedicated Short Range Communications (DSRC) Message Set Dictionary," *SAE Standard J2735*, November 2009.

[10] W. Milliken and D. Milliken, *Race Car Vehicle Dynamics*. Warrendale, PA: SAE, 1995.

[11] R. Rajamani, *Vehicle Dynamics and Control*. New York: Springer, 2012.

[12] T. Gillespie, *Fundamentals of Vehicle Dynamics*. Warrendale, PA: SAE, 1992.

[13] W. Milliken, D. Milliken, and M. Olley, *Chassis Design: Principles and Analysis*. Warrendale, PA: SAE, 2002.

[14] NHTSA, "The national advanced driving simulator (NADS)." `http://www.nhtsa.gov/Research/Driver+Simulation+(NADS)/The+National+Advanced+Driving+Simulator+(NADS)`. Online; accessed June 11, 2014.

[15] M. K. Salaani, "Development and Validation of a Vehicle Model for the National Advanced Driving Simulator." Doctoral Dissertation, The Ohio State University, 1996.

[16] Mechanical Simulation Corporation, "Product datasheet - adams/car." `http://www.mscsoftware.com/sites/default/files/ds_adams-car_ltr_w_0.pdf`. Online; accessed June 11, 2014.

[17] Mechanical Simulation Corporation, "Trucksim brochure." `http://www.carsim.com/downloads/pdf/trucksim_handout.pdf`. Online; accessed June 11, 2014.

[18] C. Ghike and T. Shim, "14 degree-of-freedom vehicle model for roll dynamics study," *SAE*, no. 2006-01-1277, 2006.

[19] D. Segal, "Highway-vehicle-object simulation model - 1976 engineering manual - validation." FHWA Report No. FHWA-RD-76-165, February 1976.

[20] K. Berntop, "Derivation of a six degrees-of-freedom ground-vehicle model for automotive applications," *Technical Report, Lund University, Department of Automatic Control*, no. ISRN LUTFD2/TFRT–7627–SE, 2006.

[21] H. B. Pacejka, *Tire and Vehicle Dynamics*. Warrendale, PA: SAE, 2002.

[22] C. Lundquist and T. Schon, "Recursive identification of cornering stiffness parameters for an enhanced single track model," *Proceedings of the 15th IFAC Symposium on System Identification*, vol. 15, no. 1, 2009.

[23] C. Sierra, E. Tseng, A. Jain, and H. Peng, "Cornering stiffness estimation based on vehicle lateral dynamics," *Vehicle System Dynamics: International Journal of Vehicle Mechanics and Mobility*, vol. 44, no. 1, 2007.

[24] D. Bevly, R. Daily, and W. Travis, "Estimation of critical tire parameters using GPS based sideslip measurements," *SAE*, no. 2006-01-1965, 2006.

[25] W. Sienel, "Estimation of the tire cornering stiffness and its application to active car steering," *Proceedings of the 36th IEEE Conference on Decision and Control*, vol. 5, no. 4744-4749, 1997.

[26] R. Anderson and D. Bevly, "Estimation of tire cornering stiffness using gps to improve model based estimation of vehicle states," *Proceedings of IEEE Intelligent Vehicles Symposium*, no. 801-806, 2005.

[27] G. Baffet, A. Charara, and D. Lechner, "Estimation of vehicle sideslip, tire force and wheel cornering stiffness," *Control Engineering Practice*, vol. 17, no. 1255-1264, 2009.

[28] J. Bernard and J. Shannan, "Simulation of heavy vehicle dynamics," *SAE*, no. 902270, 1990.

[29] D. Williams, "The mathematical theory of the snaking of two-wheeled trailers, with practical rules and devices for preventing snaking," *Proceedings of the Institution of Mechanical Engineers: Automobile Division*, 1951. pp. 175-190.

[30] S. Rao, "Development of a Hardware in the Loop Simulation System for Heavy Truck ESC Evaluation and Trailer Parameter and State Estimation." Doctoral Dissertation, The Ohio State University, 2013.

[31] L. Alexander, M. Donath, M. Hennessey, V. Morellas, and C. Shankwitz, "A lateral dynamic model of a tractor–trailer: Experimental validation." MN DOT Report, Contract 73168 TOC 174, November 1996.

[32] M. Salaani, "The application of understeer gradient in stability analysis of articulated vehicles," *International Journal of Heavy Vehicle Systems*, vol. 16, no. 1/2, 2009.

[33] A. Hac, D. Fulk, and H. Chen, "Stability and control considerations of vehicle-trailer combination," *SAE*, no. 2008-01-1228, 2008.

[34] W. Deng and X. Kang, "Parametric study on vehicle-trailer dynamics for stability control," *SAE*, no. 2006-01-1965, 2003.

[35] M. Luijten, "Lateral dynamic behaviour of articulated commercial vehicles." Master's thesis, Eindhoven University of Technology, August 2010.

[36] Z. Bareket and P. Fancher, "Truck or bus dynamic modeling for a driving simulator," *Technical Report, University of Michigan, Transportation Research Institute*, no. UMTRI-91-26, 1991.

[37] R. Ervin, C. Winkler, J. Bernard, and R. Gupta, "Effects of tire properties on truck and bus handling." DOT Report UM-HSRI-76-11, June 1976.

[38] R. E. Kalman, "A new approach to linear filtering and prediction problems," *Transactions of the ASME, Journal of Basic Engineering*, no. 82, 1960. pp. 35-45.

[39] J. Farrell, *Aided Navigation: GPS with High Rate Sensors*. New York: McGraw-Hill, 2008.

[40] A. Gelb, *Applied Optimal Estimation*. Cambridge, Mass.: The MIT Press, 1974.

[41] R. Plessis, *Poor Man's Explanation of Kalman Filtering or How I Stopped Worrying and Learned to Love Matrix Inversion*. Monterey, Cali.: Taygeta Scientific, 1967.

[42] M. Rajamani and J. Rawlings, "Estimation of the disturbance structure from data using semidefinite programming and optimal weighting," *Texas-Wisconsin Modeling and Control Consortium*, no. 2007-02, 2007.

[43] L. Perko, *Differential Equations and Dynamical Systems*. New York: Springer, 1996. Second edition.

[44] D. Simon, *Optimal State Estimation*. New Jersey: Wiley, 2006.

[45] D. Greenwood, *Principles of Dynamics*. New Jersey: Prentice Hall, 1987. Second edition.

[46] L. Chu, Y. Fang, M. Shang, J. Guo, and F. Zhou, “Estimation of articulation angle for tractor semi-trailer based on state observer,” *International Conference on Measuring Technology and Mechatronics Automation*, 2010.

[47] A. Dunn, “Jacknife Stability of Articulated Ttractor Semitrailer Vehicles with High-Output Brakes and Jackknife Detection on Low Coefficient Surfaces.” Doctoral Dissertation, The Ohio State University, 2003.

[48] S. Zhou, S. Zhang, and G. Zhao, “Jackknife control on tractor semi-trailer during emergency braking,” *Advanced Materials Research*, vol. 299-300, no. 1303-1306, 2011.

[49] D. Wesemeier and R. Isermann, “Identification of vehicle parameters using stationary driving maneuvers,” *Control Engineering Practice*, vol. 17, no. 1426-1431, 2009.

[50] S. You, J. Hahn, and H. Lee, “New adaptive approaches to real-time estimation of vehicle sideslip angle,” *Control Engineering Practice*, vol. 17, no. 1367-1379, 2009.

[51] Truck Bus Control And Communications Network Committee, “Serial control and communications heavy duty vehicle network,” *SAE Standard J1939*, August 2013.

[52] ITS International, “New york’s award-winning traffic control system,” January 2013. Online; accessed May 15, 2014.

[53] R. Wessel, “Bermuda’s rfid vehicle registration system could save 2 million per year,” *RFID Journal*, May 2007. Online; accessed May 15, 2014.

[54] WABCO, “Product brochure: Electronically controlled air suspension.” `http://www.wabco-auto.com/uploads/media/Product_Brochure-Trucks-Buses.pdf`. Online; accessed May 15, 2014.

[55] Vishay Precision Group, “Product brochure: Air suspension weighing system.” `http://www.vishaypg.com/docs/32001/airscale.pdf`. Online; accessed May 15, 2014.

[56] Air Weigh, “Product brochure: Quickload tractor scale.” `http://www.air-weighscales.com/Content/AirWeigh/Uploads/QLT_brochure_Website_.pdf`. Online; accessed May 15, 2014.

Appendix A

DETAILS OF FIVE-AXLE MATHEMATICAL MODELS

A.1 Diagrams

This section contains diagrams defining the parameters, tire forces, and virtual displacements of the five-axle model. Alongside the diagrams, equations are presented that model tire lateral forces and define generalized forces.

A.1.1 Model

Figure A.1 shows the states, lateral tire forces, and parameters of the five-axle model.

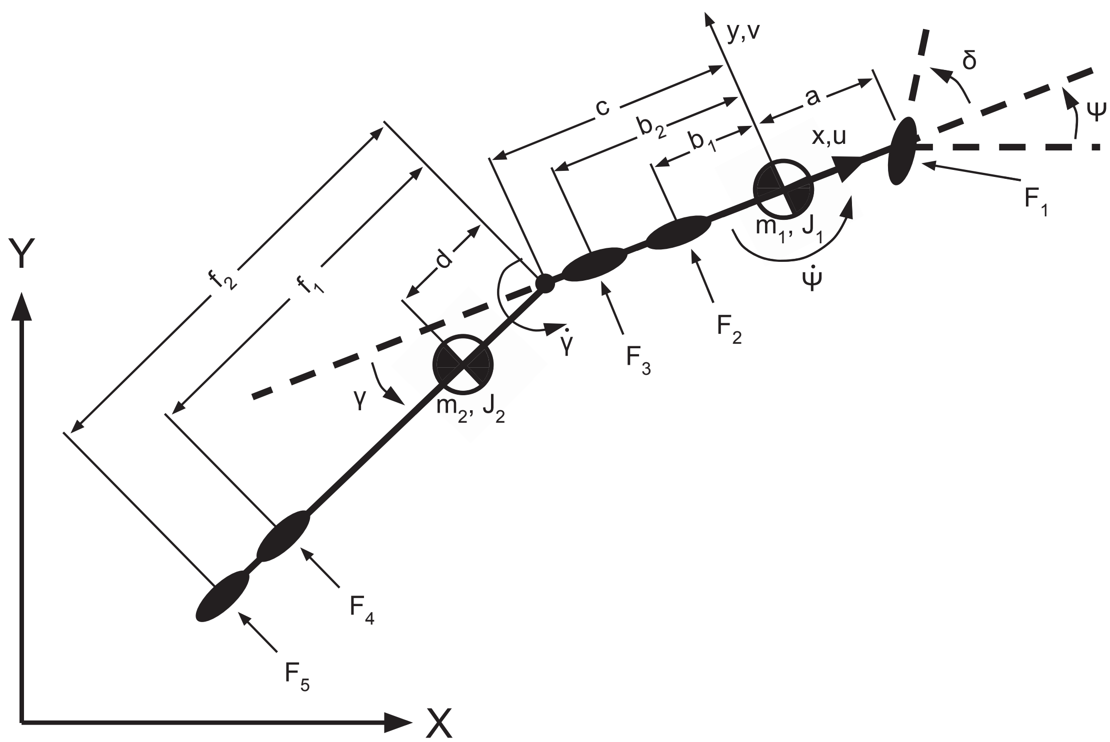

Figure A.1: Five-Axle Articulated Bicycle Model Parameters

A.1.2 Slip Angle Diagrams and Expressions

Figure A.2 is a kinematic diagram of the steer axle and is used to derive the slip angle expression. Equation A.1 models the corresponding tire force. Note that it is valid for both the three- and five-axle models.

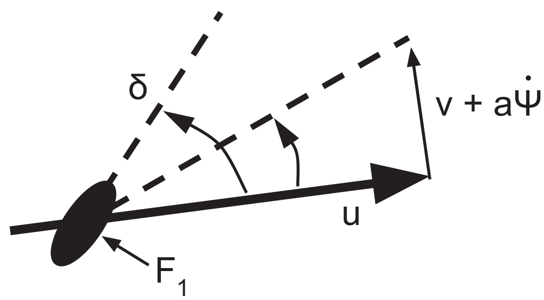

Figure A.2: Kinematic Diagram of Steer Axle

$$F_1 = C_{\alpha 1}\alpha_1 = C_{\alpha 1}\left(\delta - \arctan\left(\frac{v + a\dot{\Psi}}{u}\right)\right) \approx C_{\alpha 1}\left(\delta - \left(\frac{v + a\dot{\Psi}}{u}\right)\right) \tag{A.1}$$

Figure A.3 is a kinematic diagram of the first drive axle and is used to derive the slip angle expression. Equation A.2 models the corresponding tire force. The diagram and expression would be similar for the second drive axle and these are not included here. Note that this expression is valid for both the three- and five-axle models.

$$F_2 = C_{\alpha 2}\alpha_2 = C_{\alpha 2}\left(-\arctan\left(\frac{v - b_1\dot{\Psi}}{u}\right)\right) \approx C_{\alpha 2}\left(\frac{b_1\dot{\Psi} - v}{u}\right) \tag{A.2}$$

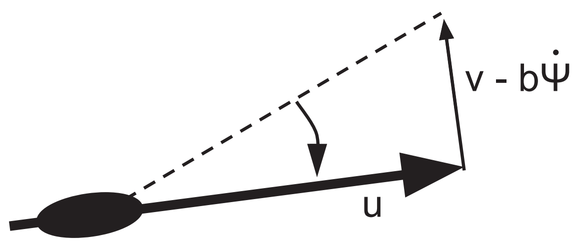

Figure A.3: Kinematic Diagram of First Drive Axle

Figure A.4 is a kinematic diagram of the first trailer axle and is used to derive the slip angle expression. Equation A.3 models the corresponding tire force. This equation shows how articulation angle acts like a steering angle for the trailer tires. The diagram and expression would be similar for the second trailer axle and these are not included here.

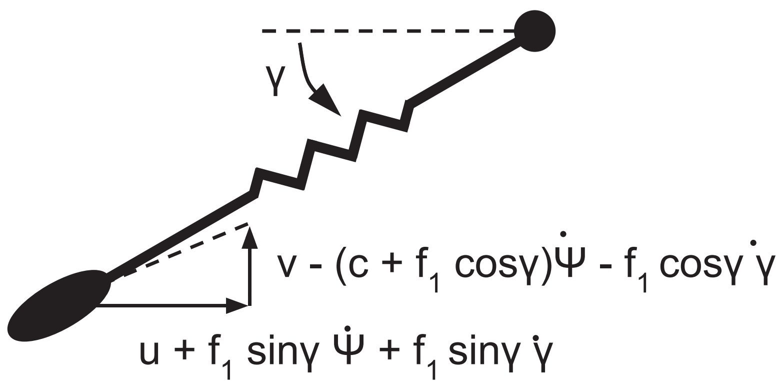

Figure A.4: Kinematic Diagram of First Trailer Axle

$$
\begin{aligned}
F_4 = C_{\alpha 4}\alpha_4 = C_{\alpha 4} &\left(\gamma - \arctan\left(\frac{v - (c + f_1 \cos\gamma)\dot{\Psi} - f_1\dot{\gamma}\cos\gamma}{u + f_1 \sin\gamma(\dot{\Psi} + \dot{\gamma})}\right)\right) \\
\approx C_{\alpha 4} &\left(\gamma - \left(\frac{v - (c + f_1 \cos\gamma)\dot{\Psi} - f_1\dot{\gamma}\cos\gamma}{u + f_1 \sin\gamma(\dot{\Psi} + \dot{\gamma})}\right)\right) \\
\approx C_{\alpha 4} &\left(\gamma - \left(\frac{v - (c + f_1 \cos\gamma)\dot{\Psi} - f_1\dot{\gamma}\cos\gamma}{u}\right)\right)
\end{aligned} \tag{A.3}
$$

A.1.3 Virtual Work Diagrams and Expressions

Virtual work diagrams and expressions for the coordinates y and γ are shown below. Those corresponding to the coordinate Ψ can be found in Section 3.2.1.

$$Q_y = \frac{W_y}{\delta y} = \cos\delta F_1 + F_2 + F_3 + \cos\gamma F_4 + \cos\gamma F_5 \tag{A.4}$$

$$Q_\gamma = \frac{W_\gamma}{\delta\gamma} = -f_1 F_4 - f_2 F_5 \tag{A.5}$$

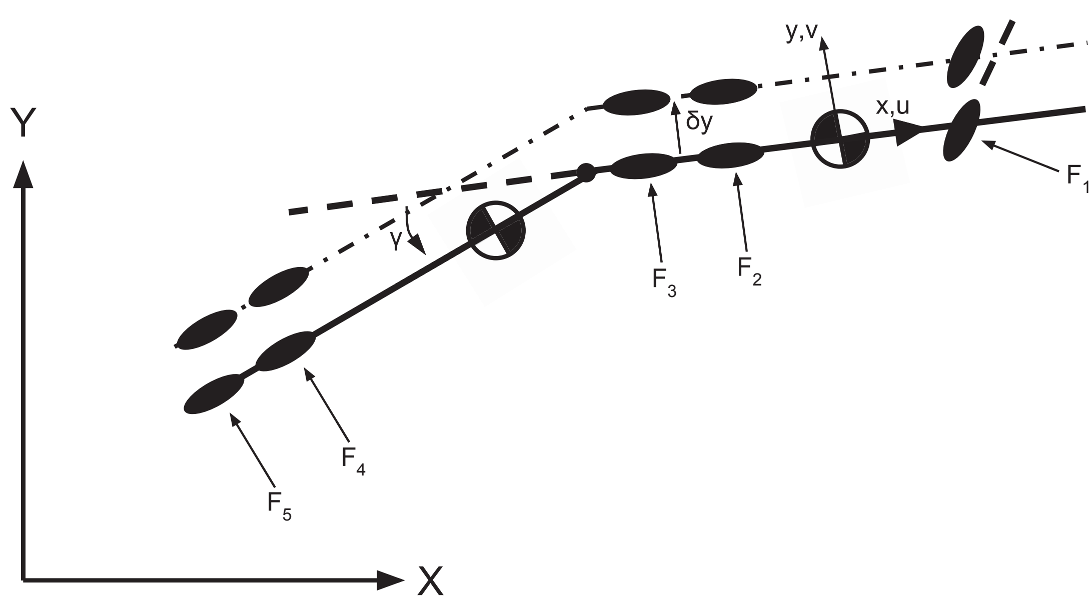

Figure A.5: Virtual Displacement by δy

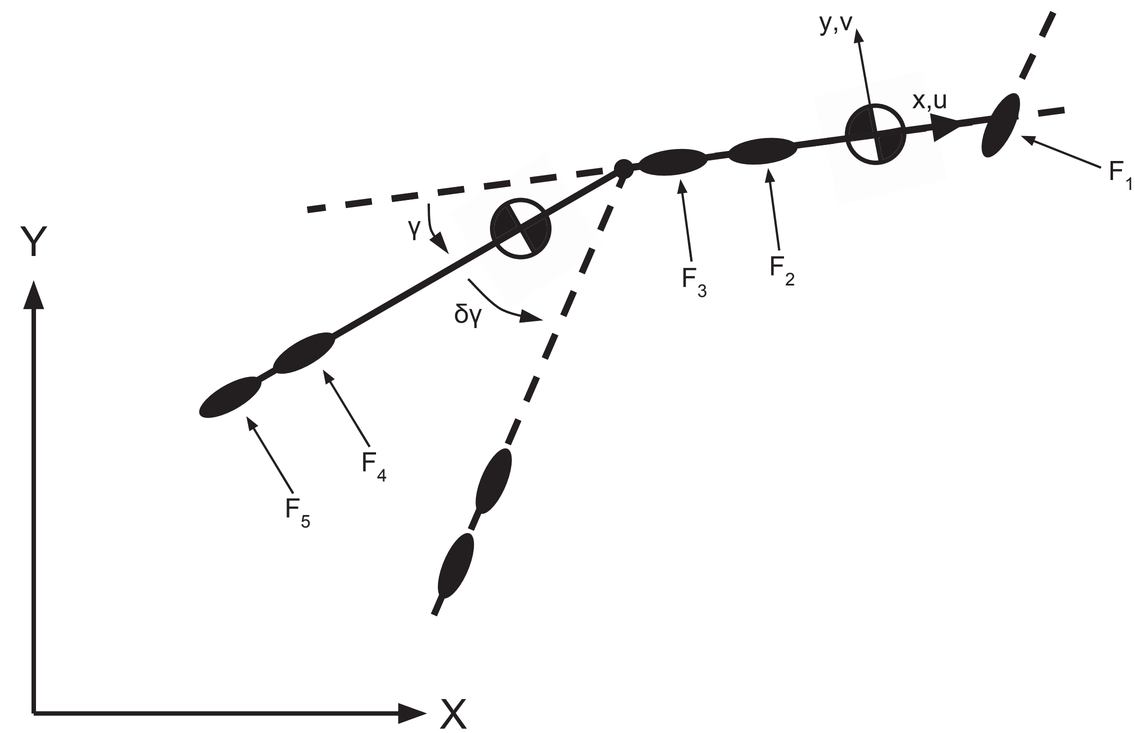

Figure A.6: Virtual Displacement by $\delta\gamma$

A.2 Model Matrices

$$\mathbf{M}_3 = \begin{bmatrix} m_1 + m_2 & -m_2(c + d\cos(\gamma)) & u(m_1 + m_2) & -m_2 d\cos(\gamma) & 0 \\ -m_2(c + d\cos(\gamma)) & J_1 + J_2 + m_2(c^2 + d^2) + 2m_2 cd\cos(\gamma) & -m_2 u(c + d\cos(\gamma)) & J_2 + m_2 d^2 + m_2 cd\cos(\gamma) & m_2 ud\cos(\gamma) \\ 0 & 0 & 1 & 0 & 0 \\ -m_2 d\cos(\gamma) & J_2 + m_2 d^2 + m_2 cd\cos(\gamma) & -2m_2 ud\cos(\gamma) & J_2 + m_2 d^2 & 0 \\ 0 & 0 & 0 & 0 & 1 \end{bmatrix} \tag{A.6}$$

$$\mathbf{M}_4 = \begin{bmatrix} m_1 + m_2 & -m_2(c + d) & u(m_1 + m_2) & -m_2 d & 0 \\ -m_2(c + d) & J_1 + J_2 + m_2(c + d)^2 & -m_2 u(c + d) & J_2 + m_2 d^2 + m_2 cd & 0 \\ 0 & 0 & 1 & 0 & 0 \\ -m_2 d & J_2 + m_2 d^2 + m_2 cd & -m_2 ud & J_2 + m_2 d^2 & 0 \\ 0 & 0 & 0 & 0 & 1 \end{bmatrix} \tag{A.7}$$

$$\mathbf{M}_6 = \begin{bmatrix} m_1 + m_2 & -m_2(c + d\cos(\gamma)) & u(m_1 + m_2) & -m_2 d\cos(\gamma) & 0 \\ -m_2(c + d\cos(\gamma)) & J_1 + J_2 + m_2(c + d\cos(\gamma))^2 & -m_2 u(c + d\cos(\gamma)) & J_2 + m_2 d\cos(\gamma)(c + d\cos(\gamma)) & 0 \\ 0 & 0 & 1 & 0 & 0 \\ -m_2 d\cos(\gamma) & J_2 + m_2((d\cos(\gamma))^2 + cd\cos(\gamma)) & -m_2 ud\cos(\gamma) & J_2 + m_2(d\cos(\gamma))^2 & 0 \\ 0 & 0 & 0 & 0 & 1 \end{bmatrix} \tag{A.8}$$

$$\mathbf{M}_7 = \begin{bmatrix} m_1 + m_2 & -m_2(c+d) & u(m_1+m_2) & -m_2 d & 0 \\ -m_2(c+d) & J_1 + J_2 + m_2(c+d)^2 & -m_2 u(c+d) & J_2 + m_2 d^2 + m_2 cd & m_2 ud \\ 0 & 0 & 1 & 0 & 0 \\ -m_2 d & J_2 + m_2 d^2 + m_2 cd & -2m_2 ud & J_2 + m_2 d^2 & 0 \\ 0 & 0 & 0 & 0 & 1 \end{bmatrix} \tag{A.9}$$

$$\mathbf{M}_8 = \begin{bmatrix} m_1 + m_2 & -m_2(c + d\cos(\gamma)) & u(m_1+m_2) & -m_2 d\cos(\gamma) & 0 \\ -m_2(c + d\cos(\gamma)) & J_1 + J_2 + m_2(c + d\cos(\gamma))^2 & -m_2 u(c + d\cos(\gamma)) & J_2 + m_2 d\cos(\gamma)(c + d\cos(\gamma)) & m2ud \\ 0 & 0 & 1 & 0 & 0 \\ -m_2 d\cos(\gamma) & J_2 + m_2((d\cos(\gamma))^2 + cd\cos(\gamma)) & -m_2 ud(1 + \cos(\gamma)) & J_2 + m_2(d\cos(\gamma))^2 & 0 \\ 0 & 0 & 0 & 0 & 1 \end{bmatrix} \tag{A.10}$$

The **K** matrices are the same for all model revisions. However, in Revisions 4 and 7 (refer to Table 3.1), $\cos(\gamma)$ is replaced by 1.

$$\mathbf{K} = \begin{bmatrix} k_{11} & k_{12} & 0 & k_{14} & k_{15} \\ k_{21} & k_{22} & 0 & k_{24} & k_{25} \\ 0 & 1 & 0 & 0 & 0 \\ k_{41} & k_{42} & 0 & k_{44} & k_{45} \\ 0 & 0 & 0 & 1 & 0 \end{bmatrix} \tag{A.11}$$

Where:

$$k_{11} = \frac{1}{u}\left[-C_{\alpha 1} - C_{\alpha 2} - C_{\alpha 3} - \cos(\gamma)C_{\alpha 4} - \cos(\gamma)C_{\alpha 5}\right]$$

$$k_{12} = \frac{1}{u}\left[-C_{\alpha 1}a + C_{\alpha 2}b_1 + C_{\alpha 3}b_2 + \cos(\gamma)C_{\alpha 4}(c + f_1\cos(\gamma)) + \cos(\gamma)C_{\alpha 5}(c + f_2\cos(\gamma))\right]$$

$$k_{14} = \frac{1}{u}\left[\cos^2(\gamma)f_1C_{\alpha 4} + \cos^2(\gamma)f_1C_{\alpha 5}\right]$$

$$k_{15} = \cos(\gamma)C_{\alpha 4} + \cos(\gamma)C_{\alpha 5}$$

$$k_{21} = \frac{1}{u}\left[-aC_{\alpha 1} + b_1C_{\alpha 2} + b_2C_{\alpha 3} + (f_1 + c\cos(\gamma))C_{\alpha 4} + (f_2 + c\cos(\gamma))C_{\alpha 5}\right]$$

$$k_{22} = \frac{1}{u}[-a^2C_{\alpha 1} - b_1^2C_{\alpha 2} - b_2^2C_{\alpha 3} - (f_1 + c\cos(\gamma))C_{\alpha 4}(c + f_1\cos(\gamma))$$
$$- (f_2 + c\cos(\gamma))C_{\alpha 5}(c + f_2\cos(\gamma))]$$

$$k_{24} = \frac{1}{u}\left[-(f_1 + c\cos(\gamma))C_{\alpha 4}f_1\cos(\gamma) - (f_2 + c\cos(\gamma))C_{\alpha 5}f_2\cos(\gamma)\right]$$

$$k_{25} = -(f_1 + c\cos(\gamma))C_{\alpha 4} - (f_2 + c\cos(\gamma))C_{\alpha 5}$$

$$k_{41} = \frac{1}{u}\left[f_1C_{\alpha 4} + f_2C_{\alpha 5}\right]$$

$$k_{42} = \frac{1}{u}\left[-f_1C_{\alpha 4}(c + f_1\cos(\gamma)) - f_2C_{\alpha 5}(c + f_2\cos(\gamma))\right]$$

$$k_{44} = \frac{1}{u}\left[-f_1^2C_{\alpha 4}\cos(\gamma) - f_2^2C_{\alpha 5}\cos(\gamma)\right]$$

$$k_{45} = -f_1C_{\alpha 4} - f_2C_{\alpha 5}$$

$$\mathbf{F} = \begin{bmatrix} \cos(\delta)C_{\alpha 1} \\ a\cos(\delta)C_{\alpha 1} \\ 0 \\ 0 \\ 0 \end{bmatrix} \tag{A.12}$$

$$\underline{\dot{x}} = \begin{pmatrix} \dot{v} \\ \ddot{\Psi} \\ \dot{\Psi} \\ \ddot{\gamma} \\ \dot{\gamma} \end{pmatrix},\ \underline{x} = \begin{pmatrix} v \\ \dot{\Psi} \\ \Psi \\ \dot{\gamma} \\ \gamma \end{pmatrix},\ u = \delta \tag{A.13}$$